Fakultät für Medizin

Klinik für Herz- und Kreislauferkrankungen

Deutsches Herzzentrum München des Freistaates Bayern

Use of intravascular optical coherence tomography for evaluation of vessel healing following coronary stent implantation and elucidation of mechanisms of stent failure (with a particular focus on neoatherosclerosis)

Erion Xhepa

Vollständiger Abdruck der von der Fakultät für Medizin der Technischen Universität München zur Erlangung des akademischen Grades eines

Doctor of Philosophy (Ph.D.)

genehmigten Dissertation.

Vorsitzender: Prof. Dr. Dr. Stefan Engelhardt

Betreuer: Prof. Dr. Adnan Kastrati

Prüfer der Dissertation:

1. Prof. Dr. Karl-Ludwig Laugwitz

2. Prof. Dr. Michael Joner

Die Dissertation wurde am 08.07.2019 bei der Fakultät für Medizin der Technischen Universität München eingereicht und durch die Fakultät für Medizin am 29.08.2019 angenommen.

TABLE OF CONTENTS

5. Discussion

LIST OF ABBREVIATIONS

ADR = antegrade dissection and re-entry

ARC = Academic Research Consortium

AWE = antegrade wire escalation

BMS = bare-metal stent

BP-DES = biodegradable-polymer drug-eluting stent

BP-SES = biodegradable-polymer sirolimus-eluting stent

BVS = bioresorbable vascular scaffolds

DP-DES = durable-polymer drug-eluting stent

DP-EES = durable-polymer everolimus-eluting stent

CTO = chronic total occlusion

DAPT = dual antiplatelet therapy

DART = dissection and re-entry technique

DES = drug-eluting stent

EES = everolimus-eluting stent

GSI= gray-scale signal intensity

ISR = in-stent restenosis

IVUS = intravascular ultrasound

LASSO = Least Absolute Shrinkage and Selection Operator

LLL = late luminal loss

MI = myocardial infarction

MLD = minimal lumen diameter

NSTEMI = non ST-elevation myocardial infarction

OCT = optical coherence tomography

%DS = percentage diameter stenosis

PCI = percutaneous coronary intervention

QCA = quantitative coronary angiography

reverse CART = reverse controlled antegrade and retrograde tracking

RWE = retrograde wire escalation

SES = sirolimus-eluting stent

ST = stent thrombosis

STAR = subintimal tracking and re-entry technique

STEMI = ST-elevation myocardial infarction

TCFA = thin-cap fibroatheroma

TLR = target lesion revascularization

TVR = target vessel revascularization

ZES = zotarolimus-eluting stent

ABSTRACT

Despite constant improvements in the outcomes of patients undergoing implantation of new-generation drug-eluting stents (DES), stent thrombosis (ST) and in-stent restenosis (ISR) continue to occur at low but significant rates and a detailed understanding of the mechanisms leading to their occurrence represents an important unmet clinical need. By allowing a detailed visualization of the vessel wall microstructure, intravascular optical coherence tomography (OCT) is particularly suited to evaluate vessel healing following implantation of different stent platforms or intervention techniques as well as to elucidate mechanisms of stent failure.

In the multicenter PRESTIGE Registry, the largest of patients presenting with stent thrombosis in the literature to date, we found that dominant etiological factors vary according to presentation: uncovered struts and underexpansion are most common in acute/subacute stent thrombosis while uncovered struts and neoatherosclerosis most common in late/very late stent thrombosis. In-stent plaque rupture represents a frequent and often fatal consequence of neoatherosclerosis and DES-implantation is independently associated with increased risk of neoatherosclerosis formation over time. In a multicenter registry of patients presenting with ISR, we found ISR lesions to display considerable intralesion neointimal heterogeneity and frequent neoatherosclerotic changes and that the latter display different time courses in DES as opposed to BMS; grey scale signal intensity analysis of restenotic neointima shows promise as a quantitative tool of neointimal characterization. Stent underexpansion was a frequent finding in both ST and ISR, underscoring its central role in triggering stent failure and highlighting the need for larger adoption of imaging-guided optimization of stent implantation as a mean to reduce the occurrence of stent failure.

In the ISAR-OCT-CTO registry, the largest study to date to specifically compare both angiographic and intravascular OCT findings following intraplaque as opposed to subintimal recanalization of chronic total occlusions (CTO), we found that intraplaque and subintimal recanalization techniques are associated with similar mid-term angiographic results. High rates of both uncovered and malapposed struts are seen following CTO recanalization, the latter particularly following use of subintimal recanalization techniques.

In a randomized comparison of a biodegradable-polymer sirolimus-eluting (BP-SES) and durable-polymer everolimus-eluting stent (DP-EES) we found no differences in terms of neointimal coverage between the stent platforms; neointimal tissue was mostly immature in both stent types, with a trend to more mature tissue in the BP-SES group. Aiming at better characterizing differences in vessel healing following implantation of BP-DES and new-generation DP-DES, we performed a meta-analysis of studies that included follow-up OCT imaging; we found that BP-DES, particularly those with thicker backbones, delay vascular healing as compared with new-generation DP-DES.

Finally, in an animal model of in-stent neoatherosclerosis, we showed that fully bioresorbable magnesium scaffolds reduce neointimal macrophage infiltration compared to stainless steel-based permanent DES and that statin treatment significantly reduces progression of neointimal macrophage infiltration in both stent types.

ZUSAMMENFASSUNG

Klinische Ergebnisse von Patienten die mittels drug-eluting stents (DES) behandelt werden verbessern sich stetig. Dennoch treten auch weiterhin Stent Thrombosen (ST) und in-Stent Restenosen (ISR) auf. Die Ereignisraten sind niedrig, bleiben jedoch klinisch relevant und unterstreichen die anhaltende klinische Herausforderung zugrundeliegende Mechanismen für Ihr Auftreten besser und detaillierter zu verstehen. Aufgrund detaillierter Darstellung der Gefäßwand und ihrer Mikrostruckturen, eignet sich die optische Kohärenztomographie sowohl zur Beurteilung der Gefäßheilung nach Implantation verschiedener Stenplattformen oder nach unterschiedlichen Interventionstechniken als auch zur Detektion von Mechanismen des Stentversagens.

Im multizentrischen PRESTIGE Register, dem in der aktuellen Literatur größten beschriebenen Stent Thrombose Register, konnten wir zeigen, dass ursächliche Mechanismen sich je nach zeitlicher Präsentation von ST unterscheiden: in akuten/subakuten ST zeigten sich hauptsächlich nicht-endothelialisierte Stentstreben und unterexpandierte Stents, in späten/sehr späten ST zeigten sich hauptsächlich nicht-endothelialisierte Stentstreben und Neoatherosklerose. Die Plaque Ruptur im Stentbereich stellt eine häufige und oft tödliche Folge der Neoatherosklerose dar. DES-Implantation und das Risiko für die Entstehung von Neoatherosklerose im Laufe der Zeit sind unabhängig miteinander assoziiert. In einem multizentrischen Register von Patienten mit ISR, zeigten sich erhebliche Unterschiede bezüglich neointimaler Charakteristika verschiedener ISR-Läsionen sowie häufig nachweisbare neoatherosklerotische Veränderungen die sich in der Entstehungsgeschwindigkeit deutlich von Neoatherosklerose in bare-metal Stents (BMS) -ISR unterscheidet. Hierbei erwies sich die „grey-scale intensitiy" Analyse als vielversprechendes Werkzeug zur Charakterisierung restenotischer Neointima. Die herausragende Rolle von Stent-Unterexpansion als zentraler Auslöser für Stentversagen spiegelt sich in deren häufigen

Beobachtung, sowohl bei ST, als auch ISR wieder. Dies unterstreicht die Notwendigkeit einer bildgebungsgesteuerten optimierten Stentimplantation als mögliches Mittel das Auftreten von Stentversagen zu reduzieren.

Das ISAR-OCT-CTO Register, stellt aktuell den größten Vergleich angiographischer und intravaskulärer OCT Ergebnisse nach intra-Plaque versus subintimaler Rekanalisation von chronischen Verschlüssen (chronic total occlusions=CTO) dar. Beide Techniken zeigten angiographisch vergleichbare mittelfristige Verlaufsergebnisse. In der OCT Bilgebung zeigten sich wiederum hohe Raten an nicht endothelialisierten und malappositionierten Stentstreben nach CTO Rekanalisation, letztere insbesondere bei subintimalen Rekanalisationstechniken.

In einem randomisierten Vergleich von Sirolimus-eluting Stents mit biodegradablen Polymer (BP-SES) und Everolimus-eluting Stents mit permanentem Polymer (DP-EES) konnten wir keinen Unterschied bezüglich des neointimalen Wachstums auf den Stentstreben der beiden Stentplattformen nachweisen. Das Neointimale Gewebe stellte sich bei beiden Stenttypen überwiegend unreif dar. Mit dem Ziel Gefäßheilung nach BP-DES und DP-DES besser zu charakterisieren, führten wir eine Meta-Analyse von Studien mit OCT Bildgebungsverlaufsuntersuchung durch. Wir konnten zeigen, dass BP-DES, insbesondere solche mit dickeren Stentstreben, im Vergleich zu DP-DES die Gefäßheilung verzögern.

Abschließend konnten wir in einem Tiermodel für in-Stent-Neoatherosklerose zeigen, dass vollständig bioresorbierbare Magnesium Scaffolds, im Vergleich zu auf rostfreien Stahl basierenden DES, Makrophgeninfiltration der Neointima reduzieren. Eine Behandlung mit Statinen reduzierte darüber hinaus signifikant die Progression der Makrophgeninfiltration in die Neointima bei beiden Stenttypen.

1. INTRODUCTION

1.1 – Evolution of coronary implants

Since the first successful non-operative dilatation of a coronary stenosis, performed by Andreas Grüntzig, a German radiologist, on 16th September 1977 at the University Hospital in Zürich [1], percutaneous coronary intervention (PCI) has evolved rapidly to become one of the most widely performed medical procedures worldwide. Initial use of balloon angioplasty for the treatment of coronary stenoses was however characterized by two main limitations: i) abrupt vessel closure secondary to vessel dissection and, ii) high rates of restenosis (in up to 40% of cases) due to a combination of acute vessel recoil, constrictive remodelling and intimal hyperplasia [2].

A potential solution to the first problem was the implantation of an expandable metal mesh, initially on a bail-out basis, in order to maintain vessel patency following balloon dilatation. Following preclinical studies, Jacques Puel and Ulrich Sigwart performed the first bare-metal stent (BMS) implantation in human coronary arteries in Toulouse, France and Lausanne, Switzerland respectively in the spring of 1986 [3, 4]. Initially conceived as a "bail-out" strategy for abrupt vessel closure in the immediate aftermath of balloon angioplasty, availability of data from the European BENESTENT [5] and the United States STRESS [6] randomized clinical trials in 1994 provided an evidence-base for extension of the use of stents to an elective basis – a development that would significantly attenuate the problem of late luminal re-narrowing (or coronary restenosis). However, the inherent thrombogenicity consequent on the exposure of metal stent struts to circulating blood resulted in a restrictive rate of thrombotic stent occlusion in the immediate aftermath of PCI despite aggressive anti-coagulant therapy with a high rate of local complications. Subsequent investigation demonstrated that a strategy based on dual antiplatelet therapy (DAPT) with aspirin and a

thienopyridine was significantly more efficacious and better tolerated [7, 8], thereby facilitating more widespread adoption of stenting into clinical practice.

Despite reduction of late restenosis occurrence compared with balloon angioplasty, the occurrence of neo-intimal hyperplasia – a process of scar tissue formation at the site of the stented segment resulting in need for repeat intervention in approximately 25% of cases – continued to represent the Achilles' heel of catheter-based intervention with BMS. Developed with the specific aim of targeting this pathophysiological process, drug-eluting stent (DES) therapy involves the incorporation into a supporting stent platform of anti-mitotic or immunosuppressive agents – with facilitated delayed elution – targeted at inhibition of smooth muscle cell proliferation, the key component of neointimal overgrowth. The advantage of this technology lies in the ability to achieve local drug effects without systemic toxicity. Controlled and sustained drug release in the initial 10-30 days post-implantation is crucial for the antirestenotic efficacy of DES. The performance of a DES is related to each of the following 3 components: namely the stent backbone, the carrier polymer (to control drug release kinetics) and the active drug. Randomized trials comparing early-generation DES and BMS showed consistent 50-70% reductions in the need for repeat revascularization [9]. However, this drastic reduction in the occurrence of in-stent restenosis (ISR) came at the price of an increased rate of stent thrombosis (ST) in the late post-implantation period (>1 year) with early generation DES as compared with BMS [9].

The underlying pathophysiological substrate for the increased incidence of very late ST with early-generation DES appeared to be a delay in vascular healing of the stented arterial segment and although this process is undoubtedly multifactorial in aetiology, it seems that inflammatory response to durable polymer coatings plays a central role [10].

Figure 1. *Principal characteristics of selected drug-eluting stents and scaffolds. Adapted from* [2].

	Durable polymer-coated stent		Biodegradable polymer-coated stent					Polymer-free drug-eluting stent		Bioresorbable drug-eluting stent
Manufacturer	Abbott/Boston	Medtronic	Biotronic	Terumo	Translumina	Boston	Biosensors	B. Braun	Biosensors	Abbott
Name	Xience/Promus	Resolute	Orsiro	Ultimaster	Yukon Choice PC	Synergy	BioMatrix	Coroflex ISAR	BioFreedom	ABSORB
Material and drug	CoCr/PtCr-EES	CoNi-ZES	CoCr-SES	CoCr-sES	316L-SES	PtCr-EES	316L-BES	316L-SES/ probucol	316L-BES	PLLA-EES
Shape										
Strut thickness	81 µm	91 µm	60 µm	80 µm	87 µm	74 µm	120 µm	65 µm	112 µm	150 µm
Coating	Circumferential		Abluminal							Circumferential

In medical technology, polymers are often classified as *durable* (or non-erodable) – resistant to degradation in the human body – or *biodegradable* – slowly degraded *in vivo* by hydrolysis of the covalent bonds that link their repeating monomer subunits. In the field of DES therapy, polymer coating has proven the most successful vehicle both for drug-loading and control of release kinetics [11, 12]. To address the potential limitation of durable polymers, DES with biodegradable-polymer (BP-DES) have been developed. The majority of BP-DES have conventional metallic backbones with a polymer matrix composed of either polylactic or polylactic-co-glycolic acid. Depending on the molecular weight and crystallinity of the polymer configuration, these polymers are converted to carbon dioxide and water in a period ranging between 6 weeks and 24 months. Consequently, BP-DES are designed to maintain the antiproliferative benefits of durable-polymer DES (DP-DES) before functionally transforming into a BMS once drug delivery and polymer biodegradation are complete [13]. Based on such characteristics, BP-DES were postulated to reduce the risk of adverse cardiac events related to ST beyond the first year that may be related to the durable polymer. Meta-analyses of randomized trials showed indeed superiority of BP-DES over early-generation DP-DES in terms of stent thrombosis and myocardial infarction [14]. However, comparisons of efficacy and safety of BP-DES with new-generation DP-DES have, taken cumulatively, failed to show a superiority of BP-

13

DES [15-18]. In the recently published long-term (10 year) follow-up of the ISAR TEST 4 randomized trial, BP-DES and new-generation DP-DES showed comparable outcomes [19].

The latest evolution of coronary implants is represented by the fully bioresorbable vascular scaffolds (BVS). BVS were designed to overcome some of the limitations associated with the use of metallic stents such as limitation of normal vasomotion and adaptive arterial remodelling, preclusion of bypass surgery and persistent, chronic foreign-body reaction eliciting inflammation. The most advanced attempt to create such a device was represented by the Absorb BVS (Abbott Vascular) which consisted of a balloon-expandable, 157 μm thick, BVS consisting of a PLLA backbone with a poly-D,L-lactide (PDLLA) coating in a 1:1 ratio with the antiproliferative drug everolimus [20]. Absorb BVS received CE marking in Europe in 2010 on the basis of data from the ABSORB clinical trial [20, 21], while the FDA approved its clinical use in 2015 following the ABSORB III clinical trial [22]. However, subsequent longer-term results have been disappointing, with increased rates of device thrombosis and target-lesion revascularization [23-26], ultimately leading to withdrawal of the Absorb BVS from the market. Despite Absorb BVS being the most largely studied BVS to date, other BVS have been developed and received CE marking approval. One of these is represented by the Magmaris scaffold (Biotronik) which is made from a refined, slow-degrading proprietary magnesium alloy, with a strut thickness of 150 μm and coated with PLLA polymer and sirolimus at a concentration of 140 μg/cm^2 [27]. Since the magnesium alloy is radiolucent, which results in poor visibility, the Magmaris scaffold has radiopaque markers made of permanent tantalum at the proximal and distal ends to improve visibility. It has a square-shaped strut and a modified electropolished strut cross-sectional profile to slow resorption and prevent fracture [27, 28]. Similar to metallic stents, magnesium scaffolds provide better tensile strength and stiffness, low acute recoil and high compliance to vessel geometry. The resorption process occurs in two main phases: an anodic reaction and then conversion to calcium phosphate [29].

1.2 – Manifestations of stent failure – Stent thrombosis and in-stent restenosis

ST represents the most feared complication of PCI, typically leading to ST-elevation myocardial infarction (STEMI) in the majority of cases [30, 31] and mortality rates that may be as high as 20-40% [30]. The already mentioned increase in the incidence of ST observed with early generation DES has not been confirmed with new-generation DES; indeed, current clinical registries and randomized clinical trials with broad inclusion criteria have shown rates of ST at or <1% after 1 year and 0.2-0.4% per year thereafter [32-35] and overall rates of early and late ST out to 3 years have halved in recent years from 3% to 1.5% [32, 33] (**Figure 2**).

Figure 2. *Incidence of stent thrombosis after bare-metal stents, early-generation DES (G1-DES) and new-generation DES (G2-DES). Adapted from [32].*
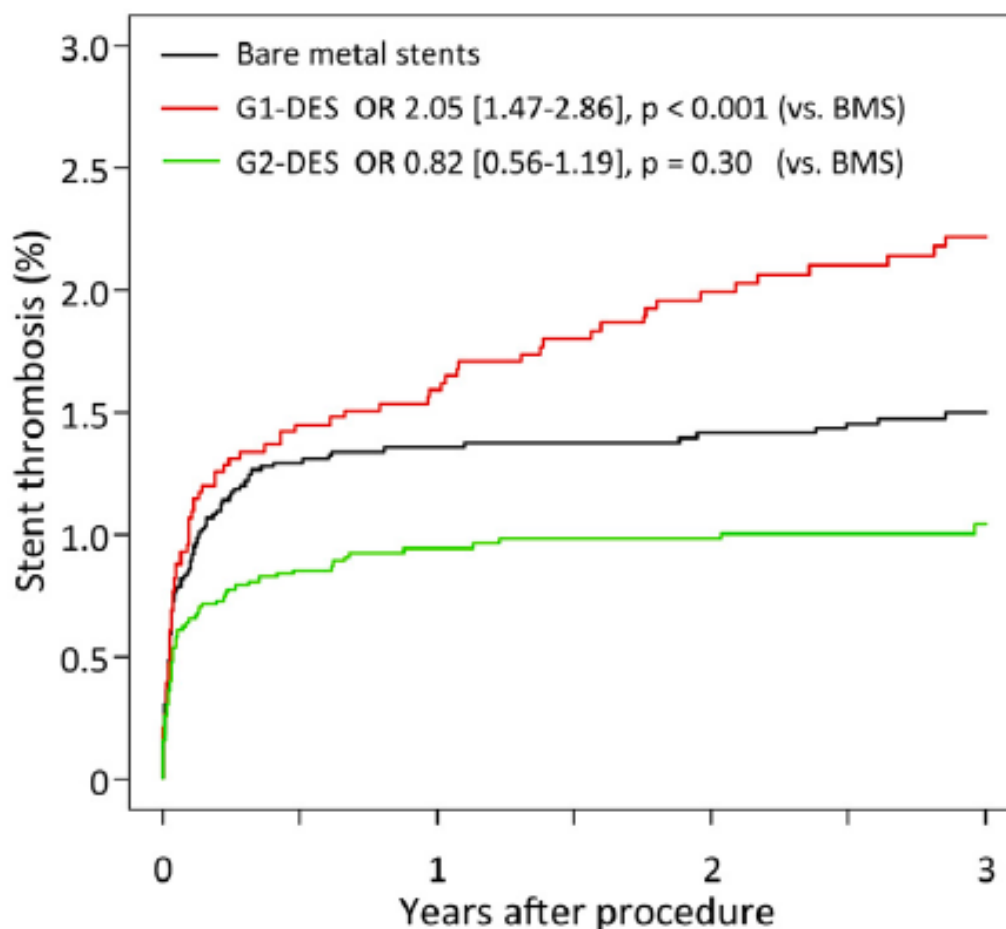
ST is characterized by angiographic or post-mortem evidence of recently formed thrombus in a previously stented segment. In order to standardize reporting across clinical trials, universal definitions were agreed upon by a group of experts known as the Academic Research Consortium (ARC) [36]. This definition classified evidence of ST as _definite ST_ (presence of an acute coronary syndrome with angiographic or post-mortem evidence of thrombus or occlusion), _probable ST_ (unexplained death within 30 days after PCI or acute myocardial infarction involving the target-vessel territory without angiographic confirmation) or _possible ST_ (any unexplained death occurring at least 30 days after the procedure); additionally, according to timing after the initial stent placement, ST is classified as _acute ST_ (occurring between 0 and 24 hours after the index PCI), _subacute ST_ (occurring between 24 hours and 30 days after the index PCI), _late ST_ (occurring between 31 and 360 days after the index PCI) and _very late ST_ (occurring beyond 360 days after the index PCI) [36, 37]. From a practical standpoint, because of differing pathophysiology and risk factors, it can be useful to dichotomize ST events in _early ST_ (ST occurring within the first 30 days after the index PCI) or _late ST_ (ST occurring beyond 30 days after the index PCI). In general, early ST is more common than late ST, accounting for ≈50-70% of all cases [38, 39].

Several risk factors for the occurrence of ST have been identified, which can be broadly classified as patient-, procedure- or device-specific. Procedural risk factors seem to play a dominant role in the occurrence of early ST; they are represented by stent undersizing, presence of residual dissection, impaired TIMI flow and residual disease proximal or distal to the stented segment. Additionally, patient-specific risk factors, such as reduced left ventricular function and impaired response to ADP-antagonist therapy appear to confer additional risk; indeed, premature discontinuation of DAPT in the initial 30 days following PCI appears to be the most important predictor of ST [40]. Although device-specific factors were thought to be of lesser importance in the occurrence of early ST, recent evidence suggests that there might be important differences with

slightly higher rates of early ST with BMS as compared with DES [41]; preclinical evaluation suggests that polymer-coating may reduce acute stent thrombogenicity by improving stent-blood interactions [42].

Although procedure-specific factors will most likely manifest as early stent failure, these factors can also impact on late ST where significant issues, such as stent undersizing or underexpansion, persist after DAPT discontinuation [39]. Stent malapposition has been often observed on intravascular imaging in patients presenting with ST [43], although the threshold at which malapposition distance and extent become relevant remain a matter of debate [44]. Patient-specific risk factors, such as impaired left ventricular function and diabetes mellitus remain important for late ST. Device-specific factors appear to be particularly important for the occurrence of late ST; several reports confirmed the presence of a small, but significant increase in the risk of ST with early generation DES [9, 41, 45]. Autopsy studies have shown that the underlying substrate for this excess risk is represented by a delayed arterial healing, a pathophysiological process characterized by impaired endothelial coverage, persistent fibrin deposition and ongoing vessel inflammation [10, 46]. Although such process is most likely multifactorial in origin, an inflammatory reaction to the durable polymer coatings used in early-generation DES appears to play a critical role [47, 48]. Delayed arterial healing has been subsequently linked not only to the occurrence of late ST but also delayed late luminal loss (late re-stenosis), persistent vasomotor dysfunction proximal and distal to the stented segment [49] and de novo in-stent atherosclerosis [50]. Current generation DES have been shown to mitigate this healing problem by incorporating thinner stent struts, more biocompatible polymer coatings and lower dosages of limus-analogue drugs [32, 33]. Additionally, in recent years, many efforts have been made to avoid the use of polymers in DES. However, the control of release kinetics of the eluted drug appears to be the crucial step in the determination of the antirestenotic efficacy of DES platforms [47, 51].

ISR occurs more frequently than ST. Large real world registries with systematic angiographic surveillance have shown rates of angiographic restenosis declining from ≈30% following implantation of BMS, to ≈15% following use of early-generation DES, to ≈12% following implantation of new-generation DES [52] (**Figure 3**). On the other hand, contemporary randomized clinical trials have shown rates of clinically relevant ISR of <5% at 12 months [53].

Figure 3. *Proportion of DES implanted and proportion of lesions with restenosis at follow-up angiography. Adapted from [52].*
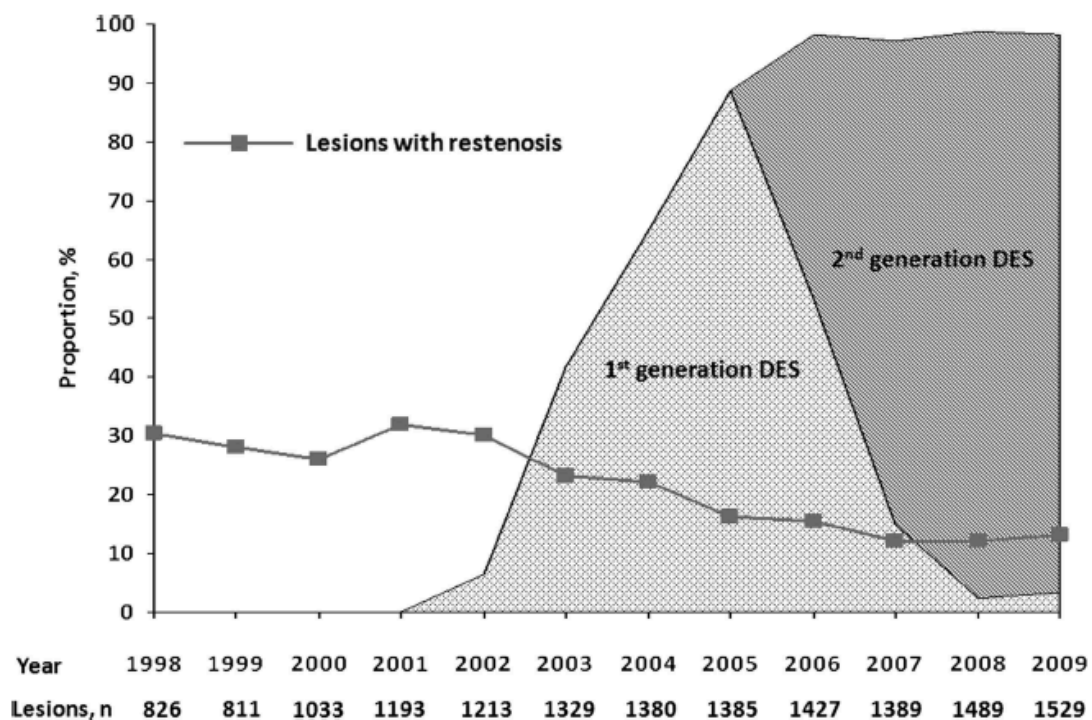
Angiographic surveillance studies have shown that neointima formation following BMS implantation tends to peak at 6 months and remain stable or regress somehow over the medium term [54, 55]. Time course of restenosis appears to be rather different following DES implantation, with ongoing erosion of luminal calibre between 6-8 months and 2-5 years following stent implantation [56, 57]. Moreover, compared with BMS-ISR, DES-ISR tends to exhibit a focal pattern, often affecting the stent edges. The finding of ongoing delayed late loss in DES beyond the 6-8 months time-window

18

supports the hypothesis of DES-associated delayed arterial healing and suggests that the temporal course of ISR with DES may be significantly right-shifted compared with BMS.

Despite representing a more benign entity than ST, occurrence of ISR may have an important impact on long-term prognosis following PCI [58] and identification of patients at risk remains of paramount importance. Analogous to ST, risk factors for the occurrence of ISR may be classified as patient-, procedure- or device-specific [52]. By reducing the extent of vessel injury at the time of implantation, thinner stent struts appear to be associated with a reduced restenotic risk compared with thicker struts [59]. Additional risk factors for the occurrence of ISR are represented by small vessel size, total stented length, complex lesion morphology, diabetes mellitus as well as stent underexpansion.

Treatment of ISR lesions is challenging and several treatment strategies (including conventional balloon angioplasty, cutting and scoring balloon therapy, debulking techniques such as rotational atherectomy, vascular brachytherapy, repeat stenting and drug-coated balloon angioplasty) have been investigated. Most patients presenting with such entity are amenable to repeat catheter intervention and the evidence available suggests the most effective strategies to be represented by repeat stenting with a new-generation DES or drug-coated balloon (DCB) angioplasty [60, 61] eventually preceded by lesion preparation with cutting/scoring balloon [62].

1.3 – Neoatherosclerosis

Neoatherosclerosis has recently been described as a novel disease entity, representing a further manifestation of atherosclerotic disease in the nascent neointimal tissue after stent implantation [50, 63]. In-stent neoatherosclerosis is histologically characterized by the accumulation of lipid-laden foamy macrophages with or without necrotic core formation and/or calcification within the neointima [63]. In-stent neoatherosclerosis has emerged as an important contributing factor to late

vascular complications including late and very late ST and late ISR. The development of neoatherosclerosis has been observed months to years following stent placement, whereas atherosclerosis in native coronary arteries advances over decades. Although the mechanisms responsible for the development of neoatherosclerosis are not fully understood to date, abnormal endothelial maturation following stent implantation is suspected to play a major role in this process. In-stent plaque rupture likely accounts for most thrombotic events associated with neoatherosclerosis. Although a significant number of autopsy and clinical imaging studies aimed to characterize the specific morphological features of neoatherosclerosis, very little is known with regards to plaque progression of this novel disease manifestation. From a histopathological standpoint it has been proposed that one of the earliest signs of neoatherosclerosis is neointimal foam cell infiltration, which often occurs between stent struts since flow dynamics (low and oscillatory shear stress, recirculation zones) likely favor progression of atherosclerotic disease in these specific regions. Another early feature is the presence of neointimal micro-calcifications. Through the influence of several factors, early neoatherosclerotic lesions progress and may eventually lead to the formation of mature atherosclerotic lesions similar to those described in native atherosclerotic plaques. These include fibrous- and fibrocalcific lesions as well as fibroatheromas within the nascent neointima. Analogous to native atherosclerosis, fibroatheromas consist of a fibrous cap covering a necrotic core composed of acellular debris, free cholesterol and extracellular matrix. Neovascularization represents a common feature of advanced fibroatheromas which can lead to vessel rupture and intraplaque hemorrhage (**Figure 4**).

Figure 4. *Representative histologic images showing various stages of in-stent neoatherosclerosis. Adapted from* [50]
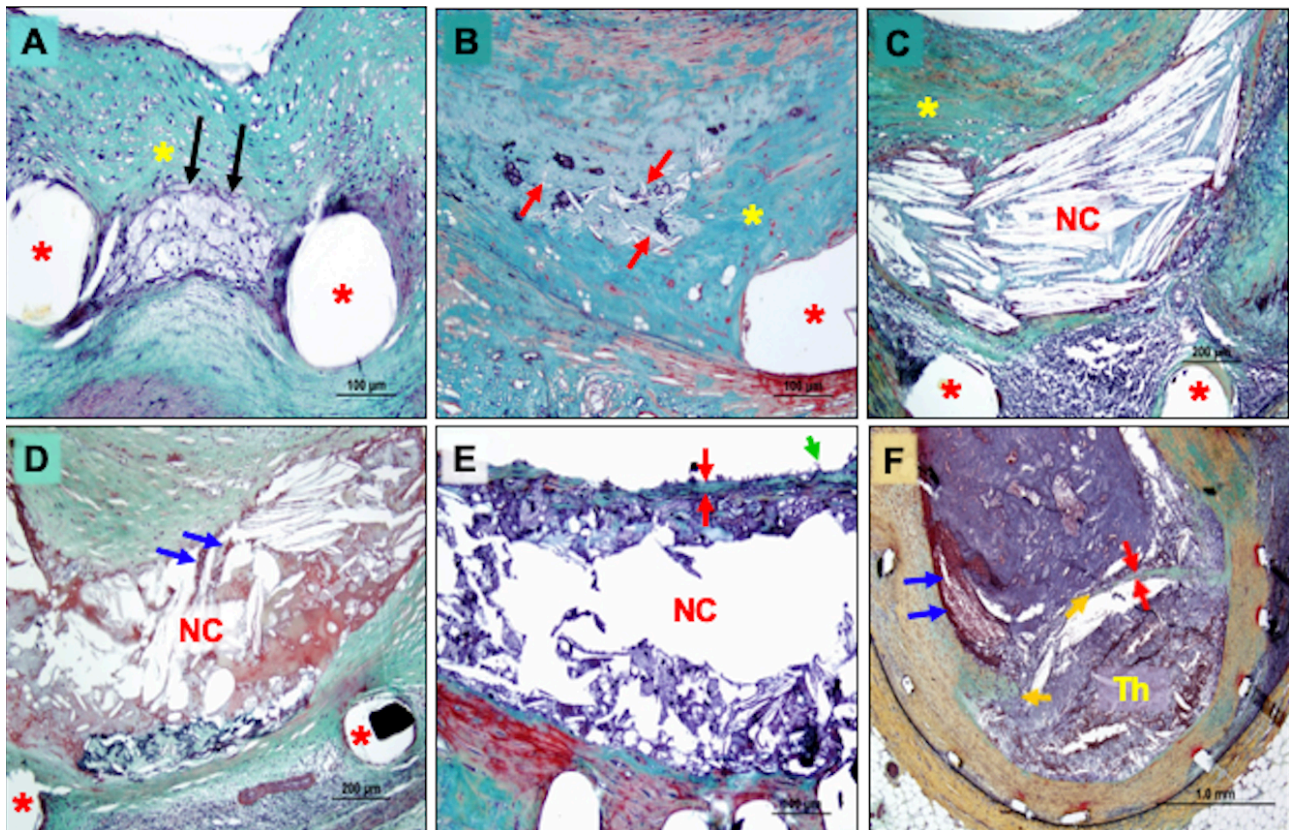
(A) Foamy macrophage clusters in peri-strut region and close to the luminal surface in a sirolimus-eluting stent. (B) Neointimal calcifications seen in the neointima of a sirolimus-eluting stent. (C) Fibroatheroma showing necrotic core (NC) within thin neointima in a SES. (D) Fibroatheroma displaying intraplaque hemorrhage most likely resulting from the rupture of micro-vessels. (E) An example of a thin-cap fibroatheroma (TCFA) characterized by a large necrotic core covered by a thin fibrous cap. (F) Vessel thrombosis resulting from plaque rupture of a TCFA within a previously stented coronary segment. *Stent strut.

The exact mechanisms leading to fibrous cap thinning in the setting of neoatherosclerosis remain incompletely elucidated, but it has been suggested that mechanisms analogous to those responsible for the progression of native atherosclerotic plaques play a central role: infiltration of macrophages into the fibrous cap and additional recruitment of mononuclear cells contribute to progression towards vulnerable lesions [64]. Overall, neoatherosclerosis represents an accelerated and possibly more unstable atherosclerotic disease-manifestation as compared to native

21

atherosclerosis [50, 63]; additionally, neoatherosclerotic changes tend to be more accentuated and appear earlier in DES compared to BMS [65]. One of the principal mechanisms responsible for the accelerated DES neoatherosclerosis appears to be the presence of incompetent and dysfunctional endothelial coverage of the stented segment characterized by poor cell-to-cell junctions, reduced expression of anti-thrombotic molecules and decreased nitric oxide production. Presence of a dysfunctional endothelial layer is in turn a direct consequence of the anti-proliferative effects of the eluted drugs [66-68] and therefore another manifestation of the delayed vascular healing following DES implantation. Poorly formed cell-to-cell junctions underlie impaired barrier function of the endothelial layer, therefore allowing greater amount of lipoproteins to enter the sub-endothelial space, thereby promoting accelerated de-novo atherosclerosis within the nascent neointima [50, 69]. The DES polymer coatings may also promote a chronic inflammation characterized by infiltration of macrophages, lymphocytes and giant cells and thereby contribute to the development of neoatherosclerosis. From a histological standpoint, necrotic core formation in the setting of neoatherosclerosis is mostly driven by macrophage apoptosis and, contrary to native vessel atherosclerosis, lipid pools are mostly absent, a feature which may facilitate earlier progression towards vulnerable plaque and in-stent plaque rupture.

1.4 – Intravascular optical coherence tomography

Although it is the most widely used method to assess the severity of coronary artery disease and to guide treatment, coronary angiography has several limitations, mainly deriving from the fact that it is a lumenogram depicting foreshortened, planar projections of the contrast filled lumen rather than imaging the diseased vessel itself. Aiming at overcoming such limitations, intravascular imaging techniques were introduced which provide tomographic or cross-sectional images of the coronary arteries [70]. Intravascular ultrasound (IVUS) represented a notable development by allowing an in

vivo visualization of structures that could previously be seen only post mortem. Intravascular optical coherence tomography (OCT), which relies on near-infrared (NIR) electromagnetic radiation (wavelength ≈1.3μm) rather than acoustic waves, was used for the first time in swine in vivo in 2000 [71]. This initial proof-of-concept study showed that OCT provided images of higher resolution compared to IVUS, allowing visualization of vascular features not captured by ultrasound such as the intimal layer, including intimal flaps and defects, disruptions of the medial layer and stent strut apposition. First-in-human confirmation of such features of intravascular OCT followed in 2002 [72-75]. By measuring the time delay of optical echoes reflected or backscattered from biological structures located beneath the endothelial layer, by a technique known as interferometry, OCT can obtain structural information as a function of depth within the tissue [76, 77] (**Figure 5**).

Figure 5. *Schematic representation of an optical coherence tomography system. Adapted from* [76]
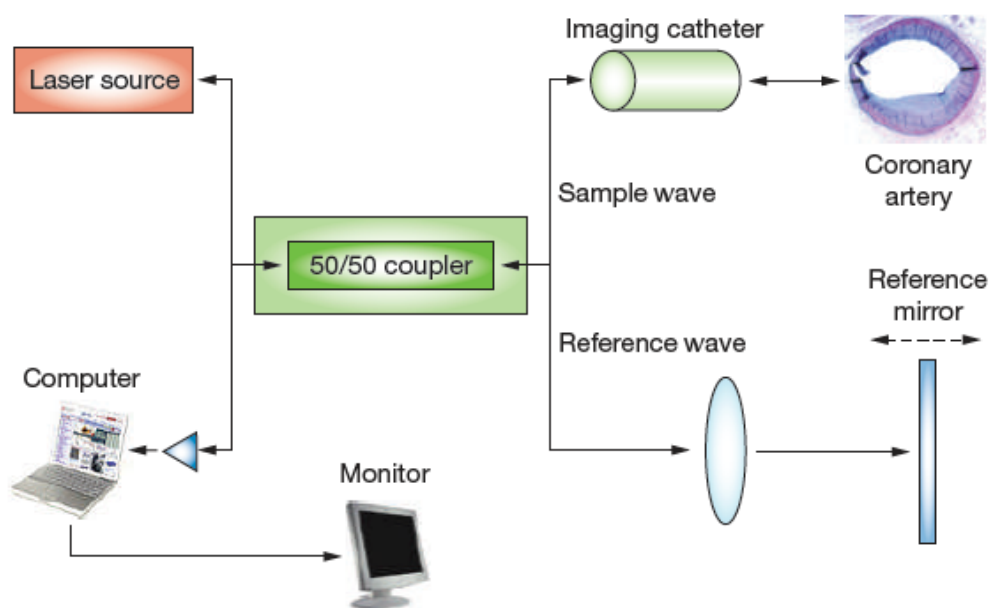
Spatial resolution, defined as the minimum distance between closely spaced objects that can be independently detected by the imaging system, is higher for intravascular OCT than for all available invasive and non-invasive imaging techniques, with an axial resolution of ≈10-15 μm which

permits in-vivo micron scale tomographic imaging of the vessel wall. Owing to its spatial resolution almost at the level of light microscopy, the term "*optical biopsy*" was coined, to underscore similarities with histological techniques and the ambition of this technology to provide in-vivo histology-like images. On the contrary, penetration depth is lower compared to IVUS, ranging typically between 0.1 mm and 2.0 mm, depending on the tissue composition of the artery. There are 2 types of intravascular OCT systems: early-generation time-domain OCT (TD-OCT) and new-generation Fourier-domain OCT systems, also known as frequency domain OCT (FD-OCT). The main difference between the two systems is that FD-OCT allows much higher imaging speeds, thereby allowing rapid, 3-dimensional pullback imaging. Another peculiarity of intravascular OCT is its inability to image through blood, since it attenuates the OCT light before it reaches the artery wall; as a consequence, intravascular OCT images are acquired as blood is flushed from the field of view.

Imaging and characterization of microstructural features of the arterial wall by means of intravascular OCT has been validated in a number of OCT-histology post-mortem correlation studies [72, 78-80]. These studies provided the foundation for the development and validation of image criteria for detecting features that correspond to tissue microstructures with high sensitivity and specificity. The detected microstructural features include macrophages [78, 81], cholesterol crystals [82], red and white thrombus [73, 83], calcium deposits [72, 80], fibrous plaques [72, 80] and lipid-rich plaques [72, 80, 84]. In 2012 an International Working Group of experts published consensus criteria aiming at standardizing the interpretation and reporting of intravascular OCT imaging [85].

Owing to these unique properties, intravascular OCT is particularly suited to investigate arterial healing following implantation of different stent platforms as well as the mechanisms underlying the principal forms of stent failure.

2. THESIS AIMS

Despite constant improvement in the outcomes of patients undergoing implantation of new-generation DES, ST and ISR continue to occur at low but significant rates and a detailed understanding of the underlying conditions in the stented segment of patients presenting with such clinical entities remain important unmet clinical needs. Due its detailed visualization of the vessel wall microstructure, intravascular OCT is particularly suited to help shedding light on the mechanisms of stent failure. Additionally, its unprecedently high spatial resolution makes intravascular OCT particularly suitable to investigate and compare patterns of vessel healing following implantation of different stent platforms as well as following different PCI techniques in specific subsets of coronary artery disease. However, a thorough investigation of low-incidence phenomena, such as ST and ISR, is only possible if several institutions join forces to allow recruitment of sufficient patient numbers in order to draw meaningful conclusions.

The principal aims of the thesis were: i) to examine intravascular OCT findings from large, real-world patient collectives presenting with both ST and ISR, aiming at deciphering the principal underlying mechanisms; ii) to investigate the frequency, time-course, relation to underlying stent type and pathogenetic role of neoatherosclerosis as a possible common pathway contributing to both types of stent failure; iii) to evaluate use of intravascular OCT as a means of surveillance of vascular healing following recanalization of coronary chronic total occlusions and to compare different recanalization techniques; iv) to assess and compare intravascular OCT-defined vessel healing patterns following implantation of BP-DES versus new-generation DP-DES; v) to assess the influence of fully bioresorbable scaffolds as compared to conventional metallic DES and of systemic statin treatment as compared to placebo on the development of neoatherosclerosis in a hypercholesterolemic animal model.

3. METHODS AND MATERIALS

3.1 Core study protocol for the PREvention of late Stent Thrombosis by an Interdisciplinary Global European effort (PRESTIGE) registry

3.1.1 Study population and patient treatment

Consecutive patients presenting with definite ST, undergoing PCI at 29 participating centers with OCT imaging capability were prospectively enrolled in the multicenter PREvention of late Stent Thrombosis by an Interdisciplinary Global European effort (PRESTIGE) registry using a centralized telephone registration system (**Figure 6**).

Figure 6. *List of European centers participating in the PRESTIGE registry.*
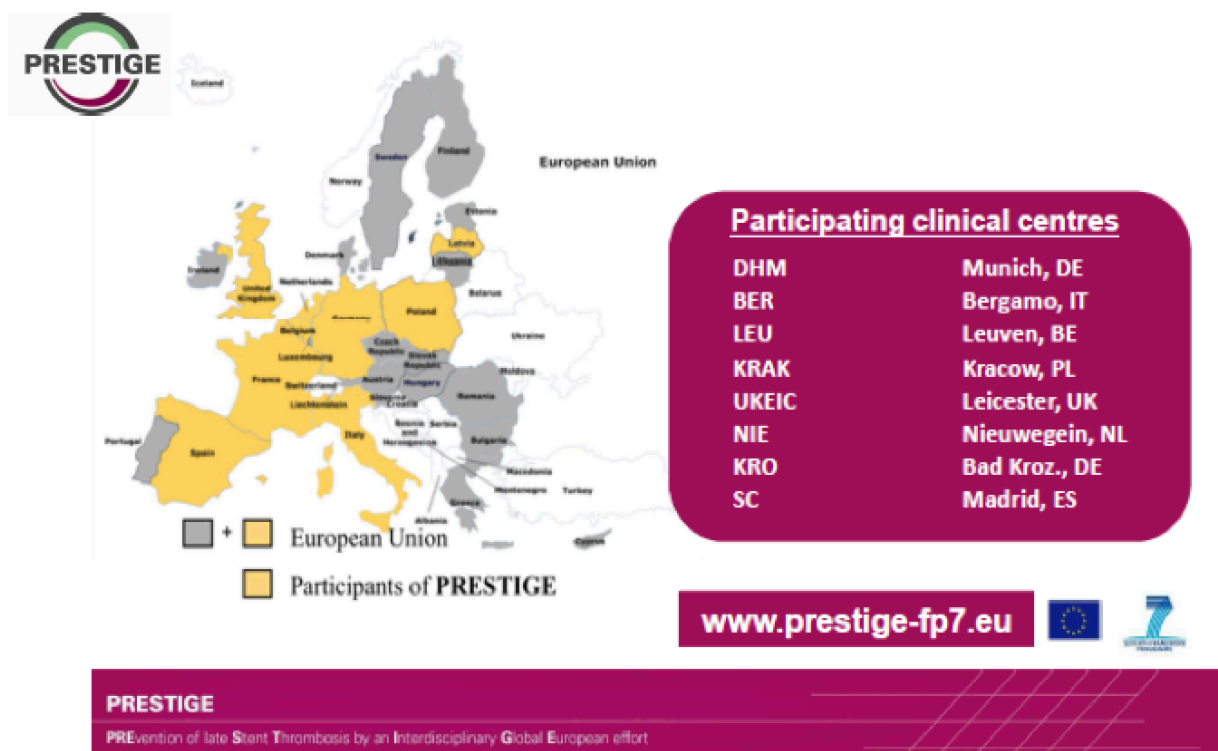
Definite ST was defined according to ARC criteria [36]. Clinical, procedural and imaging data were collected according to a standardized protocol and entered in a central electronic database. Type of underlying stent was classified as BMS, early-generation DES (durable polymer sirolimus-

eluting stents [Cypher, Cordis, Warren, New Jersey], durable polymer paclitaxel-eluting stents [Taxus, Boston Scientific, Natick, Massachusetts] or durable polymer zotarolimus-eluting stents [Endeavor, Medtronic Inc., Santa Rosa, California]), new-generation DES (all other metallic backbone DES), or bioresorbable DES [32]. The study complied with the Declaration of Helsinki. The ethical review committee at each participating institution approved the study and all patients provided written informed consent. The study was funded by the European Union under the Seventh Framework Program FP7/2007-2013, grant agreement n° HEALTH-F2-2010-260309 (PRESTIGE).

3.1.2 Study Procedures

Patients enrolled in the PRESTIGE registry underwent PCI according to local practices. After angiographic confirmation of ST, a guidewire was advanced distally in the culprit vessel across the site of occlusion. The use of intravascular OCT before and after PCI procedures was recommended in all patients. Use of thrombectomy with manual aspiration was encouraged to restore effective TIMI flow and to reduce residual thrombus before OCT image acquisition [85]. In selected cases small balloon dilation (≤ 2.0 mm in diameter) at low pressure was permitted if image quality remained insufficient after thrombectomy. However, OCT image acquisition was discouraged in patients presenting in a medical condition precluding safe OCT acquisition (e.g. unstable electrical or hemodynamic conditions or reported chronic renal insufficiency) [85].

An oral loading dose of platelet adenosine diphosphate (ADP)-receptor antagonist was administered to all patients prior to or at the time of the intervention. During the procedure, patients were treated with intravenous heparin or bivalirudin. Use of glycoprotein inhibitors was at the discretion of the treating physician.

3.1.3 OCT data acquisition

Following administration of intracoronary nitrates, OCT was performed with non-occlusive imaging technique using commercially-available OCT imaging systems (C7XR, Ilumien or Ilumien Optis, St. Jude Medical, St. Paul, MN, USA). In brief, after restoration of flow, a rapid exchange imaging catheter (Dragonfly™ or Dragonfly Duo™, St. Jude Medical, St. Paul, MN, USA) was advanced beyond the stented segment. An OCT pullback of the entire stented segment, including distal and proximal reference sites, was performed with contrast injection through the guiding catheter at 3-5 ml/sec. If the stented segment was too long to be imaged in a single pullback, an additional pullback was acquired using angiographic landmarks for appropriate imaging catheter position and view.

3.1.4 OCT quantitative analysis

Raw data of OCT image acquisitions were collected and sent to a centralized core laboratory (ISAResearch Center, Munich, Germany) for off-line analyses. Each OCT sequence was assessed and measured by independent readers experienced in OCT imaging analysis, blinded to patient characteristics and timing of ST. Initially, a quality screening of the entire sequence was performed to confirm sufficient quality of imaging to permit the analysis. Reasons for exclusion were insufficient image quality due to poor clearance of blood, missed region of interest with incomplete stent visualization, excessive remaining thrombus obscuring the stent assessment, or presence of imaging artifacts precluding the analysis. Non-analyzable frames were defined as frames with less than a total of 45° of visible lumen border (e.g. due to presence of thrombus or side branch). Stent struts located across the ostium of side branches were excluded from the analysis of coverage and apposition. Quantitative and morphometric analyses were performed every 1 mm along the entire

Xhepa, E. Use of OCT for the evaluation of vessel healing following stenting and mechanisms of stent failure

target segment. Dedicated software (St. Jude Medical, St. Paul, MN, USA) was used for quantification (**Figure 7**).

Figure 7. *Outline of work flow of core lab analysis. Adapted from* [86].
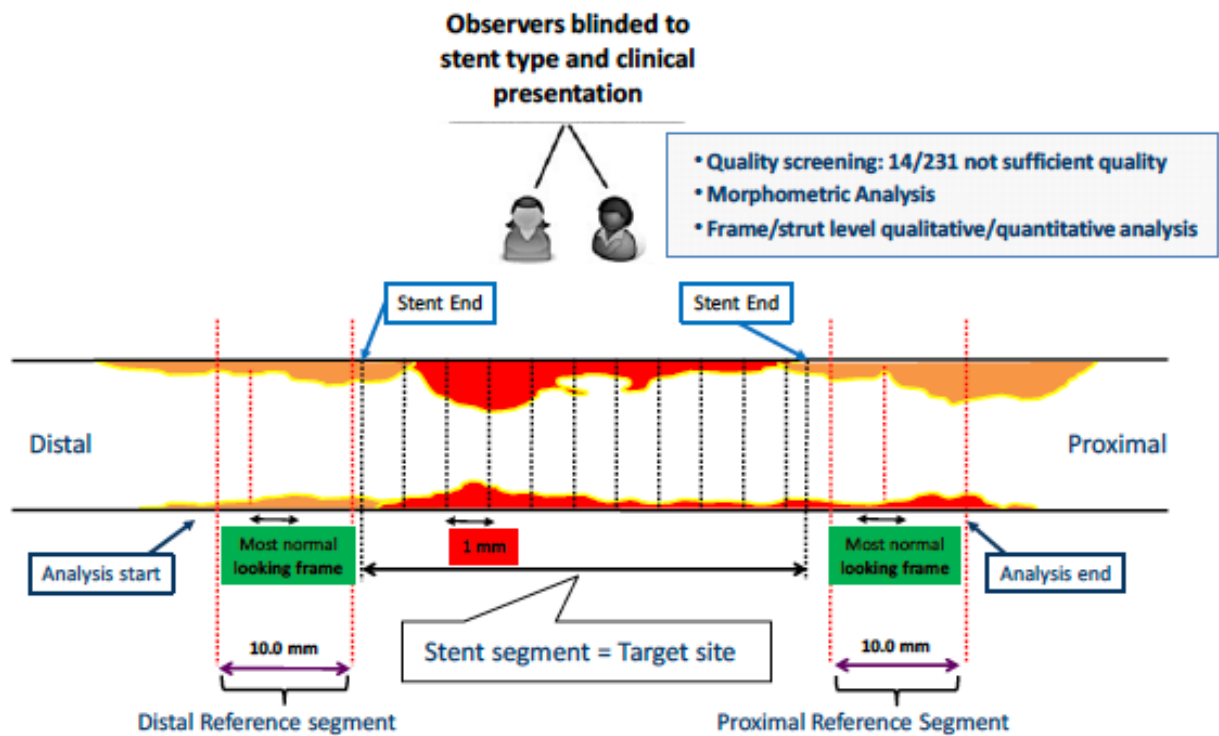
Metallic stent struts were identified as bright, signal-intense structures with blooming and dorsal shadowing; polymeric bioresorbable stent struts appear as a "black box" area surrounded by bright reflecting frames without abluminal shadowing [87]. The first and last analyzed frame at the stented segment was defined as the OCT frame allowing the drawing of a complete circumference using the strut contour, where struts were present in at least 3⁄4 of the perimeter. Distal and proximal reference measurements were performed in none or minimally diseased cross-sections within 10 mm from the stent edges. For morphometric analysis, standard definitions of cross-sectional area (CSA) and diameter were applied as previously reported [85]. Stent and lumen CSA were measured throughout the entire length of the stent. Lumen area was not assessed in presence of remaining thrombus obscuring the luminal border in at least one third of the luminal circumference.

Mean reference area was calculated as the sum of the distal and proximal non-stented reference lumen area divided by 2. In case the pullback did not include analyzable distal and proximal non-stented reference segments, the reference area was derived from the proximal and distal most stented segment. Stent expansion index was calculated as minimum stent area divided by mean reference area.

Presence of thrombus, stent strut coverage, stent strut apposition, inter-strut cavities, degree and type of neointimal tissue characteristics consistent with neoatherosclerosis were evaluated at frame level. Thrombus was defined as intraluminal protruding mass with irregular borders with or without adherence to stent struts or luminal tissue. The greatest longitudinal thrombus extent was calculated using the number of consecutive frames with any thrombus. Strut coverage was adjudicated on a frame-level basis. Struts were considered uncovered if any part of the strut was visibly exposed to the lumen. Conversely, struts covered by visible thrombus were classified as thrombus covered struts and counted separately in the analysis. The number of consecutive frames with uncovered struts was counted and the greatest longitudinal extent of uncovered struts was measured. Incomplete stent strut apposition was considered present when the axial distance between the strut's surface to the luminal surface was greater than the strut thickness (including polymer, if present) including a correction factor to account for strut blooming artifact. Readers blinded to stent type performed the assessment of malapposition. After finishing all measurements, stent type was unblinded and appropriate cut-off values were used to determine coverage and malapposition for each patient. Distance of malapposition was derived from the distance between the luminal surface of the strut and the lumen contour. Maximum malapposition distance and area of malapposition were recorded. The maximum length of malapposition was derived by the number of consecutive frames with malapposed struts. Inter-strut cavities (or coronary in-stent evaginations) were defined as the presence of an outward bulge in the luminal

vessel contour between apposed struts with a maximum depth of the bulge greater than 1/3 of the lumen diameter. Atherosclerotic changes of the neointima (neoatherosclerosis) were defined by the presence of one or more of the following: lipid laden tissue within the stent, defined as a signal-poor region with diffuse border and light signal attenuation, possibly masking deep strut detection; thin-cap fibroatheroma (TCFA), defined as plaque with lipid-laden tissue with a fibrous cap thickness ≤ 65 μm at the thinnest measured point, or neointimal calcification, characterized by a signal-poor region with sharp demarcation within the overlying neointima [50, 88]. In the core lab analysis, neoatherosclerosis was adjudicated when lipid-laden tissue or TCFA involved more than 50% of the analyzable arc at the involved cross-section.

3.1.5 Imaging adjudication committee OCT analysis

An imaging adjudication committee adjudicated the findings at the time of stent thrombosis based on systematic review of all acquired and analyzable OCT pullbacks according to a pre-specified protocol. OCT images were analyzed without knowledge of patient/stent characteristics or timing of stent thrombosis. Each OCT pullback was assessed in both longitudinal and cross-sectional views for the presence of a single dominant finding at stent thrombosis. If no single dominant finding was assessed, this was recorded. Additional findings assessed to be of lesser relevance were adjudicated as contributory. In case of disagreement, decision was made by consensus. The following categories were considered for visual adjudication: stent underexpansion (defined as stent area <80% of the mean of proximal and distal vessel reference area), edge dissection (proximal or distal to the stented segment, involving the intima and/or media with a circumferential extent at least of 1/3 of the vessel contour and a longitudinal extent greater than 3 mm), overlapping stents, stent fracture, uncovered stent struts, malapposed stent struts, presence of inter-stent cavities, in-stent restenosis and neoatherosclerosis in the presence of plaque rupture or in association with thin cap fibroatheroma

adjacent to the site of maximum thrombus burden). Restenosis was defined as the presence of >50% diameter stenosis in the stented segment. If none of these characteristics was present, the label 'no contributing factor identifiable' was recorded.

3.1.6 Statistical analysis

Continuous data are presented as mean (SD) or median [25th-75th percentiles]. Categorical data are presented as observed frequencies and proportions (%). Patients were analyzed according to time interval between index stenting and stent thrombosis presentation, classified as acute (<24 hours), subacute (24 hours-30 days), late (>30 days-1 year) and very late (>1 year) [36]. Differences between groups were assessed for statistical significance using a Wilcoxon rank-sum test or a Kruskal-Wallis test for continuous data and chi-squared test (or Fisher's exact test where the expected cell value was < 5) for categorical variables. The statistical analysis was performed using SAS/STAT software, Version 9.4 (TS2M3, SAS Institute, Cary, NC, USA). Repeatability data were analysed by calculating the within-patient standard deviation and repeatability coefficient [89], and the intra-class correlation coefficient, described by Shrout and Fleiss for the case when all patients are rated by the same raters who are assumed to be a random subset of all possible raters [90]. Generalized linear mixed regression models were applied to estimate mean differences among timing groups for frame level based parameters to account for clustering effects. Time was used as a fixed effect and a random intercept was applied per patient to estimate the predicted probability. All tests were 2-sided and assessed at a significance level of 5%. Due to the exploratory nature of the analysis, no adjustment was made for multiple testing.

3.2 Core study protocol for the in-stent restenosis registry

3.2.1 Study population and angiographic data analysis

Patients presenting with ischemic symptoms and/or evidence of myocardial ischemia in three European centers (Deutsches Herzzentrum, Munich, Germany; Hospital Universitario de La Princesa and Hospital Universitario Clínico San Carlos, Madrid, Spain) and undergoing intravascular OCT prior to PCI for ISR, were included in this study. Baseline and post-procedural angiograms were recorded and assessed off-line in a core laboratory (ISAResearch Center, Munich, Germany) with an automated edge-detection system (Medis Medical Imaging Systems, Leiden, The Netherlands). The angiographic pattern of ISR was classified according to the Mehran's classification [91].

3.2.2 OCT data acquisition and morphometric analysis

Raw data of OCT image acquisitions were sent to a centralized core laboratory (ISAResearch Center, Munich, Germany). Acquisition and morphometric analysis of intravascular OCT imaging has been previously described in the Sections 3.1.3 and 3.1.4 of the "Core study protocol for the PRESTIGE Registry".

3.2.3 Qualitative neointimal characterization and gray-scale signal intensity analysis

Characterization of neointimal tissue was performed at the frame displaying the maximal percentage area stenosis (%AS), as well as the 5 preceding and following analyzed frames; in other words, a 10 mm segment was analyzed, given a %AS of at least 50% was present in each frame. Each frame was subdivided in 4 quadrants (90°) and the neointimal characteristics separately characterized for each of them. Based on its optical characteristics, neointimal tissue was categorized as homogeneous, heterogeneous or layered. Atherosclerotic changes of the neointima were defined by the presence of one or more of the following: macrophage infiltration and/or lipid-laden tissue within the stent and neointimal calcification [50] (**Figure 8**).

Figure 8. *Representative images of optical coherence tomography findings in patients presenting with in-stent restenosis. Adapted from [92]*
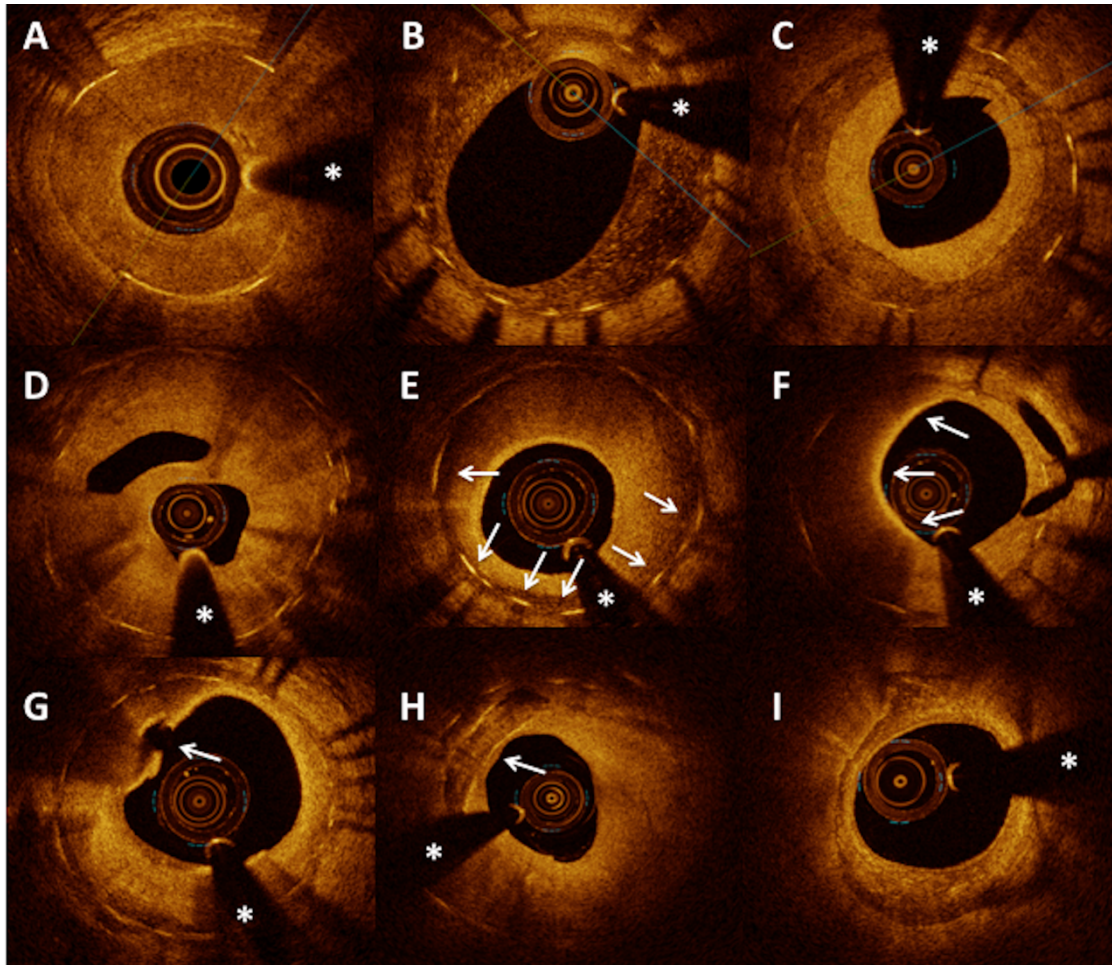
A. In-stent restenosis with homogeneous neointimal pattern; B: In-stent restenosis with heterogeneous neointimal pattern; C: In-stent restenosis with a layered neointimal pattern; D: Severe in-stent restenosis with a bridging architecture of the neointima; E: Peri-strut low-intensity areas (arrows); F: Macrophage infiltration involving a 180° neointimal arc (arrows from 6 to 12 o'clock); G: Neoatherosclerosis and ruptured thin-cap fibroatheroma (arrow); H: Neointimal calcification (arrow); I: Severe concentric in-stent calcification and neoatherosclerosis obscuring underlying stent struts; * = guidewire artifact

Quantitative analysis of the neointimal tissue by means of gray-scale signal intensity (GSI) analysis was performed on a per quadrant basis. GSI analysis has been previously shown to accurately differentiate between mature and immature neointimal tissue following coronary

stenting [93, 94]. Analyses were performed using Image J software (free-ware available at https://imagej.nih.gov/ij/index.html).

Figure 9. *Gray-scale signal intensity analysis. Adapted from [92]*
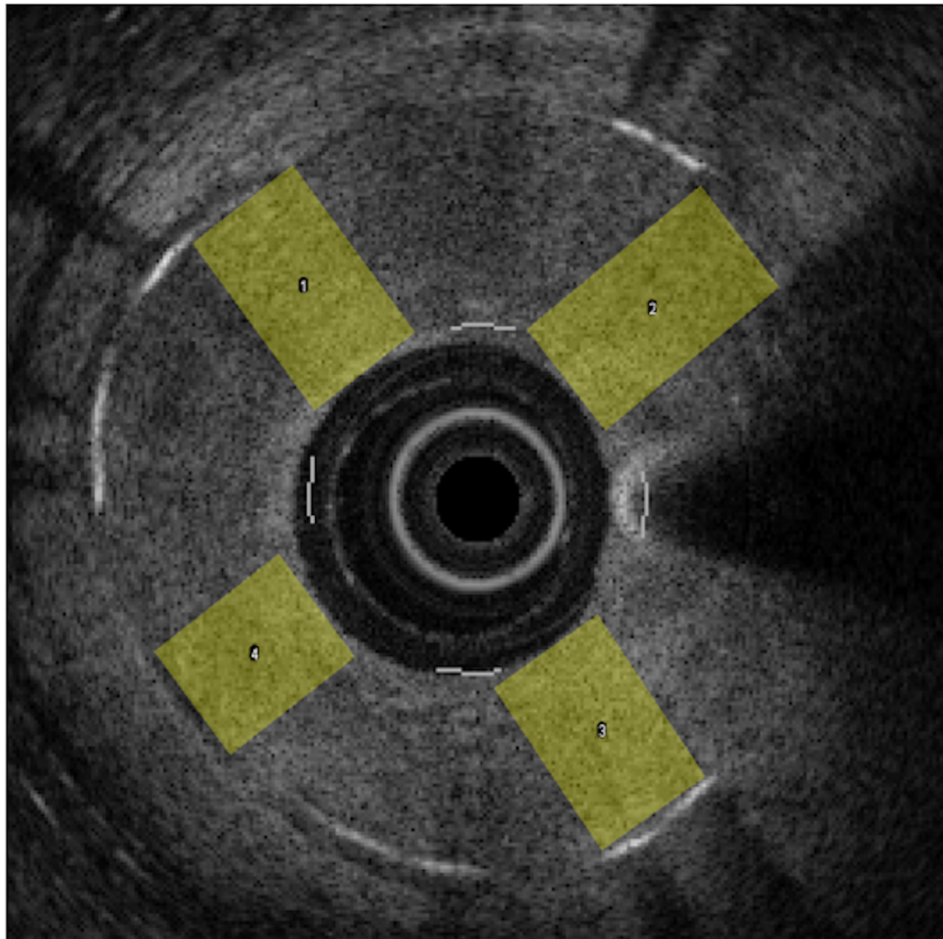
OCT cross-section converted to a gray-scale image with superimposed regions of interest in 4 different quadrants.

3.2.4 Statistical analysis

Continuous data are presented as mean±SD or median (25th-75th percentiles) depending on the distribution pattern of the variable. Categorical data are presented as frequencies or proportions (%). Differences between groups were assessed using the student's *t* test, Wilcoxon rank sum test, Kruskal-Wallis or one-way analysis of variance for continuous variables and the chi-square test (or Fischer's exact test where the expected cell value was <5) for categorical variables. Pairwise multiple

comparisons were performed by means of the Tukey's test. To account for the clustered nature of the data, a generalized linear mixed model was conducted for the analysis of OCT data. The model contained a fixed-effects term (either neointimal type or stent type) and a random-effects term (patient for frame-level analysis and patient and frame for strut-level analysis). Predictors of neointimal pattern as well as of NA were assessed by means of multivariable analysis. The selection of variables for the multivariable model was performed using the LASSO regression method [95] after entering all relevant clinical, angiographic and OCT parameters as candidates. The degree of agreement between reviewers was quantified using Cohen's κ test for concordance. All tests were 2-sided and assessed at a significance level of 5%. The statistical analysis was performed by means of R software (version 3.5.1, *R Foundation for Statistical Computing*, Vienna, Austria) and SPSS Version 23 (IBM Corp, Armonk, New York).

3.3 Core study protocol for the ISAR-OCT-CTO registry

3.3.1 Study population and definitions

Patients undergoing angiographic and intravascular OCT follow-up 6-9 months after successful CTO recanalization were included in the ISAR-OCT-CTO registry. An informed consent was obtained prior to each scheduled procedure. Clinical, procedural and imaging data were collected according to a standardized protocol and entered in a central electronic database.

Lesion complexity was assessed by means of the J-CTO score [96]. The technique used to achieve vessel recanalization was categorized as antegrade wire escalation (AWE), retrograde wire escalation (RWE), antegrade dissection and reentry (ADR) or reverse controlled antegrade and retrograde tracking (reverse CART). Use of dedicated instruments (CrossBoss catheter/Stingray™ LP system; Boston Scientific, Natick; Massachusetts), rotablation, anchoring balloon and type of interventional collaterals (septal, epicardial or saphenous vein graft) were also recorded. Dual antiplatelet therapy was prescribed for at least 12 months following successful CTO recanalization.

3.3.2 Study endpoints

The study endpoints were percentage diameter stenosis (%DS) and late luminal loss (LLL) (angiographic endpoints) as well as rates of uncovered and malapposed struts (OCT endpoints) in each recanalization strategy group; secondary OCT endpoints were mean neointimal thickness, % of lesions with >10% uncovered or malapposed struts and malapposition distance and length.

3.3.3 Angiographic and OCT data acquisition and analysis

Baseline, post-procedural and follow-up angiograms were recorded and assessed off-line in a core laboratory (ISAResearch Center, Munich, Germany) with an automated edge-detection system (Medis Medical Imaging Systems, Leiden, The Netherlands).

Acquisition and morphometric analysis of intravascular OCT imaging has been previously described in the Sections 3.1.3 and 3.1.4 of the "Core study protocol for the PRESTIGE Registry". All measurements were performed in a centralized core laboratory (ISAResearch Center, Munich, Germany).

3.3.4 Statistical analysis

Continuous data are presented as median (25th-75th percentiles) and categorical data as observed frequencies or proportions (%). Differences between groups were assessed using the Wilcoxon rank sum test for continuous variables and the chi-square test (or Fischer's exact test where the expected cell value was <5) for categorical variables.

To account for the clustered nature of the data, a generalized linear mixed model was conducted for the analysis of OCT data. The model contained a fixed-effects term (recanalization technique) and a random-effects term (patient for frame-level analysis and patient and frame for

strut-level analysis). Correlates of presence of uncovered or malapposed struts were assessed by means of multivariable analysis. The selection of variables for the multivariable model was performed using the LASSO (Least Absolute Shrinkage and Selection Operator) regression method [95] after entering all clinical, angiographic and procedural parameters as candidates. All tests were 2-sided and assessed at a significance level of 5%. The statistical analysis was performed by means of the R software (version 3.5.1, *R Foundation for Statistical Computing*, Vienna, Austria).

3.4 Core study protocol for a randomized comparison of vascular response to biodegradable-polymer sirolimus-eluting and durable-polymer everolimus-eluting stents

3.4.1 Test devices

We compared a sirolimus-eluting stent with biodegradable polymer coating (BP-SES) (Orsiro, Biotronik AG, Buelach, Switzerland) that consists of a thin-strut 60-80 μm cobalt chromium stent (60 μm for diameters from 2.25 to 3.0 mm and 80 μm for diameters from 3.5 to 4.0 mm) with a biodegradable Poly-L-lactic acid (PLLA) coating eluting sirolimus at a drug dose of 140 μg/mm2 within 12-14 weeks to a thin-strut 81 μm cobalt-chromium stent with a permanent polymer coating containing everolimus at a dose density of 100 μg/mm2 (DP-EES) (Xience PRIME, Abbott Vascular, Santa Clara, CA, USA) designed to release 80 % of the everolimus within the first 30 days after stent deployment.

3.4.2 Study population and protocol

A total of 39 patients were randomly assigned to BP-SES (n = 19) and DP-EES (n = 20) in a single centre, randomized (1:1), open-label, two-arm clinical trial comparing BP-SES with DP-EES. Written informed consent to participation was obtained from all patients. This study was approved by the local ethics committee and registered at clinicaltrials.gov (study identifier: NCT01594736). Patients

with stable and unstable angina pectoris were eligible for inclusion in this trial. Patients with acute myocardial infarction were excluded.

All index interventions were performed using standard techniques. Pre-dilatation, post-dilatation, and usage of intravascular ultrasound or OCT were left to the operator's discretion. Prior to the index procedure, all patients received aspirin at a dose of 100mg and a 600mg loading dose of clopidogrel. After the procedure, all patients were advised to continue on aspirin (100 mg daily) and statins unless there were contraindications. Clopidogrel (75 mg daily) was prescribed for at least 1 year after stent implantation. Data were collected and entered into a computer database by specialized personnel of the Clinical Data Management Centre (ISAR Centre, Munich, Germany). All events were adjudicated and classified by an experienced event adjudication committee blinded to the treatment groups.

3.4.3 Study endpoints

The primary endpoint was neointimal tissue coverage at 6-months follow-up, which was assessed as mean neointimal thickness (NIT) and percentage of uncovered struts. Secondary endpoints included apposition of stent struts and tissue characterization of the nascent neointimal tissue above stent struts.

3.4.4 OCT image acquisition and analysis

Acquisition and morphometric analysis of intravascular OCT imaging has been previously described in the Sections 3.1.3 and 3.1.4 of the "Core study protocol for the PRESTIGE Registry".

Neointimal tissue characterization was performed as previously described [93]. Exclusion criteria for GSI analysis were: presence of stent struts penetrating into a necrotic core, stent struts overlying areas of severe calcification, bifurcation stenting and malapposition as all these variables

may influence signal intensity of grey scales. Mean grey scale intensity was measured within neointimal tissue above stent struts using an Image J software algorithm (National Institutes of Health, Bethesda, MD, USA). A cut-off of 109.7 after normalization to the guide wire level was used to adjudicate mature neointimal tissue as preciously described [93].

3.4.5 Statistical analysis

Data are presented as mean value ± standard deviation or median with interquartile range (IQR) depending on the distribution. The distribution was tested using the Kolmogorov-Smirnov test. Categorical variables were compared using Pearson's chi-squared test with Yates' continuity correction and Fisher's exact test. Continuous variables were compared using the Welch's t-test if normally distributed or the Kruskal-Wallis rank sum test if not normally distributed. The analysis of primary and secondary endpoints was planned on an intention-to-treat basis. To account for the clustered nature of the data, generalized estimated equations were conducted for strut-level and frame-level OCT analysis to compare BP-SES and PP-EES. All statistical analyses were two-tailed and p-values ≤0.05 were considered statistically significant. Analyses were performed with R 2.15.1 (The R foundation for Statistical Computing, Vienna, Austria) and JMP 9.0.2 (SAS Institute Inc., Cary, NC, USA) statistical software.

3.5 Analysis protocol for meta-analysis of intravascular OCT imaging trials evaluating vascular response to biodegradable-polymer versus new-generation durable-polymer DES

3.5.1 Included studies

We searched Medline, Embase, the Cochrane Central register of Controlled Trials (CENTRAL), scientific sessions abstract and relevant websites for investigations of PCI-patients assigned to BP-DES or new-generation DP-DES and OCT imaging at follow-up. For this report, stent platforms other

than early-generation sirolimus-eluting stents (SES/Cypher, Cordis, Warren, NJ, US), paclitaxel-eluting stents (Taxus, Boston Scientific, Natick, MA, US) and fast-release zotarolimus-eluting stents (ZES/Endeavor, Medtronic, Santa Rosa, CA, US) were considered new-generation DP-DES. No restrictions concerning language or publication status were imposed. Inclusion criteria were: i) OCT imaging performed between >1 and 12 months after BP-DES or new-generation DP-DES implantation; and ii) description of OCT imaging protocols. Comparisons other than BP-DES versus new-generation DP-DES were excluded.

Two investigators independently assessed publications for eligibility at title and/or abstract level. Studies that met inclusion criteria were selected for further analysis. Risk of bias was independently evaluated for each study by the same investigators in accordance with The Cochrane Collaboration method [97].

3.5.2 Endpoints and definitions

The primary outcome of the analysis was neointimal hyperplasia (NIH) thickness and the co-primary outcome was the incidence of lesions with uncovered struts. The main secondary outcome was the incidence of lesions with malapposed struts. Other secondary outcomes of interest were NIH area, NIH volume and target lesion/vessel revascularization (TLR/TVR). All endpoints were evaluated in accordance with intention-to-treat principle and definitions reported in the original protocols.

3.5.3 Meta-analytic methods

Odds ratio and the weighted mean difference with 95% confidence intervals were used to compare the outcomes of interest between BP-DES and new-generation DP-DES and pooled using the Mantel-Haenszel random-effect model (DerSimonian and Laird). Heterogeneity between trials was quantified using the I^2 statistic accompanied by a χ^2 test; I^2 values around 25%, 50% and 75% were

suggested to indicate low, moderate, or high heterogeneity, respectively [98]. In addition, we estimated the between-study variance (τ^2). The possibility of small study effects resulting from publication bias or other biases was examined for main primary outcome by means of visual inspection of funnel plots of the ORs of individual trials against their standard errors, accompanied by a statistical test of asymmetry [99]. An influence analysis, in which meta-analysis estimates are computed omitting one study at a time, was performed for the risk estimation of the main primary outcome. Using a χ^2 test for subgroup by treatment interaction, we determined whether certain covariates were associated with risk estimation for the main primary outcome. The covariates investigated were: the time-point of OCT imaging ($\leq$6 months vs. $\geq$6 months after index PCI), the strut thickness ($\leq$100 μm vs. $\geq$100 μm) or the antiproliferative drug (sirolimus vs. biolimus) of BP-DES platforms, the minimum number of participants in each included trial ($\leq$40 patients vs. $\geq$40 patients), and the inclusion of patients with diabetes (yes vs. no) or acute MI (yes vs. no). The study was reported in compliance with the preferred reporting items for systematic reviews and meta-analyses (PRISMA) statement [100]. All analyses were performed in RevMan (Review Manager, Version 5.3, The Cochrane Collaboration, Copenhagen, Denmark) and R (version 3.3.2; R foundation for Statistical Computing, Vienna, Austria).

3.6 Study protocol for assessing the influence of fully bioresorbable scaffolds as compared to conventional metallic DES and statin treatment as compared to placebo on the development of neoatherosclerosis in a hypercholesterolemic animal model
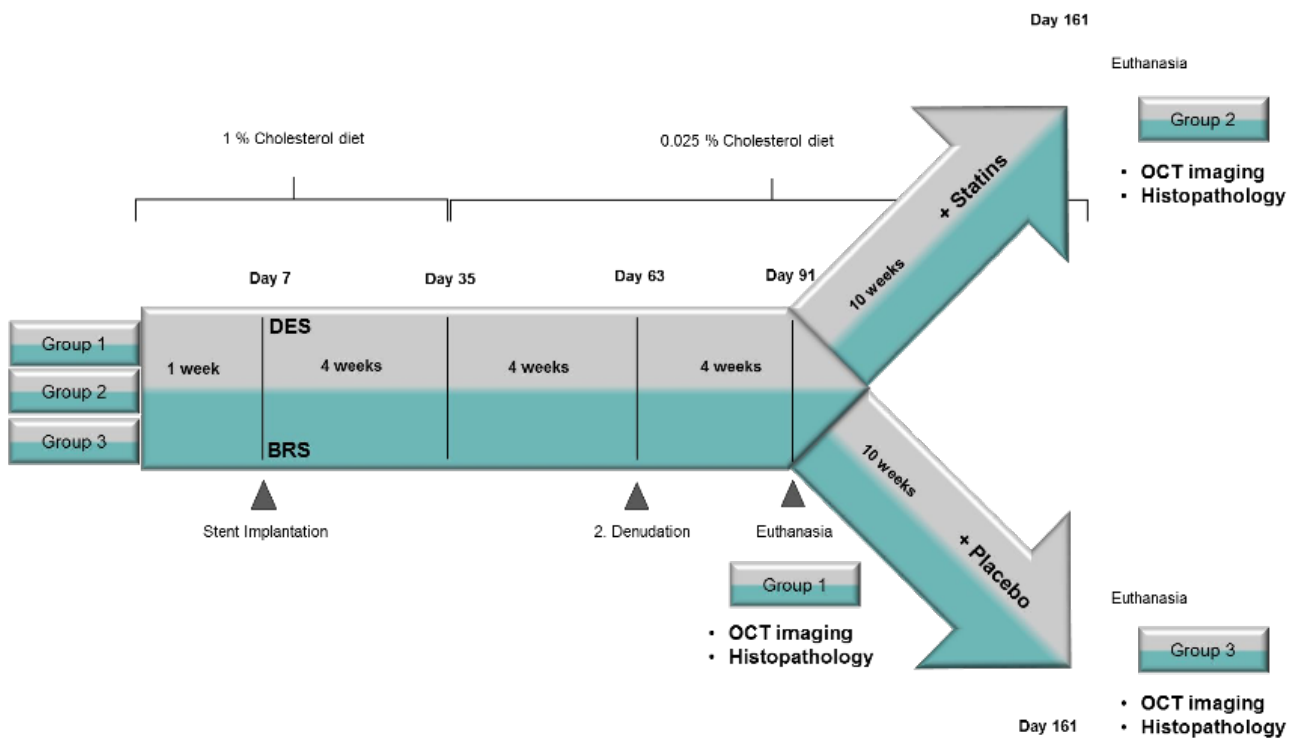
3.6.1 Study design

In a total of 33 rabbits a bioresorbable scaffold (BVS; n=33) and a permanent metallic DES (n=33) of equivalent geometry and design were randomly allocated to implantation into the right and left iliac artery. 22 rabbits were randomized to statin treatment (n=11, group 2) or placebo (n=11, group 3),

while another 11 rabbits were terminated after 91 days (n=11, group 1) for evaluation of neoatherosclerosis formation prior to receiving systemic therapy.

All animals were fed a cholesterol diet. After 7 days, denudation of the iliac arteries was performed using a Fogarty catheter as previously described [101] followed by implantation of BVS and DES, respectively. On day 63, repeat balloon injury of the stented segment was performed to accelerate neoatherosclerosis formation. Animals of group 1 were terminated after 91 days while animals of group 2 and 3 (n=11 each) were started on statin therapy (atorvastatin 3mg/kg/d) or placebo and terminated after 161 days (**Figure 10**).

Figure 10. *Study flow chart.*

3.6.2 Study devices

In this study, a fully bioresorbable magnesium scaffold (Magmaris®, Biotronik AG, Bülach, Switzerland) was compared with a custom-designed 316L stainless steel DES (Biotronik AG, Bülach,

Switzerland) of equivalent geometry and design. Both BVS and DES were of the same size (3.0 x 15mm), had a 6 crown 2 link design with a strut-thickness of 150 μm and used PLLA-coating to elute sirolimus at a concentration of 140 μg/cm^2.

3.6.3 Animal model of neoatherosclerosis

The rabbit model was approved by the government ("Regierung von Oberbayern", file number 55.2.1.54-2532-40-16) and was in accordance with the German Animal Welfare Act (version May 18, 2006, amended in March 29, 2017) as well as directive 2010/63/EU of the European Parliament on the protection of animals used for scientific purposes.

33 New Zealand White rabbits (3.0 to 4.0 kg, 3 to 4 months of age, Charles River, France) were used for this preclinical animal model of in-stent neoatherosclerosis which has been previously been established at our institution. Animals were fed a 1% cholesterol diet (Altromin Spezialfutter GmbH, Lage, Germany) for 7 days prior to balloon denudation of the iliac arteries, followed by stent implantation. After another 4 weeks of high cholesterol diet (1%), animals were switched to a 0.025% cholesterol diet (Altromin Spezialfutter GmbH, Lage, Germany) at day 35 and continued on this diet until euthanasia. Blood samples were drawn on day 0, 7, 35, 63, 91, 126 and 161 for measurement of serum cholesterol and liver enzymes. Routine health checks including documentation of animal weight were performed three times a week.

3.6.4 Stent implantation, drug treatment and tissue harvest

On day 7, balloon denudation of the iliac arteries was performed using a 3F Fogarty catheter before stents (3.0 x 15mm, Biotronik AG, Bülach Switzerland) were implanted under fluoroscopic guidance at nominal pressure of 10ATM (Magmaris®-BRS, Biotronik AG, Bülach, Switzerland) or 12ATM (316L SS-DES, Biotronik AG, Bülach Switzerland). Following implantation, vessel patency was documented

by angiography. Animals received acetylsalicylic acid daily (40mg/d) until the end of the experiment. Additionally, heparin (150IU/kg) was administered during the procedure. On day 63, repeat denudation was performed to accelerate neoatherosclerosis formation. Animals received buprenorphine for a minimum of 24 hours after the interventions for post-procedural analgesia. On day 91, a subset of animals (n=11) was terminated to determine the magnitude of neoatherosclerosis formation prior to randomization to statin treatment or placebo. The remaining animals (n=22) were randomized to statin (Atorvastatin Hennig® 10mg) treatment (n=11) at an established dose of 3 mg/kg/d [102] per os or placebo (tap water per os) (n=11) and housed until day 161 to investigate changes in neoatherosclerosis progression over time. Euthanasia was induced by an overdose of pentobarbital, while rabbits were in deep anesthesia. OCT imaging was performed immediately after euthanasia. Afterwards, iliac arteries were perfusion-fixed before they were processed for histopathological and immunohistochemical staining.

3.6.5 Histopathological and immunohistochemical processing

Stented arteries were embedded in MMA (methyl methacrylate). A total of 5 in-stent sections (10 μm thickness) were cut from each artery using a laser microtome (TissueSurgeon, LLS Rowiak LaserLabSolutions GmbH, Hannover, Germany) and subsequently stained with HE (hematoxylin-eosin) and VVG (Verhoeff-van Giesson). For immunohistochemistry, sections were stained using rabbit-specific antibodies against RAM-11 (DAKO, Glostrup, Denmark, dilution 1:100). Dako EnVision™ Mouse Secondary Antibody kit was used. Staining was performed using a fully-automated stainer (Leica Bond RX™, Leica Biosystems Nussloch GmbH, Nussloch, Germany).

3.6.6 Neoatherosclerosis score in histology

Infiltration of foamy macrophages was assessed in histological sections after HE staining using a quadrant-based scoring-system comprising the depth of foam cell infiltration into the neointimal tissue along the vascular circumference: score 1: no foamy macrophage infiltration; score 2: foamy macrophage infiltration in superficial tissue layers; score 3: foamy macrophage infiltration in deeper tissue layers; score 4: foamy macrophages in both superficial and deeper tissue layers. Mean values per cross-section were derived from individual data points at each quadrant. Final average score per vessel was derived from all 5 in-stent sections.

3.6.7 OCT neoatherosclerosis score

For neoatherosclerosis scoring OCT frames were evaluated for the presence of infiltrating macrophages with significant light attenuation [88] as well as hypo-intense areas with adjoining light attenuation. In every frame the extent of infiltrating macrophages into the neointimal tissue was scored semi-quantitatively relative to the circumference of the vessel using an ordinal score: score 1: no macrophage infiltration; score 2: macrophage infiltration in <25% of the circumference; score 3: macrophage infiltration in 25-50% of the circumference; score 4: macrophage infiltration in 50-75% of the circumference; score 5: macrophage infiltration in > 75% of the circumference. Final average score per vessel was derived from all in-stent OCT frames.

3.6.8 Statistical analysis

Continuous data are reported as mean with standard deviation in case of normal distribution and as median with interquartile range in case of non-parametric distribution. Distribution of data was confirmed by Wilk-Shapiro goodness of fit-test. Wilcoxon Kruskal-Wallis rank sums test was used to calculate the significance of differences between medians of non-parametric data, while ANOVA

was used for group comparison of parametric data. A p-value of $p < 0.05$ was considered statistically significant.

To account for the clustered nature of data and the inter-correlation of treatment assignments (BRS and DES assigned to statin and placebo) generalized estimating equations (GEE) modeling was used. For parametric data a linear model and for non-parametric data a gamma regression model with log link function was applied. Results are presented as estimated means with lower and upper 95% confidence interval (CI). To assess effects among local (BRS/DES) and systemic (statin/placebo) treatment, a p of interaction was calculated. A p-value of $p<0.05$ was considered statistically significant. All analyses were carried out using JMP (software version 12.0, Cary, NC, USA) and SPSS (IBM SPSS Statistics version 22.0, IBM Corp., New York, USA).

4. RESULTS

4.1 Optical coherence tomography findings in patients presenting with stent thrombosis

- *Detailed analysis of OCT images acquired in the setting of ST was feasible in the selected patients included in the PRESTIGE registry*

A total of 675 patients with ST were enrolled in the PRESTIGE registry at participating centers. Of these patients, 231 underwent OCT imaging at the time of presentation. Fourteen patients had image quality precluding further analysis. The remaining 217 patients comprised the primary study cohort for the current analysis (**Figure 11**).

Figure 11. *Study flow chart.*
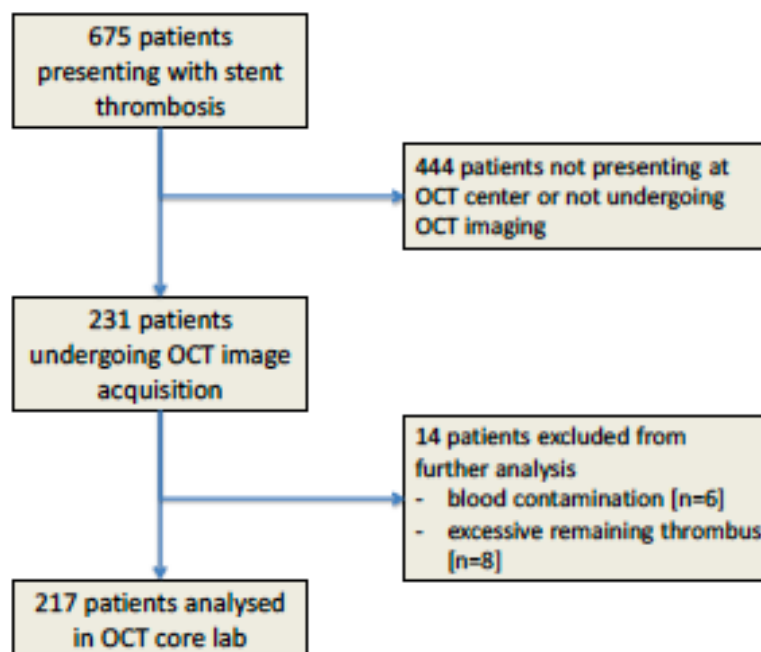
Overall 62 (28.6%) patients presented with acute/subacute and 155 (71.4%) with late/very late stent thrombosis. Median time from index stenting to presentation with stent thrombosis was 4 (2; 8) days and 1804 (692; 2953) days respectively. Regarding clinical presentation, 158 patients

(73.8%) presented with ST-elevation myocardial infarction (STEMI), 46 (21.5%) with non-STEMI (NSTEMI) and 10 (4.7%) with unstable angina. The left anterior descending (LAD) artery was the most commonly involved culprit vessel. A total of 333 stents were implanted in target vessels presenting stent thrombosis: 110 (33.0%) BMS, 45 (13.9%) first generation DES, 163 (50.3%) newer generation DES, 3 DES of unknown type, and 6 (1.8%) bioresorbable stents; in 6 patients (1.8%) the stent type could not be determined.

- ***The rate of stent underexpansion was high across all groups and highest in patients with subacute ST***

OCT morphometric analysis showed a stent expansion index <0.8 in 44.4% of all patients. In the subgroup of patients with subacute stent thrombosis, mean expansion index was 0.7±0.2 and a stent expansion index <0.8 was observed in 65.8% of these patients.

- ***Both uncovered and malapposed struts were frequently found in patients with ST; both decreased over time, although more than half of lesions with very late ST had frames with uncovered struts and more than a third had malapposed struts***

OCT analysis of stent-vessel interaction (**Table 1**) included a total of 5704 frames with a mean number of 26.5±13.2 frames per patient. 96.7% of target regions showed at least one frame with any remaining thrombus.

The number of lesions with any frame showing uncovered struts significantly decreased according to the time of presentation: 100%, 89.1%, 76.2%, 54.1% for acute, subacute, late and very late stent thrombosis (p<0.001). In patients presenting with acute or subacute stent thrombosis a median of 100% of frames were uncovered or covered with thrombus, as compared with 50.0% and 11.4% in patients with late or very late stent thrombosis (p<0.001).

Table 1: *OCT analysis of stent-vessel interaction in patients presenting with stent thrombosis classified according to time*

	Overall (N=215)	Acute stent thrombosis (N=15)	Subacute stent thrombosis (N=47)	Late stent thrombosis (N=21)	Very late stent thrombosis (N=134)	p-value
Lesion-level analysis						
Number of frames analyzed per lesion	26.5±13.2	24.9±12.9	29.0±13.3	29.8±13.0	25.4±13.2	0.16
Any frames with thrombus	208/215 (96.7%)	15/15 (100%)	46/46 (100%)	21/21 (100%)	126/133 (94.7%)	0.40
Any frames with malapposed struts	111/215 (51.6%)	13/15 (86.7%)	35/46 (76.1%)	13/21 (61.9%)	50/133 (37.6%)	<0.001
Any frames with uncovered struts	144/215 (67.0%)	15/15 (100%)	41/46 (89.1%)	16/21 (76.2%)	72/133 (54.1%)	<0.001
Any frames with interstrut cavities	45/215 (20.9%)	0/15 (0%)	3/46 (6.5%)	7/21 (33.3%)	35/133 (26.3%)	0.001
Any frames with neoatherosclerosis	58/215 (27.0%)	0/15 (0%)	0/46 (0%)	0/21 (0%)	58/133 (43.6%)	<0.001
Frame-level analysis						
Coverage						
Frames with uncovered struts, n	6.6±8.5	15.7±7.1	13.3±9.5	9.8±11.3	2.8±4.5	<0.001
Percentage of frames with uncovered struts (%)	14.3 (0; 52.4)	65 (52.9; 92.0)	55.8 (31.8; 80.6)	21.7 (5.6; 56.8)	4.2 (0; 16.1)	<0.001

Maximum length of consecutive uncovered struts (mm)	5.3±7.2	14.3±6.3	11.9±8.9	5.7±5.9	2.0±3.4	<0.001
Frames with struts covered by thrombus, n	3.3±4.7	5.3±4.8	7.2±6.3	2.4±3.3	1.9±3.2	<0.001
Frames with struts covered by thrombus, %	6.5 (0; 25.0)	18.8 (8.0; 41.7)	28.0 (12.2; 50.0)	0 (0; 23.5)	0 (0; 12.5)	<0.001
Maximum length of frames containing thrombus (mm)	12.1±10.4	16.7±7.7	19.7±13.4	9.6±6.6	9.3±8.4	<0.001
Frames with uncovered struts or struts covered by thrombus, n	9.9±11.0	21.0±6.8	20.5±11.1	12.2±12.1	4.7±6.7	<0.001
Frames with uncovered struts or struts covered by thrombus, %	33.3 (2.6; 87.5)	100 (95.8; 100)	100 (86.4; 100)	50.0 (21.7; 70.5)	11.4 (0; 35.3)	<0.001
Apposition						
Frames with malapposed struts, n	2.6±4.3	6.0±6.2	3.3±4.5	4.6±6.1	1.7±3.2	<0.001
Frames with malapposed struts, %	2.4 (0; 20.0)	25.0 (7.7; 45.5)	10.6 (1.8; 26.7)	4.3 (0; 27.3)	0.0 (0; 9.3)	<0.001
Maximum length of consecutive malapposed struts (mm)	1.8±2.9	4.1±5.5	2.1±2.4	2.8±3.8	1.2±2.3	<0.001
Malapposition area (mm^2)	0.2±0.6	0.5±0.9	0.2±0.4	0.5±1.3	0.2±0.4	0.02
maximum malapposition area (mm^2)	1.1±2.3	1.9±3.3	0.7±1.0	1.8±3.0	1.0±2.3	0.049
Maximum malapposition distance (mm)	0.1±0.2	0.1±0.2	0.1±0.1	0.1±0.2	0.1±0.2	0.008
Neoatherosclerosis						
Frames with neoatherosclerosis, n	2.3±4.9	0.0±0.0	0.0±0.0	0.0±0.0	3.8±5.8	<0.001

Frames with neoatherosclerosis, %	0 (0; 8.10)	0 (0; 0)	0 (0; 0)	0 (0; 0)	0 (0, 30.5)	<0.001
Inter-strut cavities					
Frames with interstrut cavities, n	0.8±2.6	0.0±0.0	0.1±0.6	2.1±4.4	1.0±2.6	0.002
Frames with interstrut cavities, %	0 (0; 0)	0.0 (0; 0)	0.0 (0; 0)	0.0 (0; 6.1)	0.0 (0; 2.9)	0.002
Maximum interstrut cavities depth (mm)	0.1±0.2	0.1 ± 0.2	0.0±0.1	0.2±0.3	0.1±0.3	0.01

Data is shown as mean ± standard deviation or median (inter quartile range)

The maximum longitudinal extent of thrombus and uncovered struts was greatest in patients with acute and subacute stent thrombosis and decreased over time. The number of lesions with any frame showing malapposed struts significantly decreased according to the time of presentation: 86.7%, 76.1%, 61.9%, 37.6% for acute, subacute, late and very late stent thrombosis (p<0.001) (**Figure 12**). A median of 25% of frames showed malapposition in patients with acute stent thrombosis compared with 10.6, 4.3 and 0.0 in patients with subacute, late and very late stent thrombosis respectively (p<0.001).

Figure 12. *OCT findings in patients presenting with ST classified according to time. Adapted from* [86]
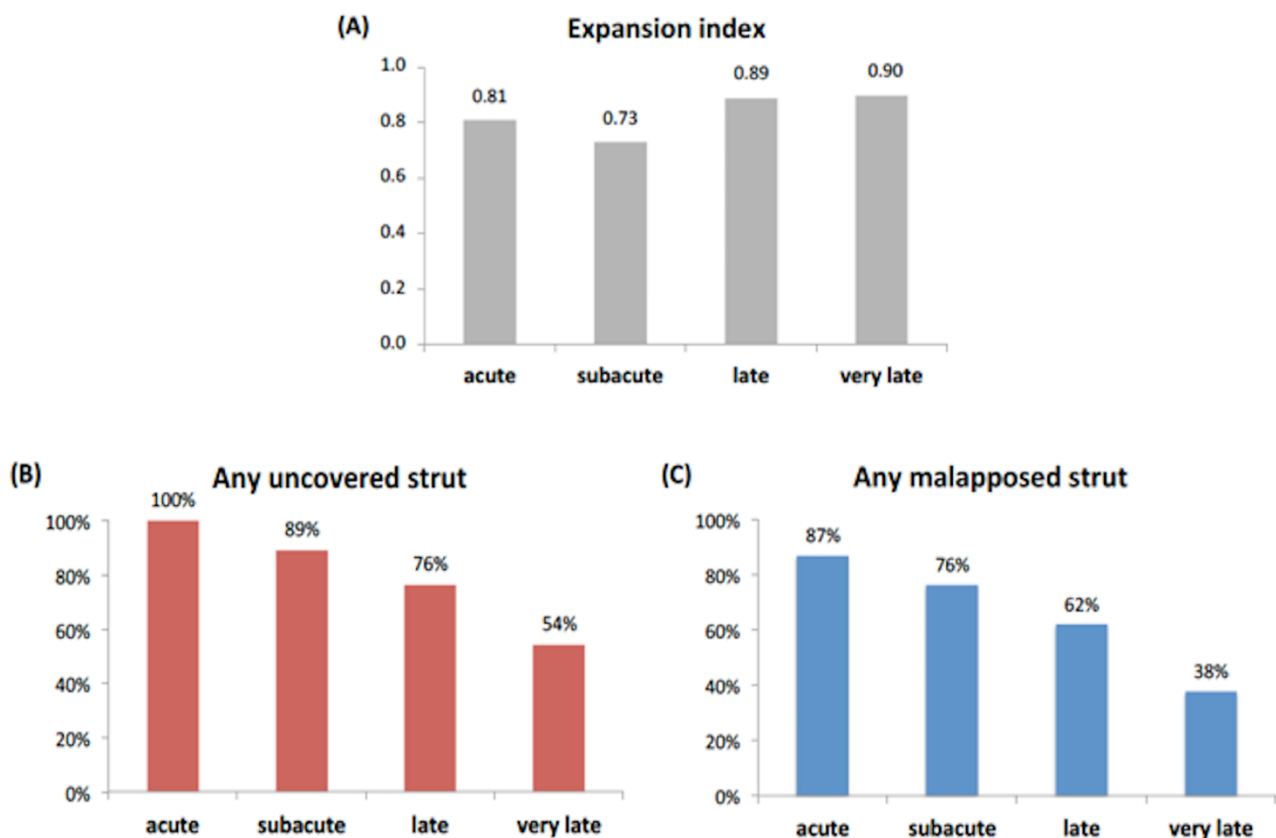
A) Mean stent expansion index. B) Proportion of patients with at least one frame with uncovered struts. C) Proportion of patients with at least one frame with malapposed struts.

- *Neoatherosclerosis was a relatively frequent finding in patients with very late ST, while it was not observed in patients with acute, subacute or late ST*

    The number of lesions showing any frames with core-lab adjudicated neoatherosclerosis or interstrut cavity significantly increased over time. In patients with acute, subacute or late ST, neoqtherosclerosis was not observed. Overall 43.6% of lesions in patients presenting with very late stent thrombosis had at least one frame with neoatherosclerosis. In these patients the median number of frames with neoatherosclerosis was 3.8.

    The predicted average probability (95% confidence interval) for any frame to have struts covered with neoatheroslcerosis or interstrut cavities was 0.0% (0.0-0.0), 0.0% (0.0-0.0), 0.0% (0.0-0,0), and 2.8% (1.3-5.9) and 0.0% (0.0-0.0), 0.1% (0.0-0.3), 1.2% (0.3-1.4), and 0.7% (0.3-1.4) for acute, subacute, late, and very late ST, respectively.


- *OCT-defined dominant causative mechanisms of ST differ according to timing of ST*

The results of the imaging adjudication committee analysis for dominant findings for acute, late and very late stent thrombosis are shown in **Figure 13**. The most commonly adjudicated dominant finding according to presentation were: acute, persistence of uncovered struts (66.7%); subacute, persistence of uncovered struts (61.7%) and underexpansion (25.5%); late, uncovered struts (33.3%) and severe restenosis (19.1%); and very late, neoatherosclerosis (31.3%) and uncovered struts (20.1%). Neoatherosclerosis was only observed as a dominant finding in patients with very late stent thrombosis.

An analysis of the imaging findings according to stent type in patients presenting with very late ST, identified a variety of causes at each time interval. Uncovered stent struts comprised a higher proportion of dominant findings in patients treated with DES. In patients with time interval

>5 years from stenting, most had been treated with BMS, and the most frequent dominant finding

in these patients was neoatherosclerosis (30/45 [66.7%]).

Figure 13. *Dominant findings identified by OCT imaging according to time interval from index stenting to presentation. Adapted from [86]*
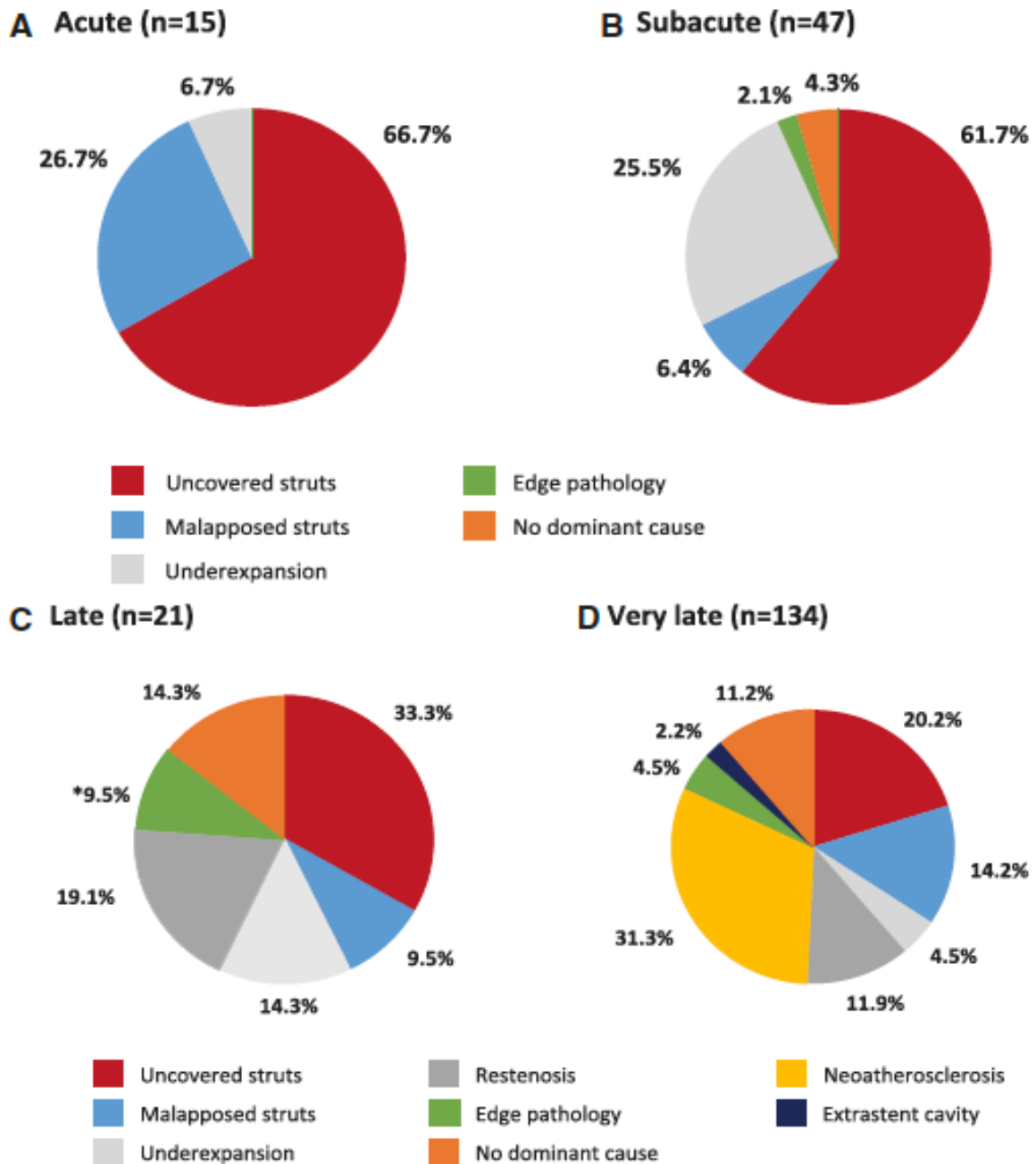
A. Acute stent thrombosis B. Subacute stent thrombosis C. Late stent thrombosis D. Very late stent thrombosis

4.2 Optical coherence tomography characterization of neoatherosclerosis in the PRESTIGE patient subgroup presenting with very late ST

- ***In-stent plaque rupture was found to be the dominant underlying cause in 40 of 134 patients (30%) presenting with very late ST at a median duration of 5.95 years from index stenting***

Neointimal lesion morphology in patients with neoatherosclerosis was assessed in a total of 6273 frames with sufficient image quality permitting core lab assessment; of those, 3283 frames located within the stented segments (52.3%), while 2990 frames were located within the adjacent non-stented segments (47.7%) within 5mm proximal or distal to the stented segment. Out of the 6273 frames, 186 (3%) were classified as fibroatheroma (19 thin-cap fibroatheroma and 165 thick-cap fibroatheroma) and 301 (4.8%) as plaque rupture; the remaining frames were classified as pathological intimal thickening and fibrocalcific plaque (in the absence of OCT-defined necrotic core) (n=5787, 92.3%); a total of 27 (0.4%) frames had significant neovascularization; calcification was seen in 1120 (17.6%) frames.

The most commonly adjudicated dominant finding for patients with neoatherosclerosis was plaque rupture in 40 of 58 lesions (69%) while 18 of 58 lesions (31%) presented with dominant mechanisms other than plaque rupture (uncovered struts, n=5; malappostion, n=2; severe stenosis, n=4; underexpansion, n=1; no dominant cause, n=4; edge segment disease, n=2)

- ***Macrophage infiltration was abundant in frames showing in-stent plaque rupture, whereas calcification was more frequent in frames without plaque rupture***

Macrophage infiltration into neointimal tissue was observed in 1582 (25.2%) frames; of the 301 frames with plaque rupture, 12 (4%) showed additional fibroatheroma in adjacent frames and 151 (50.2%) showed macrophage infiltration. Calcification was also observed in 12 (4%) frames with plaque rupture. Mean cap thickness measured 115±15μm. Macrophage infiltration was more often

observed in frames with plaque rupture vs. those without (151/301, [50.2%] vs. 1431/5972, [24%], p<0.0001). Conversely, calcification was more frequently observed in frames without plaque rupture (1108/5972, [18.6%] vs. 12/301, [4%], p<0.0001).

- ***Implantation of DES was significantly associated with formation of neoatherosclerosis, while previous myocardial infarction in patients with neoatherosclerosis was strongly associated with plaque rupture***

Multivariate Cox regression analysis (**Figure 14**) showed a 2.2-fold increased risk to develop neoatherosclerosis after implantation of DES relative to BMS (HR 2.22; 95% confidence interval: 1.15-4.30, p=0.02). The median follow-up duration was 7.8 years (5.0-11.5 years) for patients with neoatherosclerosis and 4.5 years (2.1-6.9 years) for patients without neoatherosclerosis.

Figure 14. *Cox proportional hazards regression analyses for neoatherosclerosis and plaque rupture. Adapted from* [103]
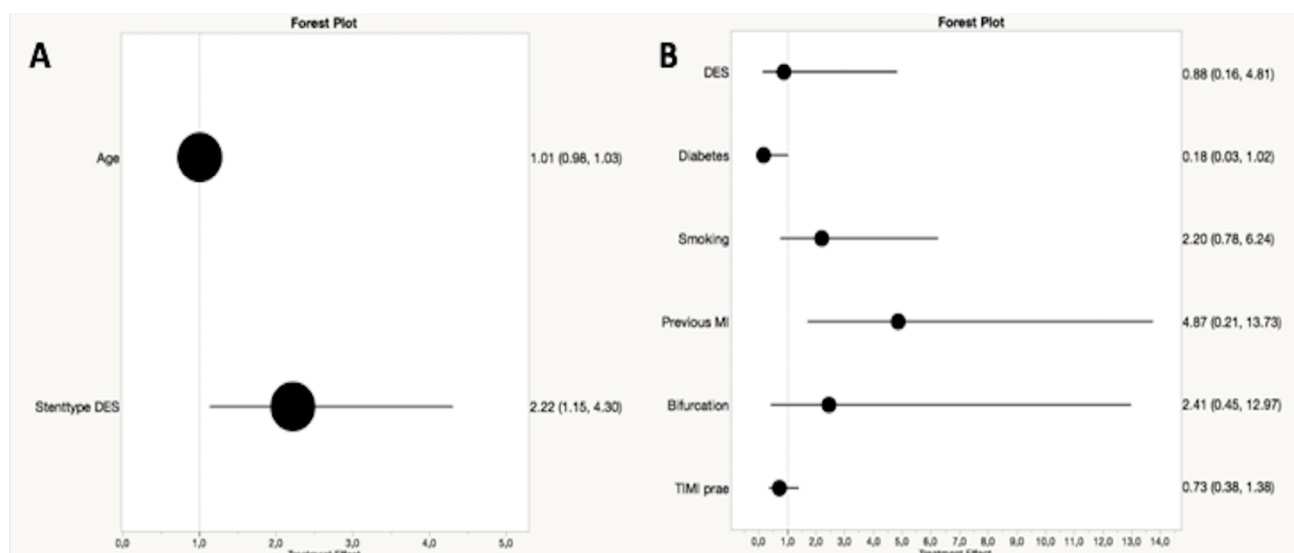
A. Forest plot illustrating hazards ratios of covariates associated with neoatherosclerosis formation.
B. Forest plot illustrating hazard ratios of covariates in patients with neoatherosclerosis associated with plaque rupture. MI = myocardial infarction; TIMI = Thrombolysis in Myocardial Infarction

Multivariate Cox regression analysis (**Figure 14**) showed a 4.9-fold higher risk of plaque rupture in patients with neoatherosclerosis and previous myocardial infarction (HR: 4.87; 95% confidence interval: 1.73 - 13.73, p=0.003). The median follow-up duration was 38.7 years (6.3-12.5 years) for patients with plaque rupture and 6.9 years (4.8-10.3 years) for patients without plaque rupture.

4.3 Optical coherence tomography findings in patients presenting with in-stent restenosis

- ***ISR lesions display considerable intralesion neointimal heterogeneity***

A total of 107 patients undergoing PCI for ISR were included, with one lesion being imaged/treated per patient; 73 lesions displayed a predominantly homogeneous and 34 lesions a predominantly non-homogeneous neointima. Underlying stent type was a BMS in 37 (34.6%), DES in 64 (59.8%) and BVS in 6 (5.6%) patients. Further classification as a function of time from index stenting showed 47 patients (14 BMS, 28 DES and 5 BVS) presenting with early (< 1 year), 20 patients (1 BMS, 18 DES and 1 BVS) with late (1-3 years) and 40 patients (22 BMS and 18 DES) with very late (> 3 years) ISR.

The qualitative analysis showed that predominantly homogeneous lesions included 4.5% (0.0-14.3) non-homogeneous quadrants, while predominantly non-homogeneous ones included 28.1% (20.3-37.5) homogeneous quadrants. There was excellent interobserver agreement regarding neointimal characterization (Cohen's κ=0.931).

- ***GSI analysis shows mean GSI values to significantly differ between neointimal categories***

GSI analysis was performed in a total of 3648 quadrants. Homogeneous quadrants were characterized by the highest mean GSI values [108.4(92.5-123.6)], followed by those with NA [88.3(72.8-104.9)], with non-homogeneous quadrants showing the lowest GSI values [79.9(61.2-95.9)] (**Figure 15**). One-way ANOVA as well as pairwise comparisons by means of the Tukey post hoc

test showed a statistically significant difference for each between group comparison (p<0.001 for all comparisons).

Figure 15. *Gray-scale signal intensity values for homogenous, non-homogeneous and neoatherosclerosis quadrants. Adapted from* [92]
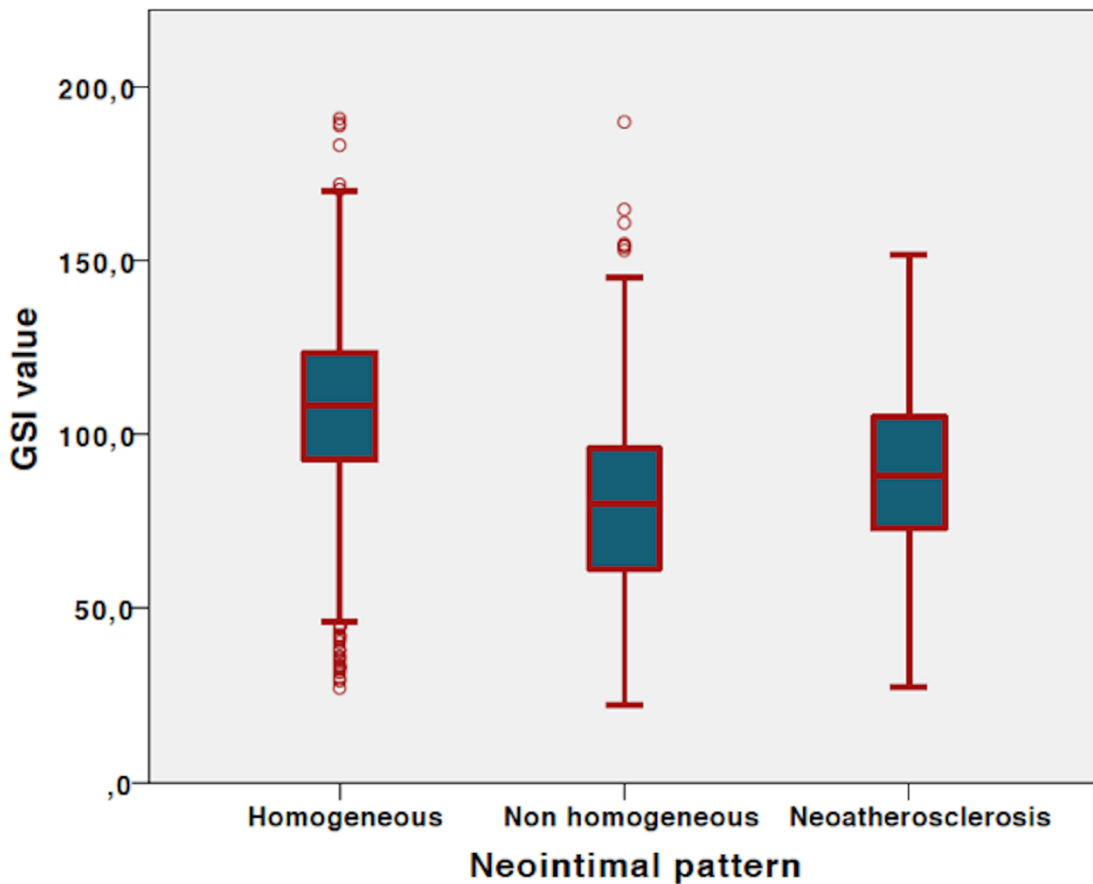

- ***Neoatherosclerosis is a not uncommon finding, develops earlier in DES compared to BMS and its presence and extent are time dependent phenomena***

Presence of any frame with neoatherosclerosis was registered in 33 (30.8%) lesions. Neoatherosclerotic changes were present in 15 (40.5%) BMS and 18 (25.7%) DES lesions (p=0.114); presence of any frame with NA was observed in 6 (12.8%) early, 6 (30.0%) late and 21 (52.5%) very late lesions (p<0.001). When analyzing presence of NA on the basis of both underlying stent type

and time from index stenting, some clear differences emerge between BMS and DES, with clustering of BMS neoatherosclerosis in the very late phase and no evidence of such changes up to 3 years (0% early, 0% late and 68.2% very late BMS lesions; p<0.001); on the contrary, DES lesions displayed an earlier appearance of NA (18.2% early, 31.6% late and 33.3% very late DES lesions; p=0.393) (**Figure 16**).

Figure 16. *Proportion of quadrants displaying neoatherosclerotic changes according to stent type and restenosis age. Adapted from* [92]
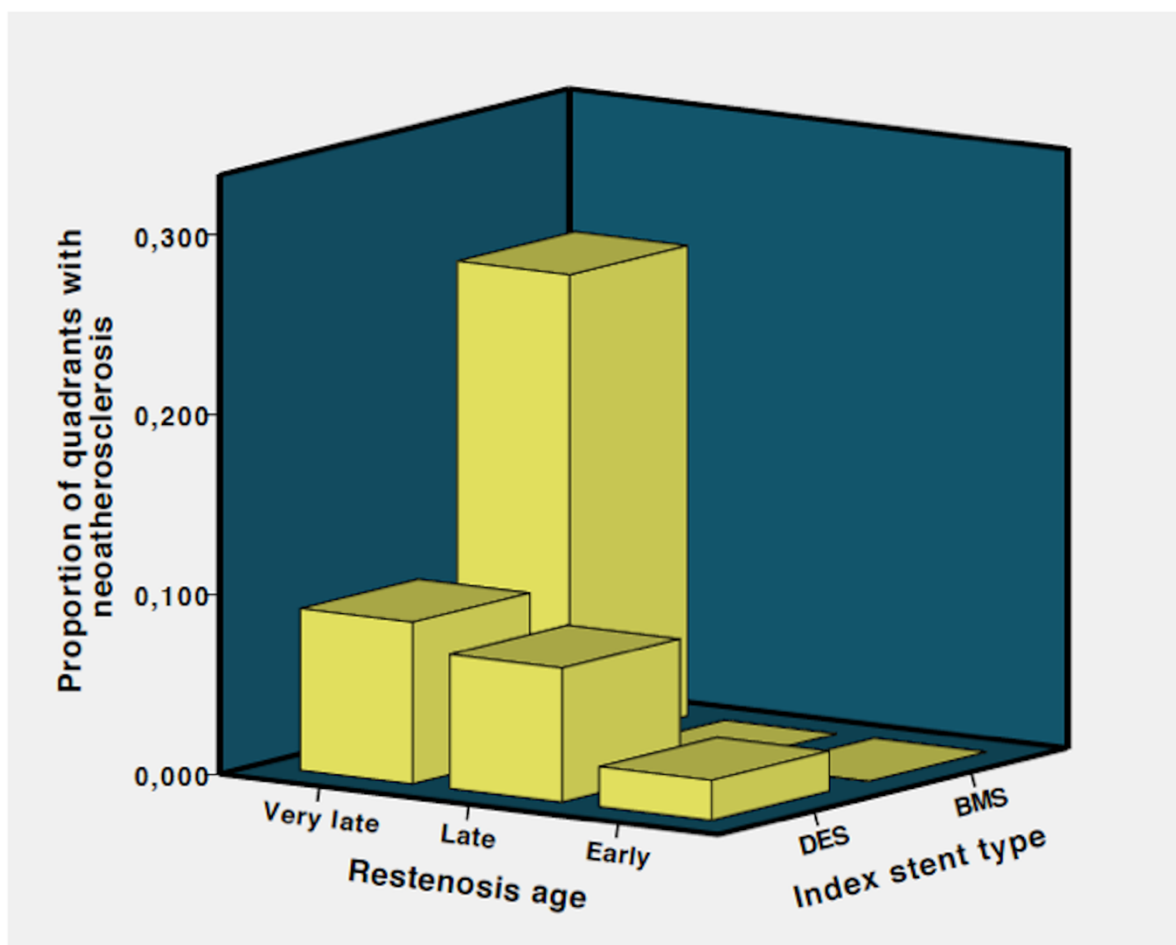
4.4 Angiographic and optical coherence tomography findings following intraplaque as opposed to subintimal recanalization of coronary chronic total occlusions – The ISAR-OCT-CTO registry

- *Use of contemporary DART is associated with similar mid-term clinical and angiographic results compared to intraplaque recanalization techniques*

Between April 2015 and April 2017, 193 CTO recanalization procedures were performed at the Deutsches Herzzentrum München. The first 75 consecutive patients undergoing angiographic and intravascular OCT imaging following successful CTO recanalization (1 CTO/patient) were included in the present report. The technique that achieved successful recanalization was intraplaque recanalization in 46 patients and DART in 29 patients. Stable angina and/or inducible myocardial ischemia were the leading indications for the recanalization procedure.

An antegrade approach (AWE) was used in the vast majority (93.5%) of the intraplaque strategy group, while RWE was adopted in only 3 (6.5%) patients of this group. Conversely, in the subintimal recanalization group, an ADR technique was used in 13 (44.8%) and a reverse CART in 16 (55.2%) of patients; mode of dissection was wire-based in 11 patients and CrossBoss-based in 2 patients of the ADR group, while mode of re-entry was Stingray-based in 10 patients and wire-based in 3 patients.

QCA of follow-up angiography showed no differences in terms of in-stent %DS [21.4 (15.5-33.5) vs. 20.8 (15.3-38.4); p=0.734], in-segment %DS [36.9 (26.4-43.1) vs. 31.2 (23.2-49.5); p=0.656, in-stent LLL [0.215 (0.063-0.495) vs. 0.230 (0.060-0.645) mm; p=0.837] or in-segment LLL [0.030 (-0.278-0.510) vs. 0.130 (-0.120-0.500) mm; p=0.395] between intraplaque and subintimal groups (**Table 2** and **Figure 17**). TLR was performed in 5 (10.9%) and 5 (17.2%) (p=0.496) patients respectively; among patients undergoing TLR, 40% were symptomatic. There were no cases of death, myocardial infarction or coronary artery bypass surgery in the study.

Table 2. *Angiographic outcomes and quantitative coronary analysis*

	Intraplaque strategy (n=46)	Subintimal strategy (n=29)	p-value
Pre-procedure			
Lesion length (mm)	36.2 (27.6-47.6)	47.8 (33.3-55.9)	0.183
RVD (mm)	2.94 (2.75-3.14)	2.99 (2.72-3.22)	0.876
Post procedure			
RVD (mm)	3.04 (2.87-3.41)	3.16 (2.87-3.34)	0.868
MLD (mm)	2.65 (2.43-2.85)	2.69 (2.31-2.91)	0.909
%DS (in-stent)	15.20 (9.28-18.78)	12.30 (10.35-15.00)	0.497
MLD (in-seg.)	2.21 (1.76-2.49)	2.32 (1.69-2.69)	0.301
%DS (in-seg.)	30.1 (20.3-41.9)	26.8 (17.9-37.5)	0.208
Follow-up			
Time interval follow-up (days)	198.0 (183.8-241.2)	200.5 (182.5-227.8)	0.803
RVD (mm)	3.03 (2.80-3.34)	3.19 (2.89-3.47)	0.397
MLD (mm)	2.39 (1.93-2.65)	2.41 (1.93-2.78)	0.734
MLD in-seg. (mm)	1.94 (1.64-2.37)	2.19 (1.63-2.63)	0.376
%DS in-stent	21.4 (15.5-33.5)	20.8 (15.3-38.4)	0.734
%DS in-seg.	36.9 (26.4-43.1)	31.2 (23.2-49.5)	0.656
LLL (mm)	0.215 (0.063-0.495)	0.230 (0.060-0.645)	0.837
LLL in-seg. (mm)	0.030 (-0.278-0.510)	0.130 (-0.120-0.500)	0.395
Binary restenosis	9 (19.6)	7 (25.0)	0.582

Data are shown as numbers (%) or median (inter quartile range)

Figure 17. *Cumulative frequency distribution curves for in-segment percentage diameter stenosis (left) and for in-stent late lumen loss (right) at angiographic follow-up according to recanalization technique*
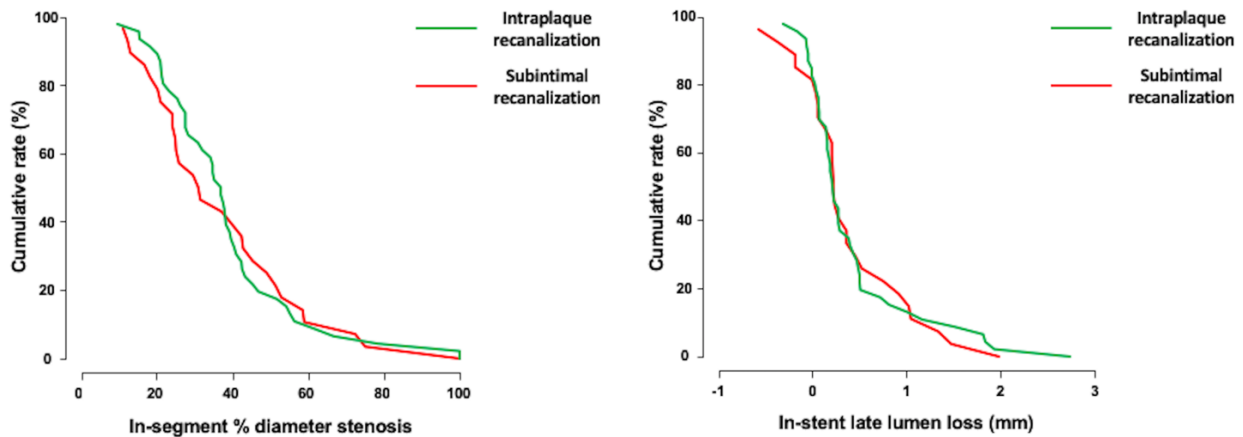
- *Rate of both uncovered and malapposed struts is high following CTO recanalization and the technique used (intraplaque vs. subintimal) independently correlates with strut malappostion but not strut coverage*

The number of analyzed struts was 27197 (2691 frames) and 19895 (1920 frames) in the intraplaque and subintimal group respectively (**Table 3**). Mean stent area [7.12 (5.61-8.93) vs. 6.93 (5.53-8.58) mm^2; p=0.487] and mean lumen area [6.46 (4.86-8.42) vs. 6.56 (4.94-9.02) mm^2; p=0.606] were comparable between groups.

OCT analysis of stent-vessel interaction showed no significant differences in terms of strut coverage (79.9% vs. 71.3%; p=0.255) or mean neointima thickness [110 (60-180) vs. 100 (60-170) μm; p=0.946] between the two groups (**Figure 18**).

Number of malapposed struts [6.6% vs. 13.6%; p<0.001], % of frames with malapposed struts [13.7 (3.0-29.8) vs. 27.1 (8.1-55.4); p=0.046], mean malapposition distance [230 (150-420) vs. 320 (180-680) μm; p=0.012] and maximal malapposition distance [540 (255-920) vs. 750 (490-1470) μm; p=0.022] were significantly higher in the subintimal recanalization group; despite not reaching

statistical significance, there was a tendency towards higher maximal malapposition length [3.0 (1.0-6.8) vs. 6.0 (2.0-13.0) mm; p=0.061] and % of lesions with >10% malapposed struts (26.1% vs. 48.3%; p=0.086] in the subintimal recanalization group (**Figure 18**).

Table 3. *Optical coherence tomography analysis of stent-vessel interaction according to recanalization technique*

	Intraplaque strategy (n=46)	Subintimal strategy (n=29)	p-value
Total nr. of frames	2691	1920	-
Total nr. of struts	27197	19895	-
Mean stent area (mm^2)	7.12 (5.61-8.93)	6.93 (5.53-8.58)	0.487
Min. stent area (mm^2)	4.59 (3.93-5.71)	4.03 (3.61-5.30)	0.215
Mean stent diam. (mm)	3.01 (2.67-3.36)	2.96 (2.64-3.30)	0.386
Max. stent diam. (mm)	3.20 (2.83-3.60)	3.18 (2.82-3.57)	0.573
Min. stent diam. (mm)	2.82 (2.50-3.15)	2.74 (2.44-3.08)	0.262
Mean lumen area (mm^2)	6.46 (4.86-8.42)	6.56 (4.94-9.02)	0.606
Max. lumen area (mm^2)	10.85 (8.69-13.07)	11.89 (8.92-14.48)	0.333
Min. lumen area (mm^2)	3.34 (2.59-4.43)	3.19 (2.29-4.85)	0.671
Mean lumen diam. (mm)	2.86 (2.48-3.26)	2.87 (2.50-3.37)	0.871
Max. lumen diam. (mm)	3.12 (2.69-3.59)	3.20 (2.74-3.79)	0.573
Min. lumen diam. (mm)	2.61 (2.25-2.96)	2.57 (2.22-3.02)	0.698
Max. % area stenosis	33.60 (21.83-49.73)	35.72 (27.57-57.11)	0.699
Max. neointimal area (mm^2)	2.17 (1.85-3.33)	2.49 (1.82-3.49)	0.469
Strut coverage (%)	79.9	71.3	0.255

% frames with uncovered struts	51.9 (33.9-76.3)	60.0 (35.2-85.1)	0.205
Lesions with >5% uncovered struts (%)	78.3	82.8	0.859
Lesions with >10% uncovered struts (%)	67.4	75.9	0.600
Mean neointima thickness (μm)	110 (60-180)	100 (60-170)	0.946
Max. neointimal thickness (μm)	510 (390-688)	600 (490-790)	0.112
Strut malapposition (%)	6.6	13.6	<0.001
% frames with malapposed struts	13.7 (3.0-29.8)	27.1 (8.1-55.4)	0.046
Lesions with >5% malapposed struts (%)	41.3	58.6	0.220
Lesions with >10% malapposed struts (%)	26.1	48.3	0.086
Mean malapposition distance (μm)	230 (150-420)	320 (180-680)	0.012
Max. malapposition distance (μm)	540 (255-920)	750 (490-1470)	0.022
Max. malapposition length (mm)	3.0 (1.0-6.8)	6.0 (2.0-13.0)	0.061

Data are shown as numbers (%) or median (inter quartile range)

Figure 18. *Illustrative example of angiography and intravascular OCT in a patient with a chronically occluded right coronary artery. Percentage of OCT-determined uncovered and malapposed stent struts according to recanalization technique.*
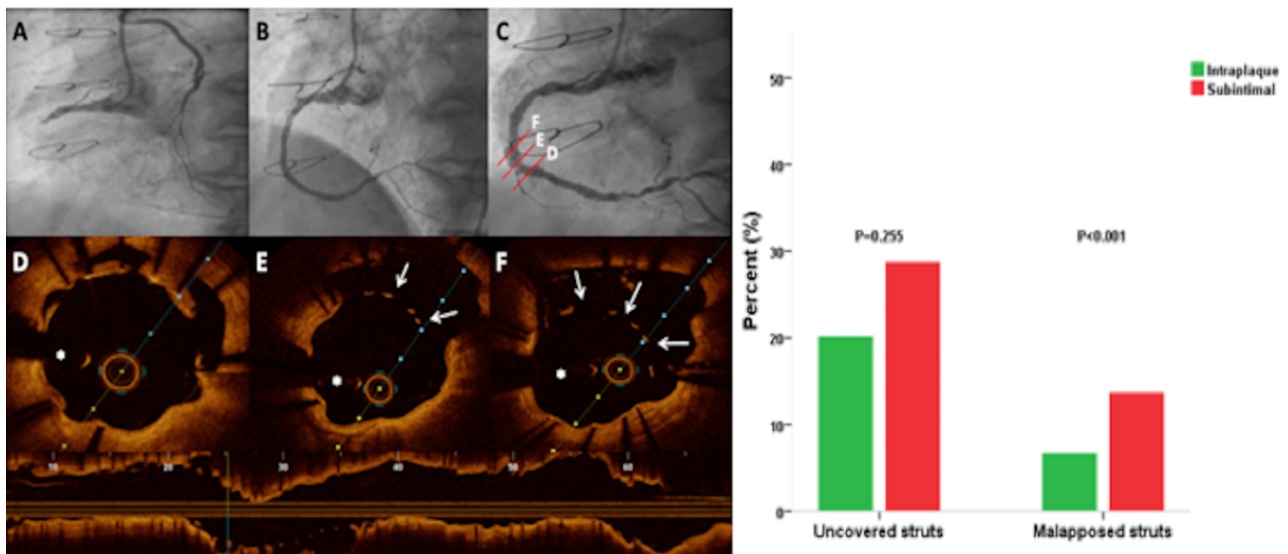
Left - A: initial dual coronary injection; B: final angiographic result after subintimal recanalization of the chronically occluded artery; C: eccentric coronary evaginations at the mid portion of the recanalized vessel visible at angiographic follow-up but not at baseline angiography. D, E and F: OCT cross-sections showing eccentric bulging of the vessel lumen and marked stent strut malapposition. Right – Percentage of uncovered and malapposed stent struts as determined by follow-up intravascular OCT according to recanalization technique.

- ***Correlates of strut coverage and strut malapposition***

Two separate multivariable models were conducted to assess the potential independent role of factors selected by the LASSO regression method regarding strut coverage and malapposition. The model for strut coverage included age, bifurcation lesion, family history, maximal stent diameter and rotablation procedure as dependent variables. Neither the technique used (intraplaque vs. subintimal) to achieve CTO recanalization (OR: 0.65; 95% CI: 0.28-1.49; p=0.314), nor the remaining variables (p>0.246 for all variables) independently correlate with strut coverage. The model for strut malapposition included age, bifurcation lesion, maximal stent diameter and rotablation procedure as dependent variables. Use of subintimal techniques remained an independent correlate of strut

malapposition (OR: 3.41; 95% CI: 1.24-9.36; p=0.017) even after adjustment for potential confounders; the remaining variables didn't independently correlate (p>0.124 for all variables) with strut malapposition.

4.5 Randomized comparison of vascular response to biodegradable-polymer sirolimus-eluting and durable-polymer everolimus-eluting stents

- ***There were no significant differences in terms of stent strut coverage or apposition at 6-8 months follow-up between patients randomly assigned to receive BP-SES or DP-EES***

A total of 29 patients were available for angiographic and OCT follow-up, with 14 patients with BP-SES (14 lesions) and 15 patients with PP-EES (15 lesions) patients eligible for the present analysis. This yielded a total of 6162 struts for coverage analysis (2889 in BP-SES and 3273 in PP-EES). For characterization of neointimal maturity, a total of 3672 neointimal regions (2030 regions in BP-SES and 1642 regions in PP-EES) above struts were assessed using grey scale intensity analysis.

Mean neointimal thickness did not differ significantly between the two groups (0.05 ± 0.08 mm vs. 0.08 ± 0.15 mm, p = 0.12). The percentage of uncovered struts was comparable between groups (456 (15.8%) vs. 571 (17.4%), p = 0.70). The number of lesions with ≥ 30% uncovered struts tended to be lower in BP-EES (14.3% (2 lesions)) as compared to PP-EES (20.0% (3 lesions)), without reaching statistical significance (p=0.68). The percentage of malapposed struts was low and comparable in both groups (1.3% in BP-SES and 2.2% in PP-EES, p = 0.27). One lesion in each group showed at least 5% malapposed struts, while 7 lesions (50.0 %) in BP-SES vs. 8 (53.3%) in PP-EES showed any malapposed strut in the stent segment (p = 0.86). Mean malapposition distance was 0.37 ± 0.21 mm in BP-SES and 0.29 ± 0.23 mm in PP-EES (p=0.50).

- ***Tissue coverage mainly consisted of immature neointima as evaluated by GSI analysis and no significant differences in terms of neointimal maturity were seen between BP-SES and PP-EES at 6-8 months follow-up***

Neointimal GSI analysis was assessed in a total of 3672 regions of interest (ROIs) above struts. 1463 ROIs were excluded from the analysis due to image quality (e.g. insufficient blood clearance, saturation artefact, etc.). After adjustment for clustering, mean GSI values in BP-SES and PP-EES did not significantly differ between groups (107.0 ± 21.8 in BP-SES vs. 99.3 ± 19.5 in PP-EES, $p = 0.44$). The number of neointimal regions with immature tissue was 1093 (53.8%) vs. 1120 (68.2%), $p = 0.31$). The rate of struts covered with mature tissue was similar between groups (937 (46.2%) in BP-SES versus 522 (31.8%) in PP-EES, $p = 0.31$).

4.6 Meta-analysis of optical coherence tomography studies comparing vascular response to biodegradable-polymer versus new-generation durable-polymer DES

- ***Thick-strut BP-DES are associated with decreased neointima growth and higher risk for uncovered struts compared to new-generation DP-DES***

The electronic search identified 10 studies, all with full-length articles [104-112], in which patients were assigned to BP-DES or new-generation DP-DES and subsequent OCT imaging at follow-up. These trials, which enrolled a total of 544 participants, were included in the final analyses. In these trials, patients with stable or unstable coronary artery disease were assigned to receive BP-DES (n=282) or new-generation DP-DES (n=262). Participants assigned to BP-DES received biolimus-eluting stents (BES, Nobori, Terumo Corporation, Japan or Biomatrix Flex, Biosensor Inc., Newport Beach, CA, USA, n=152), or sirolimus-eluting stents (SES, Orsiro, Biotronik, Bülach, Switzerland, Ultimaster, Terumo Corporation, Japan or Itrix, AMG International BmbH, Raesfeld-Borken, Germany, n=130). The overwhelming majority of participants assigned to DP-DES received everolimus-eluting stent (EES,

Xience V/Xience Prime, Abbott Vascular, Santa Clara, CA, USA; Promus/Promus Element, Boston Scientific, Natick, MA, USA, n=239), while zotarolimus-eluting stents (ZES, Resolute/Resolute Integrity, Medtronis, Santa Rosa, CA, USA, n=23) represented the comparator DP-DES in one trial.

Among participants who were originally enrolled, 447 patients (82.1%) with 480 treated lesions had analyzable OCT pullbacks at follow-up. The total number of analysed struts was 118129 (n=61455 and n=56674 for lesions treated with BP-DES and new-generation DP-DES, respectively. OCT imaging was performed as a weighted median follow-up of 7 months.

Figure 19. *Illustrative Forest plots for primary outcomes with BP-DES vs. new-generation DP-DES. Weighted mean difference for (A) neointima hyperplasia thickness (µm) and odds ratio for (B) lesions with uncovered struts with BP-DES vs. new-generation DP-DES. The diamonds indicate the point estimates and the left and right ends of the lines the (95% CI).*
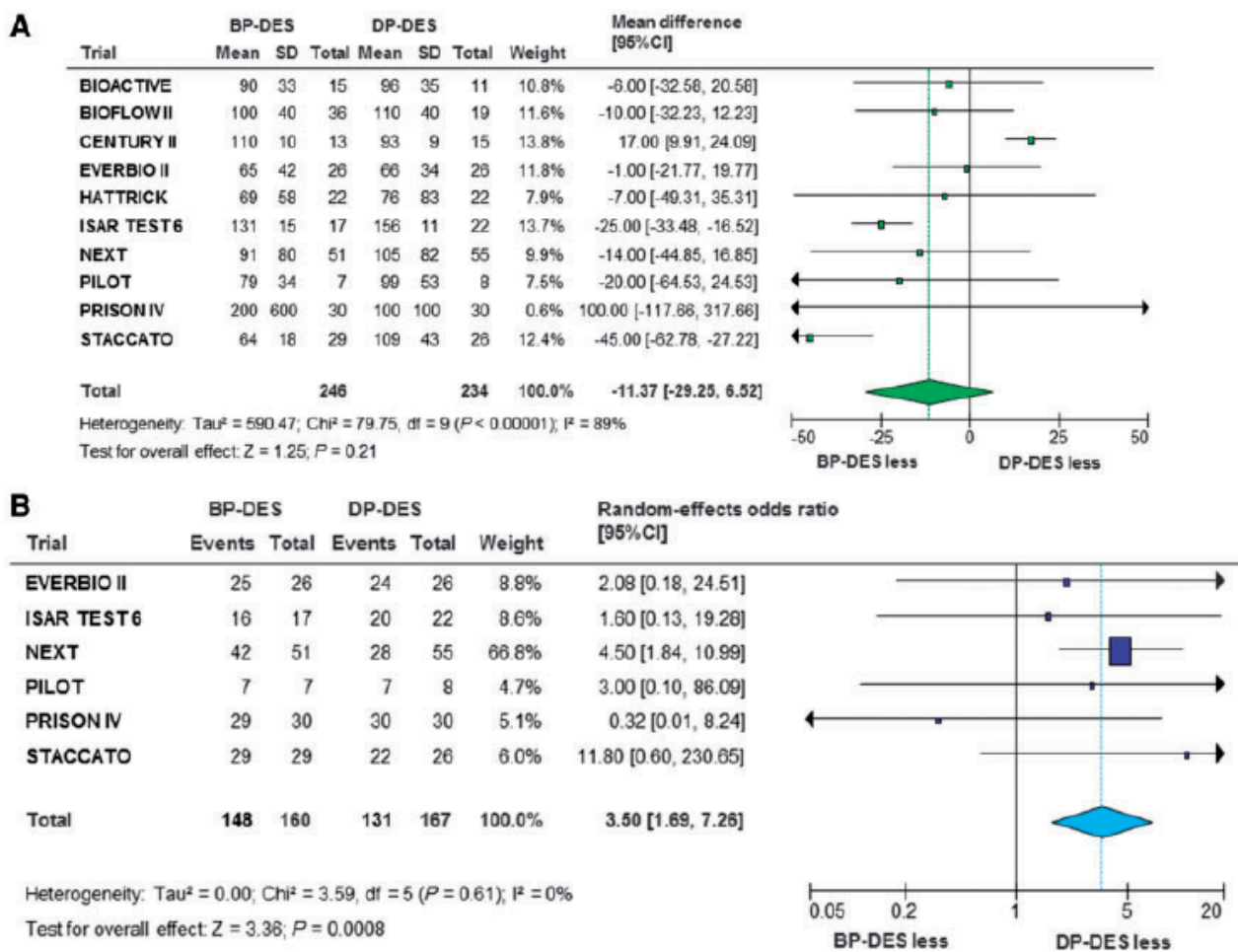
Forest plots for primary outcomes are displayed in **Figure 19.** Neointima thickness, the main primary outcome, was assessed in 436 lesions. Lesions treated with BP-DES showed no difference in terms of neointima thickness as compared to those treated with new-generation DP-DES [range 64-200 µm vs. 66-156 µm; -11.37 (-29.25, 6.52; p=0.21]. There was a high heterogeneity for this risk estimate (I^2=89%). Assessment of strut coverage, the co-primary outcome, was possible for 327 lesions, 279 of which were reported to be uncovered (85.3). Lesions treated with BP-DES vs- new-generation DP-DES showed a higher risk for any uncovered strut [92.5% vs. 78.4%; 3.50 (1.69-7.26), p=0.0008; I^2=0%]. Notably, 90 lesions presented >10% uncovered struts with no significant differences between BP-DES and new-generation DP-DES [44.1% vs. 43.2%; 1.14 (0.42-3.14), p=0.80; I^2=59%].

Analysis of stent strut apposition was performed in 327 lesions and 134 (40.9%) of these were reported to have malapposed struts. Lesions treated with BP-DES vs. new-generation DES showed a trend towards higher risk for any malapposed strut [48.1% vs. 34.1%; 2.01 (0.98-4.12), p=0.06; I^2=42%]. The mean percentage of malapposed struts was significantly higher with BP-DES as compared to new-generation DES [range 0.48-4.2 vs. 0.2-4.3; 0.65 (0.12, 1.17); p=0.02; I^2=4%]. Notably, 21 lesions presented >5% malapposed struts without significant differences between BP-DES and new-generation DES.

Neointimal area was assessed in 426 lesions. Lesions treated with BP-DES showed lower neointimal area as compared to those treated with new-generation DP-DES [range 0.38-1.31 mm^2 vs. 0.52-1.56 mm^2; -0.12 (-0.24, -0.00); p=0.046; I^2=55%]. Neointimal volume was assessed in 266 lesions. Lesions treated with BP-DES showed no difference in terms of neointimal volume compared to those treated with new-generation DP-DES [range 7-17.7 mm^3 vs. 8.4-16.5 mm^3; 0.26 (-3.21, 3.74); p=0.19; I^2=27%].

Finally, the subgroup analyses showed that the time point of OCT imaging, the antiproliferative drug eluted from BP-DES, the number of participants in each included trial, the inclusion of patients with diabetes or acute myocardial infarction were not associated with th estimated odds ratio of the primary outcome. Conversely, strut thickness of BP-DES displayed a significant interaction with the treatment effect for the primary outcome (p_{int}=0.043). Indeed, lesions treated with thick-struts (>100 µm) BP-DES were associated with lower neointima thickness as compared to those treated with new-generation DP-DES [-20.39 (-33.83, -6.95), p=0.003; I^2=39%].

4.7 Influence of fully bioresorbable magnesium scaffolds as compared to conventional metallic DES and systemic statin treatment as compared to placebo on the development of neoatherosclerosis in a hypercholesterolemic animal model

- *Magnesium-based BVS showed decreased neointimal macrophage infiltration relative to stainless steel-based permanent DES, while atorvastatin treatment significantly reduced progression of neointimal macrophage infiltration in both BRS and DES, as confirmed by histopathological assessment*

Of the 33 rabbits included in the study, 2 animals died of cholesterol induced liver failure. Two additional animals had to be excluded from the analysis due to total thrombotic occlusion of a stented vessel (one rabbit with thrombosis in BRS, one with thrombosis in DES). Accordingly, a total of 9 animals were available in group 1 (day 91). A total of 10 animals each remained in groups 2 and 3, respectively until day 161.

- *Neoatherosclerosis scoring by histology*

BRS showed a significantly lower estimated score of foamy macrophage infiltration compared to DES [score 1.16 (1.12, 1.21) vs. 1.53 (1.41, 1.65); mean reduction -0.391; p<0.0001]. Statin treatment

resulted in a significant reduction of foamy macrophage infiltration relative to placebo (score 1.23 (1.14, 1.32) vs. 1.45 (1.36, 1.54); mean reduction -0.286; p=0.001) (**Table 4**).

Table 4. *Results of histopathological analysis of group 2 and 3 after 161 days (10 rabbits/group)*

		neoatherosclerosis score					% stenosis				
		Mean	Lower 95% CI	Upper 95% CI	p-value	B- value	Mean	Lower 95% CI	Upper 95% CI	p-value	B-value
Treatment	BRS, n=10	1.16	1.12	1.21	0.0001*	-0.391	68.64	64.82	72.69	0.0001*	0.679
	DES, n=10	1.53	1.41	1.65			35.53	32.33	39.04		
Group	Statin, n=10	1.23	1.14	1.32	0.001*	-0.286	49.33	44.22	55.03	0.977	0.018
	Placebo, n=10	1.45	1.36	1.54			49.43	45.39	53.84		
P interaction		0.005*					0.577				

Values are presented as estimated means with upper and lower 95% CI. A p<0.05 was considered statistically significant (*). B-values represent mean reductions. Wilcoxon Kruskal-Wallis (non-parametric) or ANOVA (parametric) was applied.

Figure 20. *Comparison and co-registration of BRS and DES*
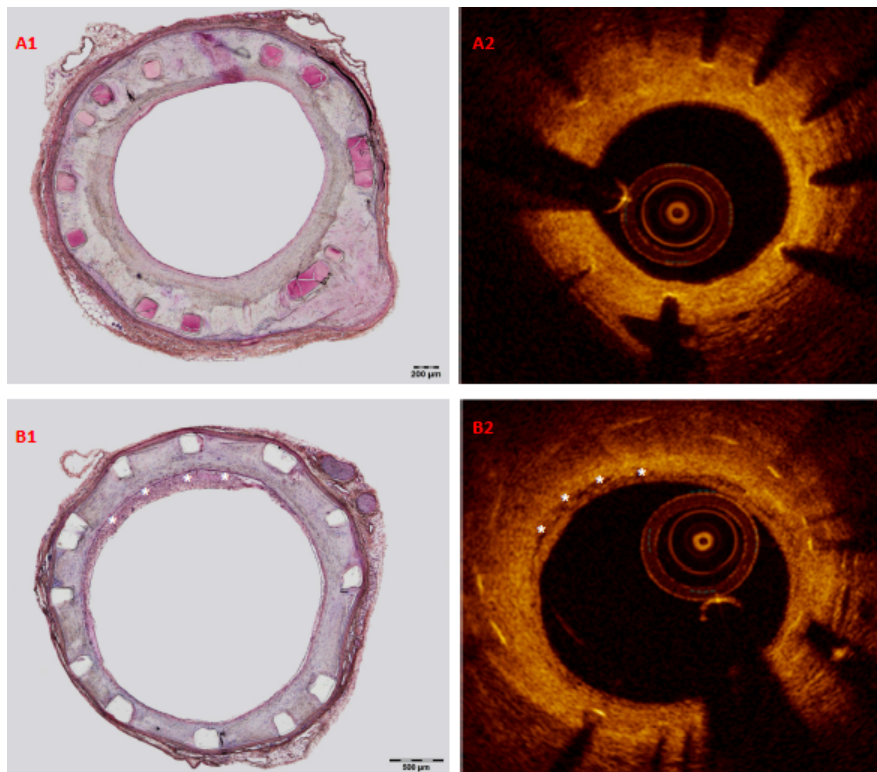
A. Sections stained for HE (A1) with corresponding OCT-frame (A2) in a BRS treated vessel.

B. Sections stained for HE (B1) with corresponding OCT-frame (B2) in a DES treated vessel.

* indicate foamy macrophage infiltration

There was significant statistical interaction (p=0.005) among stent type and treatment allocation to statin vs. placebo. **<u>Figure 20</u>** shows representative co-registration of HE-stained histological slides and OCT-frames in BRS and DES, respectively.

- ***Neoatherosclerosis scoring by OCT***

An overview of the results is presented in **<u>Table 5</u>**. BRS showed a significantly lower estimated score of macrophage infiltration by OCT compared to DES (score 1.20 (1.08, 1.34) vs. 2.09 (1.83, 2.39); mean reduction -0.606; p<0.0001. There was no statistically significant difference in animals receiving statin treatment relative to placebo by OCT (score 1.57 (1.32, 1.87) vs. 1.60 (1.44, 1.77); mean reduction -0.70; p=0.873).

<u>Table 5</u>. *Results of OCT analysis of group 2 and 3 after 161 days (n=10 rabbits per group)*

		Neoatherosclerosis score					%stenosis				
		Mean	Lower 95% CI	Upper 95% CI	p-value	B-value	Mean	Lower 95% CI	Upper 95% CI	p-value	B-value
Treatment	BRS, n=10	1.20	1.08	1.34	0.0001*	-0.606	47.00	41.44	53.32	0.0001*	0.875
	DES, n=10	2.09	1.83	2.39			21.77	18.82	25.20		
Group	Statin, n=10	1.57	1.32	1.87	0.873	-0.070	32.31	27.03	38.61	0.857	0.125
	Placebo, n=10	1.60	1.44	1.77			31.68	28.14	35.67		
P interaction		0.435					0.222				

Values are presented as estimated means with upper and lower 95% CI. A p<0.05 was considered statistically significant (*). B-values represent mean reductions. Wilcoxon Kruskal-Wallis (non-parametric) or ANOVA (parametric) was applied.

- ***Morphometric analysis in OCT and histopathology***

<u>Table 4</u> and **<u>Table 5</u>** show the results of morphometric assessment of stented vessels after 161 days by histopathology and OCT. There was significantly greater neointimal area in BRS relative to DES by OCT-based assessment (1.86mm^2 vs. 1.32mm^2; +0.611 in BRS; p<0.0001) and histology (3.22mm^2

vs. 2.27mm^2; +0.987 in BRS; p<0.0001). This resulted in increased percentage stenosis in BRS treated arteries relative to DES (47% in BRS vs. 21.8% in DES; p<0.0001 in OCT analysis and 68.6% vs. 35.5%; p<0.0001 in histological analysis).

- ***Histological and immunohistological staining***

Neointimal tissue consisted of smooth muscle cells in a proteoglycan-rich matrix. Inflammation of neointimal tissue was generally mild to moderate with a tendency towards greater inflammation in BRS relative to DES (inflammation score: 1.53 in BRS vs. 1.24 in DES, p=0.106). Cholesterol crystals were frequently observed in deeper tissue layers in both BRS and DES. Giant cells were mainly observed within the peri-strut regions (% giant cells: 9.33% in BRS vs. 7.70% in DES, p=0.335). In segments stained for RAM11, macrophage infiltration was frequently observed within the sub-intimal tissue in DES, while BRS showed scattered macrophages within the peri-strut tissue (**Figure 21**).

Figure 21. *RAM-11 staining in BRS and DES stented vessels*
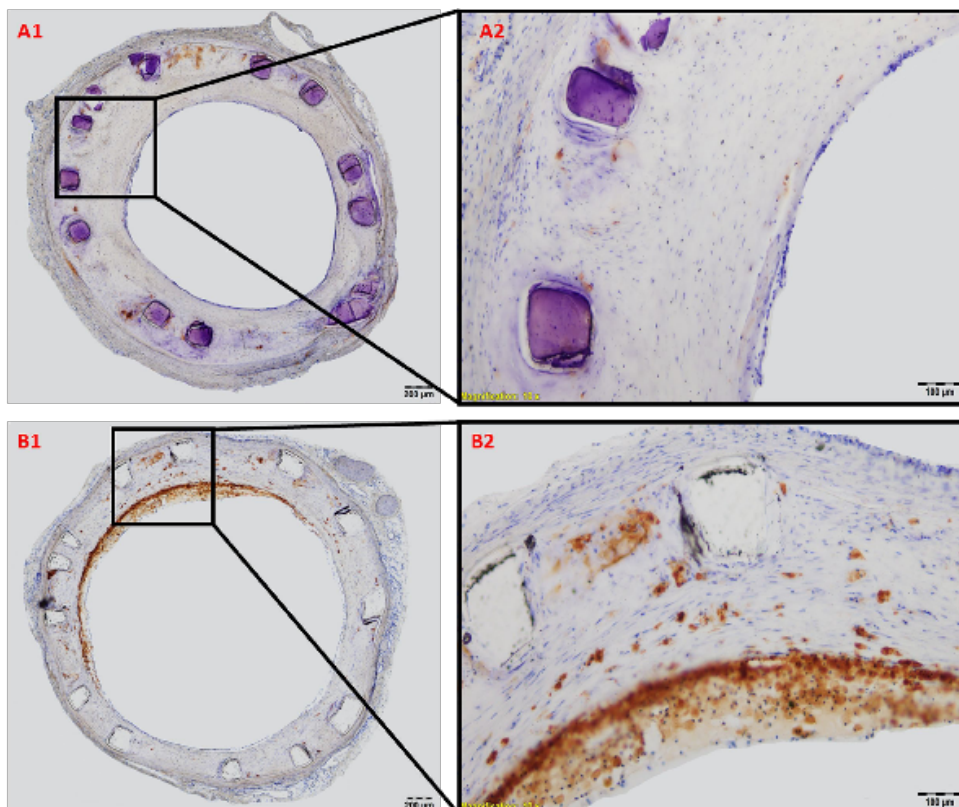
A. Overview of a RAM-11 stained section from a BRS (A1) with 40x magnification (A2). Sparse macrophage infiltration is detectable in peri-strut neointimal tissue. B. Overview of a RAM-11 stained section from a DES (B1), with 40x magnification (B2). Superficial foamy macrophage infiltration is visible in about 50% of the vessel circumference.

5. DISCUSSION

5.1 Optical coherence tomography findings in patients presenting with stent thrombosis

In the largest registry of patients presenting with stent thrombosis in the literature to date, that enrolled patients presenting with both early and late/very late stent thrombosis containing a high proportion of current generation DES and undergoing imaging in the acute setting using current generation OCT systems the key findings were:

- detailed analysis of OCT images acquired in the setting of stent thrombosis was feasible in the selected patients included in this registry

- the rate of stent underexpansion was high across all groups and highest in patients with subacute stent thrombosis

- both uncovered struts and malapposed struts were frequently found in patients with stent thrombosis; both decreased over time, though more than half of lesions with very late stent thrombosis had frames with uncovered struts and more than a third had malapposed struts

- neoatherosclerosis was a not uncommon finding in patients with very late stent thrombosis.

When categorizing patients according to timing of stent thrombosis, some clear messages emerge. In patients presenting with acute/subacute stent thrombosis, uncovered and malapposed stent struts along with underexpansion of the stented coronary segment were identified as key morphological features of stent thrombosis by OCT. While it is not unexpected that uncovered stent struts were frequently observed early after stent implantation, this emphasizes the inherent thrombogenicity of stents in this phase, when neointimal healing and re-endothelialization are incomplete. Similarly, although the relevance of stent malapposition in isolation is often discussed, the finding of high rates of malapposition in our report is in line with other reports [113, 114]. Indeed, the relevance of flow disturbance, especially occurrence of non-streamlined flow along malapposed

stent struts has recently been shown to be of relevance with regards to acute thrombogenicity of stents [115].

The high prevalence of stent underexpansion is a noteworthy observation and is in keeping with the known association between acute procedural results and stent thrombosis [39]. A stent expansion index <0.8 was observed in more than 40% of patients and approximately two-thirds of patients with subacute stent thrombosis had stent expansion indices <0.8. In addition, stent underexpansion was adjudicated as the dominant cause of stent thrombosis in 25% of these patients.

In patients presenting with late/very late stent thrombosis, a more heterogeneous profile was observed, with uncovered/malapposed stent struts, underexpansion and severe restenosis predominant features within the first year and in-stent neoatherosclerosis beyond 1-year. Indeed although both uncovered and malapposed struts decreased over time, more than half of lesions with very late stent thrombosis had frames with uncovered struts and more than a third had malapposed struts. In addition, severe restenosis in the treated segment was relatively frequently observed. This underlines the association between stent thrombosis and in-stent restenosis as part of the spectrum of stent failure [37, 116]. The link can be explained by deceleration of flow within the restenotic stented segment, which causes a shift towards pro-coagulatory pathways [117].

In our study we found that in-stent neoatherosclerosis – i.e. development of de novo atherosclerosis inside the implanted stent – was an important cause of stent thrombosis beyond one year cases. Although the diagnosis of neoatherosclerosis can be challenging in the presence of residual overlying thrombus and its definition remains a matter of some debate, these observations are consistent with findings in late stent failure from autopsy studies, which have documented presence of neoatherosclerosis in around 30% of selected autopsy cases and premature and accelerated formation in DES as compared with uncoated stents [50]. One explanation for the more

accelerated course in DES is the greater delay in endothelial healing and lack of endothelial integrity within the stented segments of DES as compared with bare metal stents. Interestingly, in the current study, neoatherosclerosis was more frequent in bare metal stents, which is likely explained by the longer duration of follow-up in these patients. Indeed, previous registries showed that duration of follow up is the most important risk factor for the occurrence of neoatherosclerosis [50, 69]. Effective measures to overcome neoatherosclerosis represent an important unmet need for future clinical investigation.

5.2 Optical coherence tomography characterization of neoatherosclerosis in the PRESTIGE patient subgroup presenting with very late ST

The current study investigated the frequency, timing and etiological factors of neoatherosclerosis in patients presenting with very late stent thrombosis to 29 European clinical centers with intravascular imaging capability. The most salient findings of the current study can be summarized as follows:

- Neoatherosclerosis was observed in 58 of 134 patients (43.3%) with VLST

- In-stent plaque rupture was found to be the dominant underlying cause in 40 of 134 patients (30 %) presenting with VLST at a median duration of 5.95 years from index stenting

- Dominant and contributing factors of VLST differed substantially among patients with and without neoatherosclerosis; plaque rupture was by far the most frequent finding in patients with neoatherosclerosis (69%), while uncovered stent struts (29%), malapposition (22%) and severe stenosis (16%) were frequent dominant factors in patients without neoatherosclerosis

- Macrophage infiltration was abundant in frames showing in-stent plaque rupture, whereas calcification was more frequent in frames without plaque rupture

- Implantation of DES was significantly associated with formation of neoatherosclerosis, while previous myocardial infarction in patients with neoatherosclerosis was strongly associated with plaque rupture

In-stent neoatherosclerosis was frequently observed in patients suffering VLST. In-stent plaque rupture was identified as dominant pathological mechanism causing VLST in 30% of patients presenting beyond the 1-year time frame. Although the aim of the current analysis was to provide insights into frequency and timing of neoatherosclerosis in a patient population presenting with VLST, where the absolute frequency of neoatherosclerosis is expectedly high, the 30% relative frequency of in-stent plaque rupture is of concern considering the enormous number of stents implanted on a global scale. One of the key findings of our as well as other reports [114, 118] is the fact that newer generation DES were consistently affected by neoatherosclerosis to a level that is similar to first generation DES.

Given the significantly longer duration of implantation in BMS relative to DES, we performed multivariate Cox regression analysis to identify factors associated with formation of neoatherosclerosis and plaque rupture. Strikingly, implantation of DES was significantly associated with formation of neoatherosclerosis. It has recently been reported that leaky endothelial cell junctions give rise to accelerated atheroma formation within the nascent neointima following DES implantation, resulting from prolonged release of anti-proliferative drugs known to impede endothelial integrity during recovery after vascular injury [50]. Therefore, neoatheroma formation may occur earlier after DES implantation when compared to BMS, which has been suggested in autopsy studies [63], recent intravascular imaging trials [119] and the current registry.

Importantly, pathology data from a large series of autopsy cases suggested that underlying vulnerable plaque type is associated the occurrence of neoatherosclerosis over time in both DES and BMS [50], which is supported by the increased risk of plaque rupture in patients with previous myocardial infarction in our study. Future prospective clinical studies are needed to confirm this intriguing hypothesis.

Foam cell infiltration of neointimal tissue has been proposed to be the earliest sign of neoatherosclerosis formation [50]. Interestingly, signal attenuation indicative of macrophage infiltration was significantly more frequent in OCT frames with plaque rupture vs. those without, suggesting that significant macrophage infiltration might be associated with plaque vulnerability in rupture-prone neoatherosclerotic lesions. Furthermore, calcification was more often observed in OCT frames without plaque rupture, confirming previous studies [120] suggesting calcification to be a marker of plaque quiescence.

5.3 Optical coherence tomography findings in patients presenting with in-stent restenosis

In the present registry which included patients from 3 European Centers undergoing intravascular OCT prior to percutaneous treatment of ISR we found that:

- ISR lesions display considerable intralesion neointimal heterogeneity
- GSI analysis shows mean GSI values to significantly differ between neointimal categories
- Neoatherosclerosis is a not uncommon finding, develops earlier in DES compared to BMS and its presence and extent are time dependent phenomena
- the rate of stent underexpansion was high in both groups.

Since the majority of studies performed to date [121-123] categorized neointimal patterns based on the optical characteristics of a single frame, we expanded the analysis to include a 10 mm

segment. We found that neointimal patterns different from the dominant one are significantly represented in the same restenotic lesion. Therefore, a detailed analysis of the neointimal characteristics of the whole stented segment seems advisable for proper classification of restenotic lesions.

The classification of neointimal tissue has been a matter of debate and more reproducible strategies have been advocated [124]. Our analysis shows that mean GSI values significantly differ between neointimal categories. These results provide initial evidence on the usefulness of GSI analysis as a valuable quantitative adjunct in neointimal characterization. However, additional evaluation, ideally in the context of an OCT-histology correlation study, seems advisable in order to define the discriminatory capacity of GSI analysis.

Neoatherosclerosis has been involved in the pathogenesis of both ISR and stent thrombosis [86, 116]. Although NA was more frequent in BMS in absolute terms, this finding should be viewed in the light of significantly longer implant duration for BMS compared to DES. Indeed, our findings support a strong time dependency of NA changes, with progressive increase in incidence with increasing time from stent implantation; indeed, time from index stenting was the only independent predictor of neoatherosclerosis. Our results are in line with those of previous registries that showed duration of follow up to be the most important risk factor for the occurrence of NA [50, 65]. The premature development of neoatheroslerosis in DES compared to BMS is a noteworthy finding, since it closely mirrors findings of previous histopathological reports based on selected autopsy cases [63].

Stent underexpansion has long been recognized as a major mechanical factor triggering ISR. In our patient collective, stent underexpansion was present in 48.5% and 61.1% of lesions respectively. These findings have important therapeutic drawbacks since recognition of stent underexpansion should prompt aggressive dilatation and eventually use of super-high-pressure

non-compliant balloons. Additionally, they underscore the importance of intravascular imaging guidance to optimize expansion during initial implantation as a mean to reduce the occurrence of ISR.

5.4 Angiographic and optical coherence tomography findings following intraplaque as opposed to subintimal recanalization of coronary chronic total occlusions – The ISAR-OCT-CTO registry

The main findings of the ISR-OCT-CTO registry, the first to specifically compare vascular healing patterns by intravascular OCT following percutaneous CTO recanalization by means of intraplaque as compared to subintimal techniques, can be summarized as follows:

- use of contemporary DART is associated with similar mid-term clinical and angiographic results compared to intraplaque recanalization techniques

- although rate of uncovered struts is high following CTO recanalization, the technique used (intraplaque vs. subintimal) does not correlate with presence of uncovered struts

- rate of strut malapposition is high following CTO recanalization, particularly if achieved by means of subintimal strategies and use of DART is an independent correlate of strut malapposition

- antegrade and retrograde DART show comparable rates of strut coverage and although absolute number of malapposed struts was significantly higher in the retrograde group, remaining indexes of malapposition did not differ between the two groups

The majority of recent observational studies showing comparable mid-term clinical outcomes between modern DART and intraplaque recanalization techniques [125-129] did not include a systematic angiographic follow-up. However, patient clinical status after CTO recanalization is not only determined by persisting patency of the recanalized vessel, but also by dynamic changes in collateral vessel supply, which in case of restenosis/reocclusion can recover to pre-recanalization

levels [130]. Therefore, as confirmed also by studies with angiographic follow-up [131] and by the low prevalence of symptoms (40%) in the patient subgroup undergoing TLR in our study , in the specific setting of CTO recanalization, failure to perform a systematic angiographic follow-up may significantly underestimate the occurrence of restenosis/re-occlusion. We found no differences in terms of MLD, %DS, LLL, binary restenosis or TLR between the two recanalization strategies. In view of the high complexity of the lesion subset being recanalized by means of DART in our patient collective (J-CTO score $\geq$3 in 65.5% of this subgroup), confirmation of comparable angiographic outcomes between the two groups is a remarkable finding, which confirms the sustained efficacy of contemporary DART.

Intravascular OCT surveillance of vessel healing patterns following successful CTO recanalization has received limited attention compared to non-occlusive coronary lesions. A limited number of studies reported reduced stent strut coverage following CTO recanalization as compared to non-CTO PCI [132]. Additionally, OCT evaluation in a patient subgroup of the ACE-CTO study confirmed high rates of both uncovered and malapposed struts in DES implanted in CTO lesions [133]. In line with these previous observations, our results confirm a high prevalence of uncovered struts following CTO recanalization. The technique used to achieve recanalization did not correlate with presence of uncovered struts in our study. Additionally, our OCT findings of comparable neointimal thickness and area between the two groups corroborate the angiographic findings and confirm sustained DART efficacy.

Congruent with previous studies [132, 133], our study confirms high rates of malapposition following CTO recanalization. Our study extends these findings by showing that virtually all indexes of malapposition display significantly higher numerical values following DART as compared to intraplaque recanalization and that use of DART is independently associated with presence of malapposed struts. Comparison of vessel healing parameters between antegrade and retrograde

DART showed no differences in terms of strut coverage and, although the absolute number of malapposed struts was significantly higher in the retrograde group, all remaining indexes of malapposition were comparable between the two groups.

There are some potential explanations for the occurrence of both reduced stent coverage and apposition in the setting of CTO PCI. One mechanism could be an increase in lumen area of chronically hypoperfused vessels following successful recanalization with resultant occurrence of stent-vessel mismatch. Additionally, use of DART is intrinsically linked to a disruption of the intimal and medial layers with resultant formation of intramural hematoma and stent implantation in the subintimal space. Resorption of intramural hematomas following recanalization represents an alternative mechanism for the occurrence of strut malapposition. Finally, optimal stent apposition, besides requiring maneuvers, such as aggressive post-dilation, which portend a higher risk of vessel perforation, might be impossible to achieve in a markedly distensible environment such as the subintimal space. Little is known regarding the patterns of vessel healing/remodeling following stent implantation in the subintimal space, since no specific histological studies have been conducted so far. Although no definitive conclusions can be drawn, since no baseline OCT was performed, the significantly higher values of virtually all indexes of malapposition following DART in our study could reflect the occurrence of a positive vessel remodeling following DART.

The finding of high rates of uncovered and malapposed struts, the latter particularly in the DART group, have important implications since both have been linked to the occurrence of stent thrombosis in pathological and clinical studies [86, 134]. Although the relevance of isolated strut malapposition is still a matter of debate, flow disturbance and the resultant increase in shear rate along malapposed stent struts have been shown to be of relevance with regards to acute stent thrombogenicity in in-vitro models [135]. Considering that the long-term clinical outcomes of subintimal stenting remain poorly investigated, the most important therapeutic implications of

these findings relate to DAPT duration. Although no cases of stent thrombosis were registered in our study, all patients were still receiving DAPT at the time of angiographic follow-up.

5.5 Randomized comparison of vascular response to biodegradable-polymer sirolimus-eluting and durable-polymer everolimus-eluting stents

We observed the following salient findings at 6-8 months follow-up after PCI comparing BP-SES to PP-EES:

- the percentage of uncovered struts was similar in both BP-SES and PP-EES (neointimal tissue coverage in >84% in both groups) and did not differ significantly between BP-SES and PP-EES

- the number of malapposed struts was low in both groups without significant differences between the two stent types

- tissue coverage mainly consisted of immature neointima as evaluated by GSI analysis. Mature neointimal tissue was more frequently observed in BP-SES as compared to PP-EES, but without statistically significant differences between groups after adjustment for clustering effects.

In the present study, 15.8% of BP-SES struts and 17.4% of PP-EES struts remained uncovered after 6 months, while 14.3% vs. 20.0% of lesions showed at least 30% uncovered stent struts. The percentage of uncovered struts in both groups was higher when compared with previous studies [104, 106, 136]. A more conservative definition of strut coverage in our study could explain some of the differences in terms of stent coverage between studies. Neointimal thickness was overall very low in both DES (0.05 ± 0.08 mm in BP-SES vs. 0.08 ± 0.15 mm in PP-EES, p = 0.12) and without significant differences between both stent types in our study.

In the present study, we assessed neointimal maturity using an algorithm for OCT grey scale intensity analysis of neointimal tissue, which we previously validated after coregistration of OCT

with histology derived from preclinical models of chronic stent implantation and human autopsy specimens from patients after stent implantation. This novel methodology might provide important insights into vascular healing responses after PCI and was used in a prospective, randomized trial for the first time.

Neointimal maturity was comparably low at 6 months in both BP-SES and PP-EES exhibiting only 46.2% of mature tissue in BP-SES and 31.8% in PP-EES without significant differences between groups. Mature tissue revealed significantly higher smooth muscle cell content and lower proteoglycan/collagen, fibrin, and inflammatory cell content as compared with immature tissue regions by histopathologic assessment in our previous validation study [93]. Our findings support comparable neointimal healing patterns in both DES without unfavourable effects caused by polymer degradation in BP-SES and rather reflect the nature of delayed neointimal healing in the early phase of DES-based PCI, which is limited by anti-proliferative effects of drug elution.

5.6 Meta-analysis of optical coherence tomography studies comparing vascular response to biodegradable-polymer versus new-generation durable-polymer DES

The main findings of this meta-analysis can be summarized as follows:

- OCT performed at a median follow-up of 7 months displays decreased neointima growth and higher risk for uncovered struts after implantation of thick-strut BP-DES

- Overall, BP-DES are associated with higher incidence of malapposed struts as compared with new-generation DP-DES

BP-DES with polylactide-based carriers were developed to overcome the biological shortcomings of early-generation DP-DES [47]. Indeed, initial OCT-based studies documented a significant improvement in vessel healing with BP-DES compared to early-generation DP-DES [137]. More recently, however, OCT studies comparing BP-DES with new-generation DP-DES led to

disappointing results [104], questioning the role of BP-DES technology with respect to new-generation, more biocompatible DP-DES. In this study we report the largest population of PCI patients assigned to BP-DES or new-generation DP-DES with OCT imaging follow-up data. Despite overall BP-DES and new-generation DP-DES displayed comparable neointimal thickness at 7-month OCT imaging, there was a high heterogeneity for this risk estimate. Indeed, in the subgroup analyses we found that thick-strut, but not thin-strut, BP-DES displayed less neointimal thickness compared to new-generation DP-DES. Our analysis confirms that thin-strut stents allow for accelerated endothelial recovery, faster integration into the vessel wall and complete re-endothelization compared to thick-strut platforms [42, 138].

Lesions treated with BP-DES presented a greater prevalence of uncovered struts as compared to those treated with new-generation DP-DES. Notably, only one out of six trials available for this risk estimate studied thin-strut BP-DES vs. new-generation DP-DES [107].

Lesions treated with BP-DES showed a tendency towards increased risk for malapposition compared to those treated with new-generation DP-DES. The lack of OCT imaging at baseline precludes a distinction between acute and late acquired stent strut malapposition. The relative contribution to stent coverage and apposition of different combinations of antiproliferative drugs and dosages, variable absorption kinetics of polymer coatings and mechanical properties of underlying stent backbones remain unclear and our results highlight once more that DES performance depends on a complex interplay between the aforementioned components. Accordingly, we were unable to decipher whether the increased risk of stent strut malapposition observed with BP-DES as compared to new-generation DP-DES is a consequence of vascular toxicity of the eluted drug, analogous to early-generation DES, or to transient inflammation secondary to sustained degradation of certain biodegradable polymer formulations investigated in this report [139].

Finally, this analysis reaffirms the excellent healing profile of contemporary DP-DES, especially of those with a fluoro-passivated permanent polymer coating, which constituted the majority of implants in the comparator group analyzed in this study. The fluoro-passivation of the durable polymer coating [140] in conjuction with the high antiproliferative effect of everolimus [141] and a thin-strut platform likely contribute to the same extent to the unprecedented safety and efficacy of these implants which should be further regarded as a benchmark for future comparative studies of vascular healing following coronary stenting.

5.7 Influence of fully bioresorbable magnesium scaffolds as compared to conventional metallic DES and systemic statin treatment as compared to placebo on the development of neoatherosclerosis in a hypercholesterolemic animal model

The current study investigated the differential magnitude of neoatherosclerosis formation after implantation of fully bioresorbable magnesium-based scaffolds and permanent metallic DES of equivalent design and geometry in an animal model of in-stent neoatherosclerosis. Furthermore, it examined the impediment of neoatherosclerosis progression as a response to statin treatment relative to placebo in both stent types up to 161 days following study initiation. With regards to these study goals, the most salient findings can be described as follows:

- Magnesium based bioresorbable scaffolds showed decreased neointimal macrophage infiltration relative to stainless steel-based permanent DES after 161 days in an animal model of neoatherosclerosis.

- There was a significant interaction between stent type and treatment allocation to atorvastatin vs. placebo with regards to reduction of neointimal macrophage infiltration.

- Atorvastatin treatment significantly reduced progression of neointimal macrophage infiltration in BRS and DES, which was confirmed by histopathological assessment.

- Magnesium based bioresorbable scaffolds showed larger neointima burden as compared to 316L SS-equivalent DES

Development of neoatherosclerosis after stent-implantation has been recognized as an important contributor to late stent-failure [86, 142]. Notably, long-term follow-up of clinical trials investigating the comparative performance of early and newer generation DES reported sustained increase in clinical events irrespective of implanted stent type over time [143]. Short of mechanistic explanation for this late increment in adverse events, preclinical and postmortem autopsy studies suggested delayed arterial healing with sustained inflammatory reaction, delayed endothelialization and formation of in-stent neoatherosclerosis to be causative in the majority of cases. Consequently, bioresorbable scaffolds were introduced to overcome these inherent limitations associated with permanent metallic DES and proposed to reduce the burden of neoatherosclerosis owing to their temporary presence, where recovery of physiological vasomotion and normalization of flow dynamics were suggested to favorably impact on plaque progression over time. However, these anticipated effects of BRS technology have not been proven in clinical practice. Indeed, bioresorbable scaffold technology has recently suffered a major set-back after release of randomized controlled clinical trial data, which showed a significantly increase in revascularization and device thrombosis rate at longer-term follow up in broad patient subsets [25, 144]. Potential mechanisms of late scaffold failure have been investigated in dedicated registries using OCT to delineate vascular morphology and suggested late strut discontinuities, malapposition, neoatherosclerosis and underexpansion of the scaffold segment to be causally associated [145]. While most of these findings can be attributed to scaffold dismantling over time, neoatherosclerosis is not specifically linked to bioresorbable scaffold technology, and was indeed forecasted to be erased with the use of BRS. However, it may be speculated that prolonged inflammation of polymeric BRS during bioresorption may increase the risk of neoatherosclerosis, yet concrete evidence is lacking

to date. In our study, we observed decreased foam cell infiltration after implantation of magnesium-based BRS relative to permanent metallic DES, which may be secondary to accelerated vascular restoration (within 6 months) after magnesium-based BRS implantation relative to the 3-year time-frame observed with first generation polymeric BRS, return to physiologic flow conditions and accelerated recovery of functional endothelial barrier function. The fact that we observed increased foamy macrophage infiltration in DES relative to BRS further strengthens this hypothesis. Future studies are needed to specifically address these points.

Atorvastatin has previously been proven to result in decreased plaque formation in hypercholesterolemic rabbits [102, 146] and there is abundant evidence of its clinical efficacy from large randomized controlled trials [147]. Atorvastatin was found to result in a highly significant 72% decrease of iliac-femoral lesion size following balloon injury in hypercholesterolemic rabbits, which was mainly attributed to significant reduction of intimal macrophages [146]. In our study, atorvastatin relative to placebo therapy resulted in significantly diminished progression of neointimal foam cell infiltration, which was independent of underlying stent type. Future prospective randomized studies are consequently needed to address this important question.

One of the main drawbacks of preclinical studies however relates to the limited transferability of findings to human disease states. Thus, rigorous comparison and validation of diseased animal models with human pathology remains an important way to maximize applicability and clinical relevance. We have previously validated the currently applied animal model against human pathology and found excellent agreement with regards to depiction of early signs of neoatherosclerosis such as foam cell infiltration within the nascent neointima following stent implantation. On the other hand, limitations exist with regards to formation of advanced stages of neoatherosclerosis, which cannot sufficiently be reproduced in this animal model to date. However, as early stages of neoatherosclerosis can most reliably be detected by OCT (i.e. macrophage

infiltration), while advanced stages (i.e. fibroatheroma) are often difficult to discern owing to limited penetration depth of OCT light, the currently applied animal model may hold great potential to gain mechanistic understanding into pathophysiology and adoption of therapeutic strategies for the treatment of neoatherosclerosis.

6. SUMMARY OF FINDINGS

- Percutaneous coronary intervention represents a highly successful treatment for obstructive coronary artery disease and patients treated with new-generation DES show excellent outcomes over the short to medium term. The two major causes of stent failure are represented by stent thrombosis and in-stent restenosis and although the incidence of both has considerably decreased in recent years, the large number of patients implanted with coronary stents worldwide makes these conditions a significant health issue. Therefore, elucidation of the pathophysiological cascades leading to these modes of stent failure has the potential to translate into strategies aimed at avoiding their occurrence and optimizing their treatment.

- Optical coherence tomography is a novel light-based imaging modality which has recently become widely available for clinical use in cardiovascular medicine. Due to its unprecedented high spatial resolution (10-15 μm), this technique permits rapid evaluation of stent coverage and apposition as well as detailed characterization of neointimal tissue and vessel wall pathology. We applied intravascular optical coherence tomography in a series of preclinical and clinical studies aimed at unraveling the principal mechanisms of stent failure as well as in the evaluation of vessel healing following use of different stent platforms and revascularization techniques.

- In the multicenter PRESTIGE Registry, the largest of patients presenting with stent thrombosis in the literature to date and including a high proportion of new-generation DES, we showed that detailed analysis of OCT images acquired in the acute setting of stent thrombosis was feasible in the selected patients included in this registry. Both uncovered and malapposed struts were frequently observed and the prevalence of both decreased over

time, though more than half of lesions with very late stent thrombosis had frames with uncovered struts and more than a third had malapposed struts. Additionally, we found that rate of stent underexpansion was high across all groups and highest in patients with subacute stent thrombosis. Finally, the dominant etiological factor varied according to presentation: uncovered struts and underexpansion were most common in acute/subacute stent thrombosis and uncovered struts and neoatherosclerosis most common in late/very late stent thrombosis.

- Further analysis of the patient subgroup presenting with very late stent thrombosis, aimed at investigating timing, frequency and pathophysiological role of neoatherosclerosis, showed that in-stent plaque rupture represents a frequent and often fatal consequence of neoatherosclerosis formation in patients suffering very late stent thrombosis. Implantation of DES was independently associated with increased risk of neoatherosclerosis formation over time, while plaque rupture often occurred in patients with neoatherosclerosis and previous myocardial infarction. Macrophage infiltration within neointimal tissue was abundant in frames showing in-stent plaque rupture, whereas calcification was more frequent in frames without plaque rupture

- In a large registry including patients from 3 European centers who underwent intravascular OCT prior to PCI for in-stent restenosis, we found that ISR lesions display considerable intralesion neointimal heterogeneity. Grey scale signal intensity analysis of neointimal tissue, applied for the first time to the characterization of restenotic neointima, showed mean GSI values to significantly differ between neointimal categories, lending support to further investigation of this methodology as a quantitative tool of neointimal characterization. Additionally, we found that neoatherosclerotic changes are frequent in ISR lesions, show different time courses in DES as opposed to BMS and their presence and extent

appear to be time dependent phenomena. Finally, we found high rates of stent underexpansion ($\approx$ 50%) in patients presenting with ISR. Whether an intravascular OCT-guided treatment of ISR, based on the dominant neointimal type, can improve outcomes of patients presenting with ISR remains to be investigated in specifically designed clinical trials.

- The high rate of stent underexpansion in patients presenting with stent thrombosis as well as those with in-stent restenosis is a remarkable finding which deserves further comment. It points out the central role of suboptimal stent expansion in the pathogenesis of both modes of stent failure and highlights the need for intravascular imaging guided optimization of stent implantation during the index procedure as a mean to reduce the occurrence of both stent thrombosis and restenosis. Adequately powered, randomized clinical trials aimed at comparing OCT-guided and angiography-guided PCI in terms of hard clinical endpoints are already underway and will help to shed light on this issue.

- In the ISAR-OCT-CTO registry, the largest study to date to specifically compare both angiographic and intravascular OCT findings following intraplaque as opposed to subintimal CTO recanalization, we found that use of contemporary DART is associated with similar mid-term clinical and angiographic results compared to intraplaque recanalization techniques. We found high rates of both uncovered and malapposed struts following CTO recanalization, the latter particularly following subintimal recanalization of occluded vessels. The technique used to achieve vessel recanalization (intraplaque vs. subintimal) independently correlates with strut malapposition, but not with strut coverage.

- In the randomized ORSIRO-OCT trial we found that neointimal coverage in BP-SES was comparable to DP-EES and averaged 83 % at 6-months of follow-up, whereas neointimal

tissue was identified as mostly immature in both DES types by OCT with a trend to more mature tissue in BP-SES at 6 months of follow-up

- In a meta-analysis of study-level data from 10 trials in which follow-up OCT imaging was used to assess vascular healing following implantation of BP-DES as opposed to new-generation DP-DES, we found that BP-DES, particularly those with thicker backbones, delay vascular healing as compared to new-generation DP-DES. The higher risk for strut malapposition observed with BP-DES as compared to new-generation DP-DES represents an important finding which requires further investigation.

- Finally, we compared the effect of stent type (bioresorbable magnesium-based scaffolds and permanent metallic DES of equivalent design and geometry) as well as statin treatment (atorvastatin vs. placebo) in an animal model of in-stent neoatherosclerosis. We found that magnesium-based bioresorbable scaffolds are characterized by decreased neointimal macrophage infiltration relative to stainless steel-based permanent DES. Additionally, atorvastatin treatment significantly reduced progression of neointimal macrophage infiltration in BRS and DES, as confirmed by histopathological assessment

7. SOURCES OF FUNDING

8. REFERENCES

1.   Gruntzig A. Transluminal dilatation of coronary-artery stenosis. *Lancet*. 1978;1:263.

2.   Byrne RA, Stone GW, Ormiston J and Kastrati A. Coronary balloon angioplasty, stents, and scaffolds. *Lancet*. 2017;390:781-792.

3.   Puel J, Joffre F, Rousseau H, Guermonprez JL, Lancelin B, Morice MC, Valeix B, Imbert C and Bounhoure JP. [Self-expanding coronary endoprosthesis in the prevention of restenosis following transluminal angioplasty. Preliminary clinical study]. *Arch Mal Coeur Vaiss*. 1987;80:1311-2.

4.   Sigwart U, Puel J, Mirkovitch V, Joffre F and Kappenberger L. Intravascular stents to prevent occlusion and restenosis after transluminal angioplasty. *N Engl J Med*. 1987;316:701-6.

5.   Serruys PW, de Jaegere P, Kiemeneij F, Macaya C, Rutsch W, Heyndrickx G, Emanuelsson H, Marco J, Legrand V, Materne P and et al. A comparison of balloon-expandable-stent implantation with balloon angioplasty in patients with coronary artery disease. Benestent Study Group. *N Engl J Med*. 1994;331:489-95.

6.   Fischman DL, Leon MB, Baim DS, Schatz RA, Savage MP, Penn I, Detre K, Veltri L, Ricci D, Nobuyoshi M and et al. A randomized comparison of coronary-stent placement and balloon angioplasty in the treatment of coronary artery disease. Stent Restenosis Study Investigators. *N Engl J Med*. 1994;331:496-501.

7.   Schomig A, Neumann FJ, Kastrati A, Schuhlen H, Blasini R, Hadamitzky M, Walter H, Zitzmann-Roth EM, Richardt G, Alt E, Schmitt C and Ulm K. A randomized comparison of antiplatelet and anticoagulant therapy after the placement of coronary-artery stents. *N Engl J Med*. 1996;334:1084-9.

8.   Leon MB, Baim DS, Popma JJ, Gordon PC, Cutlip DE, Ho KK, Giambartolomei A, Diver DJ, Lasorda DM, Williams DO, Pocock SJ and Kuntz RE. A clinical trial comparing three antithrombotic-

drug regimens after coronary-artery stenting. Stent Anticoagulation Restenosis Study Investigators. *N Engl J Med*. 1998;339:1665-71.

9.   Stettler C, Wandel S, Allemann S, Kastrati A, Morice MC, Schomig A, Pfisterer ME, Stone GW, Leon MB, de Lezo JS, Goy JJ, Park SJ, Sabate M, Suttorp MJ, Kelbaek H, Spaulding C, Menichelli M, Vermeersch P, Dirksen MT, Cervinka P, Petronio AS, Nordmann AJ, Diem P, Meier B, Zwahlen M, Reichenbach S, Trelle S, Windecker S and Juni P. Outcomes associated with drug-eluting and bare-metal stents: a collaborative network meta-analysis. *Lancet*. 2007;370:937-48.

10.   Finn AV, Nakazawa G, Joner M, Kolodgie FD, Mont EK, Gold HK and Virmani R. Vascular responses to drug eluting stents: importance of delayed healing. *Arterioscler Thromb Vasc Biol*. 2007;27:1500-10.

11.   Commandeur S, van Beusekom HM and van der Giessen WJ. Polymers, drug release, and drug-eluting stents. *J Interv Cardiol*. 2006;19:500-6.

12.   Pendyala L, Jabara R, Robinson K and Chronos N. Passive and active polymer coatings for intracoronary stents: novel devices to promote arterial healing. *J Interv Cardiol*. 2009;22:37-48.

13.   Vorpahl M, Finn AV, Nakano M and Virmani R. The bioabsorption process: tissue and cellular mechanisms and outcomes. *EuroIntervention*. 2009;5 Suppl F:F28-35.

14.   Navarese EP, Tandjung K, Claessen B, Andreotti F, Kowalewski M, Kandzari DE, Kereiakes DJ, Waksman R, Mauri L, Meredith IT, Finn AV, Kim HS, Kubica J, Suryapranata H, Aprami TM, Di Pasquale G, von Birgelen C and Kedhi E. Safety and efficacy outcomes of first and second generation durable polymer drug eluting stents and biodegradable polymer biolimus eluting stents in clinical practice: comprehensive network meta-analysis. *BMJ*. 2013;347:f6530.

15.   Stefanini GG, Byrne RA, Serruys PW, de Waha A, Meier B, Massberg S, Juni P, Schomig A, Windecker S and Kastrati A. Biodegradable polymer drug-eluting stents reduce the risk of stent thrombosis at 4 years in patients undergoing percutaneous coronary intervention: a pooled

analysis of individual patient data from the ISAR-TEST 3, ISAR-TEST 4, and LEADERS randomized trials. *Eur Heart J*. 2012;33:1214-22.

16.   Kang SH, Park KW, Kang DY, Lim WH, Park KT, Han JK, Kang HJ, Koo BK, Oh BH, Park YB, Kandzari DE, Cohen DJ, Hwang SS and Kim HS. Biodegradable-polymer drug-eluting stents vs. bare metal stents vs. durable-polymer drug-eluting stents: a systematic review and Bayesian approach network meta-analysis. *Eur Heart J*. 2014;35:1147-58.

17.   Palmerini T, Biondi-Zoccai G, Della Riva D, Mariani A, Sabate M, Smits PC, Kaiser C, D'Ascenzo F, Frati G, Mancone M, Genereux P and Stone GW. Clinical outcomes with bioabsorbable polymer- versus durable polymer-based drug-eluting and bare-metal stents: evidence from a comprehensive network meta-analysis. *J Am Coll Cardiol*. 2014;63:299-307.

18.   El-Hayek G, Bangalore S, Casso Dominguez A, Devireddy C, Jaber W, Kumar G, Mavromatis K, Tamis-Holland J and Samady H. Meta-Analysis of Randomized Clinical Trials Comparing Biodegradable Polymer Drug-Eluting Stent to Second-Generation Durable Polymer Drug-Eluting Stents. *JACC Cardiovasc Interv*. 2017;10:462-473.

19.   Kufner S, Joner M, Thannheimer A, Hoppmann P, Ibrahim T, Mayer K, Cassese S, Laugwitz KL, Schunkert H, Kastrati A, Byrne RA and Investigators I-T. Ten-Year Clinical Outcomes From a Trial of Three Limus-Eluting Stents With Different Polymer Coatings in Patients With Coronary Artery Disease. *Circulation*. 2019;139:325-333.

20.   Serruys PW, Onuma Y, Dudek D, Smits PC, Koolen J, Chevalier B, de Bruyne B, Thuesen L, McClean D, van Geuns RJ, Windecker S, Whitbourn R, Meredith I, Dorange C, Veldhof S, Hebert KM, Sudhir K, Garcia-Garcia HM and Ormiston JA. Evaluation of the second generation of a bioresorbable everolimus-eluting vascular scaffold for the treatment of de novo coronary artery stenosis: 12-month clinical and imaging outcomes. *J Am Coll Cardiol*. 2011;58:1578-88.

21.   Serruys PW, Onuma Y, Ormiston JA, de Bruyne B, Regar E, Dudek D, Thuesen L, Smits PC, Chevalier B, McClean D, Koolen J, Windecker S, Whitbourn R, Meredith I, Dorange C, Veldhof S, Miquel-Hebert K, Rapoza R and Garcia-Garcia HM. Evaluation of the second generation of a bioresorbable everolimus drug-eluting vascular scaffold for treatment of de novo coronary artery stenosis: six-month clinical and imaging outcomes. *Circulation*. 2010;122:2301-12.

22.   Ellis SG, Kereiakes DJ, Metzger DC, Caputo RP, Rizik DG, Teirstein PS, Litt MR, Kini A, Kabour A, Marx SO, Popma JJ, McGreevy R, Zhang Z, Simonton C, Stone GW and Investigators AI. Everolimus-Eluting Bioresorbable Scaffolds for Coronary Artery Disease. *N Engl J Med*. 2015;373:1905-15.

23.   Cassese S, Byrne RA, Ndrepepa G, Kufner S, Wiebe J, Repp J, Schunkert H, Fusaro M, Kimura T and Kastrati A. Everolimus-eluting bioresorbable vascular scaffolds versus everolimus-eluting metallic stents: a meta-analysis of randomised controlled trials. *Lancet*. 2016;387:537-44.

24.   Serruys PW, Chevalier B, Sotomi Y, Cequier A, Carrie D, Piek JJ, Van Boven AJ, Dominici M, Dudek D, McClean D, Helqvist S, Haude M, Reith S, de Sousa Almeida M, Campo G, Iniguez A, Sabate M, Windecker S and Onuma Y. Comparison of an everolimus-eluting bioresorbable scaffold with an everolimus-eluting metallic stent for the treatment of coronary artery stenosis (ABSORB II): a 3 year, randomised, controlled, single-blind, multicentre clinical trial. *Lancet*. 2016;388:2479-2491.

25.   Wykrzykowska JJ, Kraak RP, Hofma SH, van der Schaaf RJ, Arkenbout EK, AJ IJ, Elias J, van Dongen IM, Tijssen RYG, Koch KT, Baan J, Jr., Vis MM, de Winter RJ, Piek JJ, Tijssen JGP, Henriques JPS and Investigators A. Bioresorbable Scaffolds versus Metallic Stents in Routine PCI. *N Engl J Med*. 2017;376:2319-2328.

26.   Ali ZA, Serruys PW, Kimura T, Gao R, Ellis SG, Kereiakes DJ, Onuma Y, Simonton C, Zhang Z and Stone GW. 2-year outcomes with the Absorb bioresorbable scaffold for treatment of coronary

artery disease: a systematic review and meta-analysis of seven randomised trials with an individual patient data substudy. *Lancet*. 2017;390:760-772.

27.   Haude M, Ince H, Abizaid A, Toelg R, Lemos PA, von Birgelen C, Christiansen EH, Wijns W, Neumann FJ, Kaiser C, Eeckhout E, Lim ST, Escaned J, Onuma Y, Garcia-Garcia HM and Waksman R. Sustained safety and performance of the second-generation drug-eluting absorbable metal scaffold in patients with de novo coronary lesions: 12-month clinical results and angiographic findings of the BIOSOLVE-II first-in-man trial. *Eur Heart J*. 2016;37:2701-9.

28.   Jinnouchi H, Torii S, Sakamoto A, Kolodgie FD, Virmani R and Finn AV. Fully bioresorbable vascular scaffolds: lessons learned and future directions. *Nat Rev Cardiol*. 2019;16:286-304.

29.   Wittchow E, Adden N, Riedmuller J, Savard C, Waksman R and Braune M. Bioresorbable drug-eluting magnesium-alloy scaffold: design and feasibility in a porcine coronary model. *EuroIntervention*. 2013;8:1441-50.

30.   Schulz S, Schuster T, Mehilli J, Byrne RA, Ellert J, Massberg S, Goedel J, Bruskina O, Ulm K, Schomig A and Kastrati A. Stent thrombosis after drug-eluting stent implantation: incidence, timing, and relation to discontinuation of clopidogrel therapy over a 4-year period. *Eur Heart J*. 2009;30:2714-21.

31.   Armstrong EJ, Feldman DN, Wang TY, Kaltenbach LA, Yeo KK, Wong SC, Spertus J, Shaw RE, Minutello RM, Moussa I, Ho KK, Rogers JH and Shunk KA. Clinical presentation, management, and outcomes of angiographically documented early, late, and very late stent thrombosis. *JACC Cardiovasc Interv*. 2012;5:131-40.

32.   Tada T, Byrne RA, Simunovic I, King LA, Cassese S, Joner M, Fusaro M, Schneider S, Schulz S, Ibrahim T, Ott I, Massberg S, Laugwitz KL and Kastrati A. Risk of stent thrombosis among bare-metal stents, first-generation drug-eluting stents, and second-generation drug-eluting stents: results from a registry of 18,334 patients. *JACC Cardiovasc Interv*. 2013;6:1267-74.

33.   Raber L, Magro M, Stefanini GG, Kalesan B, van Domburg RT, Onuma Y, Wenaweser P, Daemen J, Meier B, Juni P, Serruys PW and Windecker S. Very late coronary stent thrombosis of a newer-generation everolimus-eluting stent compared with early-generation drug-eluting stents: a prospective cohort study. *Circulation*. 2012;125:1110-21.

34.   Stone GW, Witzenbichler B, Weisz G, Rinaldi MJ, Neumann FJ, Metzger DC, Henry TD, Cox DA, Duffy PL, Mazzaferri E, Gurbel PA, Xu K, Parise H, Kirtane AJ, Brodie BR, Mehran R, Stuckey TD and Investigators A-D. Platelet reactivity and clinical outcomes after coronary artery implantation of drug-eluting stents (ADAPT-DES): a prospective multicentre registry study. *Lancet*. 2013;382:614-23.

35.   Byrne RA, Serruys PW, Baumbach A, Escaned J, Fajadet J, James S, Joner M, Oktay S, Juni P, Kastrati A, Sianos G, Stefanini GG, Wijns W and Windecker S. Report of a European Society of Cardiology-European Association of Percutaneous Cardiovascular Interventions task force on the evaluation of coronary stents in Europe: executive summary. *Eur Heart J*. 2015;36:2608-20.

36.   Cutlip DE, Windecker S, Mehran R, Boam A, Cohen DJ, van Es GA, Steg PG, Morel MA, Mauri L, Vranckx P, McFadden E, Lansky A, Hamon M, Krucoff MW, Serruys PW and Academic Research C. Clinical end points in coronary stent trials: a case for standardized definitions. *Circulation*. 2007;115:2344-51.

37.   Byrne RA, Joner M and Kastrati A. Stent thrombosis and restenosis: what have we learned and where are we going? The Andreas Gruntzig Lecture ESC 2014. *Eur Heart J*. 2015;36:3320-31.

38.   Kimura T, Morimoto T, Kozuma K, Honda Y, Kume T, Aizawa T, Mitsudo K, Miyazaki S, Yamaguchi T, Hiyoshi E, Nishimura E, Isshiki T and Investigators R. Comparisons of baseline demographics, clinical presentation, and long-term outcome among patients with early, late, and very late stent thrombosis of sirolimus-eluting stents: Observations from the Registry of Stent Thrombosis for Review and Reevaluation (RESTART). *Circulation*. 2010;122:52-61.

39.   van Werkum JW, Heestermans AA, Zomer AC, Kelder JC, Suttorp MJ, Rensing BJ, Koolen JJ, Brueren BR, Dambrink JH, Hautvast RW, Verheugt FW and ten Berg JM. Predictors of coronary stent thrombosis: the Dutch Stent Thrombosis Registry. *J Am Coll Cardiol*. 2009;53:1399-409.

40.   Iakovou I, Schmidt T, Bonizzoni E, Ge L, Sangiorgi GM, Stankovic G, Airoldi F, Chieffo A, Montorfano M, Carlino M, Michev I, Corvaja N, Briguori C, Gerckens U, Grube E and Colombo A. Incidence, predictors, and outcome of thrombosis after successful implantation of drug-eluting stents. *JAMA*. 2005;293:2126-30.

41.   Kastrati A, Mehilli J, Pache J, Kaiser C, Valgimigli M, Kelbaek H, Menichelli M, Sabate M, Suttorp MJ, Baumgart D, Seyfarth M, Pfisterer ME and Schomig A. Analysis of 14 trials comparing sirolimus-eluting stents with bare-metal stents. *N Engl J Med*. 2007;356:1030-9.

42.   Kolandaivelu K, Swaminathan R, Gibson WJ, Kolachalama VB, Nguyen-Ehrenreich KL, Giddings VL, Coleman L, Wong GK and Edelman ER. Stent thrombogenicity early in high-risk interventional settings is driven by stent design and deployment and protected by polymer-drug coatings. *Circulation*. 2011;123:1400-9.

43.   Attizzani GF, Capodanno D, Ohno Y and Tamburino C. Mechanisms, pathophysiology, and clinical aspects of incomplete stent apposition. *J Am Coll Cardiol*. 2014;63:1355-67.

44.   Foin N, Gutierrez-Chico JL, Nakatani S, Torii R, Bourantas CV, Sen S, Nijjer S, Petraco R, Kousera C, Ghione M, Onuma Y, Garcia-Garcia HM, Francis DP, Wong P, Di Mario C, Davies JE and Serruys PW. Incomplete stent apposition causes high shear flow disturbances and delay in neointimal coverage as a function of strut to wall detachment distance: implications for the management of incomplete stent apposition. *Circ Cardiovasc Interv*. 2014;7:180-9.

45.   Stone GW, Moses JW, Ellis SG, Schofer J, Dawkins KD, Morice MC, Colombo A, Schampaert E, Grube E, Kirtane AJ, Cutlip DE, Fahy M, Pocock SJ, Mehran R and Leon MB. Safety and efficacy of sirolimus- and paclitaxel-eluting coronary stents. *N Engl J Med*. 2007;356:998-1008.

46. Joner M, Finn AV, Farb A, Mont EK, Kolodgie FD, Ladich E, Kutys R, Skorija K, Gold HK and Virmani R. Pathology of drug-eluting stents in humans: delayed healing and late thrombotic risk. *J Am Coll Cardiol*. 2006;48:193-202.

47. Byrne RA, Joner M and Kastrati A. Polymer coatings and delayed arterial healing following drug-eluting stent implantation. *Minerva Cardioangiol*. 2009;57:567-84.

48. Luscher TF, Steffel J, Eberli FR, Joner M, Nakazawa G, Tanner FC and Virmani R. Drug-eluting stent and coronary thrombosis: biological mechanisms and clinical implications. *Circulation*. 2007;115:1051-8.

49. Togni M, Raber L, Cocchia R, Wenaweser P, Cook S, Windecker S, Meier B and Hess OM. Local vascular dysfunction after coronary paclitaxel-eluting stent implantation. *Int J Cardiol*. 2007;120:212-20.

50. Otsuka F, Byrne RA, Yahagi K, Mori H, Ladich E, Fowler DR, Kutys R, Xhepa E, Kastrati A, Virmani R and Joner M. Neoatherosclerosis: overview of histopathologic findings and implications for intravascular imaging assessment. *Eur Heart J*. 2015;36:2147-59.

51. Acharya G and Park K. Mechanisms of controlled drug release from drug-eluting stents. *Adv Drug Deliv Rev*. 2006;58:387-401.

52. Cassese S, Byrne RA, Tada T, Pinieck S, Joner M, Ibrahim T, King LA, Fusaro M, Laugwitz KL and Kastrati A. Incidence and predictors of restenosis after coronary stenting in 10 004 patients with surveillance angiography. *Heart*. 2014;100:153-9.

53. Raungaard B, Jensen LO, Tilsted HH, Christiansen EH, Maeng M, Terkelsen CJ, Krusell LR, Kaltoft A, Kristensen SD, Botker HE, Thuesen L, Aaroe J, Jensen SE, Villadsen AB, Thayssen P, Veien KT, Hansen KN, Junker A, Madsen M, Ravkilde J, Lassen JF and Scandinavian Organization for Randomized Trials with Clinical O. Zotarolimus-eluting durable-polymer-coated stent versus a biolimus-eluting biodegradable-polymer-coated stent in unselected patients undergoing

percutaneous coronary intervention (SORT OUT VI): a randomised non-inferiority trial. *Lancet*. 2015;385:1527-35.

54.   Kastrati A, Schomig A, Dietz R, Neumann FJ and Richardt G. Time course of restenosis during the first year after emergency coronary stenting. *Circulation*. 1993;87:1498-505.

55.   Kimura T, Yokoi H, Nakagawa Y, Tamura T, Kaburagi S, Sawada Y, Sato Y, Yokoi H, Hamasaki N, Nosaka H and et al. Three-year follow-up after implantation of metallic coronary-artery stents. *N Engl J Med*. 1996;334:561-6.

56.   Byrne RA, Iijima R, Mehilli J, Pinieck S, Bruskina O, Schomig A and Kastrati A. Durability of antirestenotic efficacy in drug-eluting stents with and without permanent polymer. *JACC Cardiovasc Interv*. 2009;2:291-9.

57.   Raber L, Wohlwend L, Wigger M, Togni M, Wandel S, Wenaweser P, Cook S, Moschovitis A, Vogel R, Kalesan B, Seiler C, Eberli F, Luscher TF, Meier B, Juni P and Windecker S. Five-year clinical and angiographic outcomes of a randomized comparison of sirolimus-eluting and paclitaxel-eluting stents: results of the Sirolimus-Eluting Versus Paclitaxel-Eluting Stents for Coronary Revascularization LATE trial. *Circulation*. 2011;123:2819-28, 6 p following 2828.

58.   Cassese S, Byrne RA, Schulz S, Hoppman P, Kreutzer J, Feuchtenberger A, Ibrahim T, Ott I, Fusaro M, Schunkert H, Laugwitz KL and Kastrati A. Prognostic role of restenosis in 10 004 patients undergoing routine control angiography after coronary stenting. *Eur Heart J*. 2015;36:94-9.

59.   Pache J, Kastrati A, Mehilli J, Schuhlen H, Dotzer F, Hausleiter J, Fleckenstein M, Neumann FJ, Sattelberger U, Schmitt C, Muller M, Dirschinger J and Schomig A. Intracoronary stenting and angiographic results: strut thickness effect on restenosis outcome (ISAR-STEREO-2) trial. *J Am Coll Cardiol*. 2003;41:1283-8.

60.   Alfonso F, Byrne RA, Rivero F and Kastrati A. Current treatment of in-stent restenosis. *J Am Coll Cardiol*. 2014;63:2659-73.

61.   Siontis GC, Stefanini GG, Mavridis D, Siontis KC, Alfonso F, Perez-Vizcayno MJ, Byrne RA, Kastrati A, Meier B, Salanti G, Juni P and Windecker S. Percutaneous coronary interventional strategies for treatment of in-stent restenosis: a network meta-analysis. *Lancet*. 2015;386:655-64.

62.   Kufner S, Joner M, Schneider S, Tolg R, Zrenner B, Repp J, Starkmann A, Xhepa E, Ibrahim T, Cassese S, Fusaro M, Ott I, Hengstenberg C, Schunkert H, Abdel-Wahab M, Laugwitz KL, Kastrati A, Byrne RA and Investigators I-D. Neointimal Modification With Scoring Balloon and Efficacy of Drug-Coated Balloon Therapy in Patients With Restenosis in Drug-Eluting Coronary Stents: A Randomized Controlled Trial. *JACC Cardiovasc Interv*. 2017;10:1332-1340.

63.   Nakazawa G, Otsuka F, Nakano M, Vorpahl M, Yazdani SK, Ladich E, Kolodgie FD, Finn AV and Virmani R. The pathology of neoatherosclerosis in human coronary implants bare-metal and drug-eluting stents. *J Am Coll Cardiol*. 2011;57:1314-22.

64.   Falk E, Nakano M, Bentzon JF, Finn AV and Virmani R. Update on acute coronary syndromes: the pathologists' view. *Eur Heart J*. 2013;34:719-28.

65.   Otsuka F, Vorpahl M, Nakano M, Foerst J, Newell JB, Sakakura K, Kutys R, Ladich E, Finn AV, Kolodgie FD and Virmani R. Pathology of second-generation everolimus-eluting stents versus first-generation sirolimus- and paclitaxel-eluting stents in humans. *Circulation*. 2014;129:211-23.

66.   Joner M, Nakazawa G, Finn AV, Quee SC, Coleman L, Acampado E, Wilson PS, Skorija K, Cheng Q, Xu X, Gold HK, Kolodgie FD and Virmani R. Endothelial cell recovery between comparator polymer-based drug-eluting stents. *J Am Coll Cardiol*. 2008;52:333-42.

67.   Nakazawa G, Nakano M, Otsuka F, Wilcox JN, Melder R, Pruitt S, Kolodgie FD and Virmani R. Evaluation of polymer-based comparator drug-eluting stents using a rabbit model of iliac artery atherosclerosis. *Circ Cardiovasc Interv*. 2011;4:38-46.

68.   Otsuka F, Finn AV, Yazdani SK, Nakano M, Kolodgie FD and Virmani R. The importance of the endothelium in atherothrombosis and coronary stenting. *Nat Rev Cardiol*. 2012;9:439-53.

69.   Nicol P, Xhepa E, Bozhko D and Joner M. Neoatherosclerosis: from basic principles to intravascular imaging. *Minerva Cardioangiol*. 2018;66:292-300.

70.   Mintz GS and Guagliumi G. Intravascular imaging in coronary artery disease. *Lancet*. 2017;390:793-809.

71.   Tearney GJ, Jang IK, Kang DH, Aretz HT, Houser SL, Brady TJ, Schlendorf K, Shishkov M and Bouma BE. Porcine coronary imaging in vivo by optical coherence tomography. *Acta Cardiol*. 2000;55:233-7.

72.   Yabushita H, Bouma BE, Houser SL, Aretz HT, Jang IK, Schlendorf KH, Kauffman CR, Shishkov M, Kang DH, Halpern EF and Tearney GJ. Characterization of human atherosclerosis by optical coherence tomography. *Circulation*. 2002;106:1640-5.

73.   Jang IK, Bouma BE, Kang DH, Park SJ, Park SW, Seung KB, Choi KB, Shishkov M, Schlendorf K, Pomerantsev E, Houser SL, Aretz HT and Tearney GJ. Visualization of coronary atherosclerotic plaques in patients using optical coherence tomography: comparison with intravascular ultrasound. *J Am Coll Cardiol*. 2002;39:604-9.

74.   Jang IK, Tearney G and Bouma B. Visualization of tissue prolapse between coronary stent struts by optical coherence tomography: comparison with intravascular ultrasound. *Circulation*. 2001;104:2754.

75.   Grube E, Gerckens U, Buellesfeld L and Fitzgerald PJ. Images in cardiovascular medicine. Intracoronary imaging with optical coherence tomography: a new high-resolution technology providing striking visualization in the coronary artery. *Circulation*. 2002;106:2409-10.

76.   Low AF, Tearney GJ, Bouma BE and Jang IK. Technology Insight: optical coherence tomography--current status and future development. *Nat Clin Pract Cardiovasc Med*. 2006;3:154-62; quiz 172.

77.   Suter MJ, Nadkarni SK, Weisz G, Tanaka A, Jaffer FA, Bouma BE and Tearney GJ. Intravascular optical imaging technology for investigating the coronary artery. *JACC Cardiovasc Imaging*. 2011;4:1022-39.

78.   Tearney GJ, Yabushita H, Houser SL, Aretz HT, Jang IK, Schlendorf KH, Kauffman CR, Shishkov M, Halpern EF and Bouma BE. Quantification of macrophage content in atherosclerotic plaques by optical coherence tomography. *Circulation*. 2003;107:113-9.

79.   Kume T, Akasaka T, Kawamoto T, Watanabe N, Toyota E, Neishi Y, Sukmawan R, Sadahira Y and Yoshida K. Assessment of coronary arterial plaque by optical coherence tomography. *Am J Cardiol*. 2006;97:1172-5.

80.   Rieber J, Meissner O, Babaryka G, Reim S, Oswald M, Koenig A, Schiele TM, Shapiro M, Theisen K, Reiser MF, Klauss V and Hoffmann U. Diagnostic accuracy of optical coherence tomography and intravascular ultrasound for the detection and characterization of atherosclerotic plaque composition in ex-vivo coronary specimens: a comparison with histology. *Coron Artery Dis*. 2006;17:425-30.

81.   MacNeill BD, Jang IK, Bouma BE, Iftimia N, Takano M, Yabushita H, Shishkov M, Kauffman CR, Houser SL, Aretz HT, DeJoseph D, Halpern EF and Tearney GJ. Focal and multi-focal plaque macrophage distributions in patients with acute and stable presentations of coronary artery disease. *J Am Coll Cardiol*. 2004;44:972-9.

82.   Tearney GJ, Jang IK and Bouma BE. Optical coherence tomography for imaging the vulnerable plaque. *J Biomed Opt*. 2006;11:021002.

83.   Kume T, Akasaka T, Kawamoto T, Ogasawara Y, Watanabe N, Toyota E, Neishi Y, Sukmawan R, Sadahira Y and Yoshida K. Assessment of coronary arterial thrombus by optical coherence tomography. *Am J Cardiol*. 2006;97:1713-7.

84.   Kume T, Okura H, Kawamoto T, Akasaka T, Toyota E, Watanabe N, Neishi Y, Sukmawan R, Sadahira Y and Yoshida K. Relationship between coronary remodeling and plaque characterization in patients without clinical evidence of coronary artery disease. *Atherosclerosis*. 2008;197:799-805.

85.   Tearney GJ, Regar E, Akasaka T, Adriaenssens T, Barlis P, Bezerra HG, Bouma B, Bruining N, Cho JM, Chowdhary S, Costa MA, de Silva R, Dijkstra J, Di Mario C, Dudek D, Falk E, Feldman MD, Fitzgerald P, Garcia-Garcia HM, Gonzalo N, Granada JF, Guagliumi G, Holm NR, Honda Y, Ikeno F, Kawasaki M, Kochman J, Koltowski L, Kubo T, Kume T, Kyono H, Lam CC, Lamouche G, Lee DP, Leon MB, Maehara A, Manfrini O, Mintz GS, Mizuno K, Morel MA, Nadkarni S, Okura H, Otake H, Pietrasik A, Prati F, Raber L, Radu MD, Rieber J, Riga M, Rollins A, Rosenberg M, Sirbu V, Serruys PW, Shimada K, Shinke T, Shite J, Siegel E, Sonoda S, Suter M, Takarada S, Tanaka A, Terashima M, Thim T, Uemura S, Ughi GJ, van Beusekom HM, van der Steen AF, van Es GA, van Soest G, Virmani R, Waxman S, Weissman NJ, Weisz G and International Working Group for Intravascular Optical Coherence T. Consensus standards for acquisition, measurement, and reporting of intravascular optical coherence tomography studies: a report from the International Working Group for Intravascular Optical Coherence Tomography Standardization and Validation. *J Am Coll Cardiol*. 2012;59:1058-72.

86.   Adriaenssens T, Joner M, Godschalk TC, Malik N, Alfonso F, Xhepa E, De Cock D, Komukai K, Tada T, Cuesta J, Sirbu V, Feldman LJ, Neumann FJ, Goodall AH, Heestermans T, Buysschaert I, Hlinomaz O, Belmans A, Desmet W, Ten Berg JM, Gershlick AH, Massberg S, Kastrati A, Guagliumi G, Byrne RA and Prevention of Late Stent Thrombosis by an Interdisciplinary Global European Effort I. Optical Coherence Tomography Findings in Patients With Coronary Stent Thrombosis: A Report of the PRESTIGE Consortium (Prevention of Late Stent Thrombosis by an Interdisciplinary Global European Effort). *Circulation*. 2017;136:1007-1021.

87.   Nakatani S, Sotomi Y, Ishibashi Y, Grundeken MJ, Tateishi H, Tenekecioglu E, Zeng Y, Suwannasom P, Regar E, Radu MD, Raber L, Bezerra H, Costa MA, Fitzgerald P, Prati F, Costa RA, Dijkstra J, Kimura T, Kozuma K, Tanabe K, Akasaka T, Di Mario C, Serruys PW and Onuma Y. Comparative analysis method of permanent metallic stents (XIENCE) and bioresorbable poly-L-lactic (PLLA) scaffolds (Absorb) on optical coherence tomography at baseline and follow-up. *EuroIntervention*. 2016;12:1498-1509.

88.   Nakano M, Vorpahl M, Otsuka F, Taniwaki M, Yazdani SK, Finn AV, Ladich ER, Kolodgie FD and Virmani R. Ex vivo assessment of vascular response to coronary stents by optical frequency domain imaging. *JACC Cardiovasc Imaging*. 2012;5:71-82.

89.   Bland JM and Altman DG. Measuring agreement in method comparison studies. *Stat Methods Med Res*. 1999;8:135-60.

90.   Shrout PE and Fleiss JL. Intraclass correlations: uses in assessing rater reliability. *Psychol Bull*. 1979;86:420-8.

91.   Mehran R, Dangas G, Abizaid AS, Mintz GS, Lansky AJ, Satler LF, Pichard AD, Kent KM, Stone GW and Leon MB. Angiographic patterns of in-stent restenosis: classification and implications for long-term outcome. *Circulation*. 1999;100:1872-8.

92.   Xhepa E, Byrne RA, Rivero F, Rroku A, Cuesta J, Ndrepepa G, Kufner S, Valiente TB, Cassese S, Garcia-Guimaraes M, Lahmann AL, Rai H, Schunkert H, Joner M, Perez-Vizcayno MJ, Gonzalo N, Alfonso F and Kastrati A. Qualitative and quantitative neointimal characterization by optical coherence tomography in patients presenting with in-stent restenosis. *Clin Res Cardiol*. 2019.

93.   Malle C, Tada T, Steigerwald K, Ughi GJ, Schuster T, Nakano M, Massberg S, Jehle J, Guagliumi G, Kastrati A, Virmani R, Byrne RA and Joner M. Tissue characterization after drug-eluting stent implantation using optical coherence tomography. *Arterioscler Thromb Vasc Biol*. 2013;33:1376-83.

94.	Koppara T, Tada T, Xhepa E, Kufner S, Byrne RA, Ibrahim T, Laugwitz KL, Kastrati A and Joner M. Randomised comparison of vascular response to biodegradable polymer sirolimus eluting and permanent polymer everolimus eluting stents: An optical coherence tomography study. *Int J Cardiol*. 2018;258:42-49.

95.	Tibshirani R. The lasso method for variable selection in the Cox model. *Stat Med*. 1997;16:385-95.

96.	Morino Y, Abe M, Morimoto T, Kimura T, Hayashi Y, Muramatsu T, Ochiai M, Noguchi Y, Kato K, Shibata Y, Hiasa Y, Doi O, Yamashita T, Hinohara T, Tanaka H, Mitsudo K and Investigators JCR. Predicting successful guidewire crossing through chronic total occlusion of native coronary lesions within 30 minutes: the J-CTO (Multicenter CTO Registry in Japan) score as a difficulty grading and time assessment tool. *JACC Cardiovasc Interv*. 2011;4:213-21.

97.	Higgins JP, Altman DG, Gotzsche PC, Juni P, Moher D, Oxman AD, Savovic J, Schulz KF, Weeks L, Sterne JA, Cochrane Bias Methods G and Cochrane Statistical Methods G. The Cochrane Collaboration's tool for assessing risk of bias in randomised trials. *BMJ*. 2011;343:d5928.

98.	Higgins JP, Thompson SG, Deeks JJ and Altman DG. Measuring inconsistency in meta-analyses. *BMJ*. 2003;327:557-60.

99.	Egger M, Davey Smith G, Schneider M and Minder C. Bias in meta-analysis detected by a simple, graphical test. *BMJ*. 1997;315:629-34.

100.	Moher D, Liberati A, Tetzlaff J, Altman DG and Group P. Preferred reporting items for systematic reviews and meta-analyses: the PRISMA statement. *PLoS Med*. 2009;6:e1000097.

101.	Joner M, Farb A, Cheng Q, Finn AV, Acampado E, Burke AP, Skorija K, Creighton W, Kolodgie FD, Gold HK and Virmani R. Pioglitazone inhibits in-stent restenosis in atherosclerotic rabbits by targeting transforming growth factor-beta and MCP-1. *Arterioscler Thromb Vasc Biol*. 2007;27:182-9.

102.	Herdeg C, Fitzke M, Oberhoff M, Baumbach A, Schroeder S and Karsch KR. Effects of atorvastatin on in-stent stenosis in normo- and hypercholesterolemic rabbits. *Int J Cardiol*. 2003;91:59-69.

103.	Joner M, Koppara T, Byrne RA, Castellanos MI, Lewerich J, Novotny J, Guagliumi G, Xhepa E, Adriaenssens T, Godschalk TC, Malik N, Alfonso F, Tada T, Neumann FJ, Desmet W, Ten Berg JM, Gershlick AH, Feldman LJ, Massberg S, Kastrati A and Prevention of PI. Neoatherosclerosis in Patients With Coronary Stent Thrombosis: Findings From Optical Coherence Tomography Imaging (A Report of the PRESTIGE Consortium). *JACC Cardiovasc Interv*. 2018;11:1340-1350.

104.	Kubo T, Akasaka T, Kozuma K, Kimura K, Fusazaki T, Okura H, Shinke T, Ino Y, Hasegawa T, Takashima H, Takamisawa I, Yamaguchi H, Igarashi K, Kadota K, Tanabe K, Nakagawa Y, Muramatsu T, Morino Y, Kimura T and Investigators N. Vascular response to drug-eluting stent with biodegradable vs. durable polymer. Optical coherence tomography substudy of the NEXT. *Circ J*. 2014;78:2408-14.

105.	Karjalainen PP, Varho V, Nammas W, Mikkelsson J, Pietila M, Ylitalo A, Airaksinen JK, Sia J, Nyman K, Biancari F and Kiviniemi T. Early neointimal coverage and vasodilator response following biodegradable polymer sirolimus-eluting vs. durable polymer zotarolimus-eluting stents in patients with acute coronary syndrome -HATTRICK-OCT trial. *Circ J*. 2015;79:360-7.

106.	Kuramitsu S, Kazuno Y, Sonoda S, Domei T, Jinnouchi H, Yamaji K, Soga Y, Shirai S, Ando K and Saito S. Vascular response to bioresorbable polymer sirolimus-eluting stent vs. permanent polymer everolimus-eluting stent at 9-month follow-up: an optical coherence tomography sub-study from the CENTURY II trial. *Eur Heart J Cardiovasc Imaging*. 2016;17:34-40.

107.	Teeuwen K, Spoormans EM, Bennett J, Dubois C, Desmet W, Ughi GJ, Belmans A, Kelder JC, Tijssen JGP, Agostoni P, Suttorp MJ and Adriaenssens T. Optical coherence tomography findings: insights from the "randomised multicentre trial investigating angiographic outcomes of hybrid

sirolimus-eluting stents with biodegradable polymer compared with everolimus-eluting stents with durable polymer in chronic total occlusions" (PRISON IV) trial. *EuroIntervention*. 2017;13:e522-e530.

108.   Tada T, Byrne RA, Schuster T, Cuni R, Kitabata H, Tiroch K, Dirninger A, Gratze F, Kaspar K, Zenker G, Joner M, Schomig A and Kastrati A. Early vascular healing with rapid breakdown biodegradable polymer sirolimus-eluting versus durable polymer everolimus-eluting stents assessed by optical coherence tomography. *Cardiovasc Revasc Med*. 2013;14:84-9.

109.   Tada T, Kastrati A, Byrne RA, Schuster T, Cuni R, King LA, Cassese S, Joner M, Pache J, Massberg S, Schomig A and Mehilli J. Randomized comparison of biolimus-eluting stents with biodegradable polymer versus everolimus-eluting stents with permanent polymer coatings assessed by optical coherence tomography. *Int J Cardiovasc Imaging*. 2014;30:495-504.

110.   Windecker S, Haude M, Neumann FJ, Stangl K, Witzenbichler B, Slagboom T, Sabate M, Goicolea J, Barragan P, Cook S, Piot C, Richardt G, Merkely B, Schneider H, Bilger J, Erne P, Waksman R, Zaugg S, Juni P and Lefevre T. Comparison of a novel biodegradable polymer sirolimus-eluting stent with a durable polymer everolimus-eluting stent: results of the randomized BIOFLOW-II trial. *Circ Cardiovasc Interv*. 2015;8:e001441.

111.   Adriaenssens T, Ughi GJ, Dubois C, De Cock D, Onsea K, Bennett J, Wiyono S, Sinnaeve P, Coosemans M, Ferdinande B, Belmans A, D'Hooge J and Desmet W. STACCATO (Assessment of Stent sTrut Apposition and Coverage in Coronary ArTeries with Optical coherence tomography in patients with STEMI, NSTEMI and stable/unstable angina undergoing everolimus vs. biolimus A9-eluting stent implantation): a randomised controlled trial. *EuroIntervention*. 2016;11:e1619-26.

112.   Kallinikou Z, Arroyo D, Togni M, Lehman S, Corpataux N, Cook M, Muller O, Baeriswyl G, Stauffer JC, Goy JJ, Puricel SG and Cook S. Vascular response to everolimus- and biolimus-eluting

coronary stents versus everolimus-eluting bioresorbable scaffolds--an optical coherence tomography substudy of the EVERBIO II trial. *Swiss Med Wkly*. 2016;146:w14274.

113.   Souteyrand G, Amabile N, Mangin L, Chabin X, Meneveau N, Cayla G, Vanzetto G, Barnay P, Trouillet C, Rioufol G, Range G, Teiger E, Delaunay R, Dubreuil O, Lhermusier T, Mulliez A, Levesque S, Belle L, Caussin C, Motreff P and Investigators P. Mechanisms of stent thrombosis analysed by optical coherence tomography: insights from the national PESTO French registry. *Eur Heart J*. 2016;37:1208-16.

114.   Taniwaki M, Radu MD, Zaugg S, Amabile N, Garcia-Garcia HM, Yamaji K, Jorgensen E, Kelbaek H, Pilgrim T, Caussin C, Zanchin T, Veugeois A, Abildgaard U, Juni P, Cook S, Koskinas KC, Windecker S and Raber L. Mechanisms of Very Late Drug-Eluting Stent Thrombosis Assessed by Optical Coherence Tomography. *Circulation*. 2016;133:650-60.

115.   Koppara T, Cheng Q, Yahagi K, Mori H, Sanchez OD, Feygin J, Wittchow E, Kolodgie FD, Virmani R and Joner M. Thrombogenicity and early vascular healing response in metallic biodegradable polymer-based and fully bioabsorbable drug-eluting stents. *Circ Cardiovasc Interv*. 2015;8:e002427.

116.   Alfonso F, Fernandez-Vina F, Medina M and Hernandez R. Neoatherosclerosis: the missing link between very late stent thrombosis and very late in-stent restenosis. *J Am Coll Cardiol*. 2013;61:e155.

117.   Koskinas KC, Chatzizisis YS, Antoniadis AP and Giannoglou GD. Role of endothelial shear stress in stent restenosis and thrombosis: pathophysiologic mechanisms and implications for clinical translation. *J Am Coll Cardiol*. 2012;59:1337-49.

118.   Lee SY, Ahn JM, Mintz GS, Hur SH, Choi SY, Kim SW, Cho JM, Hong SJ, Kim JW, Hong YJ, Lee SG, Shin DH, Kim JS, Kim BK, Ko YG, Choi D, Jang Y, Park SJ and Hong MK. Characteristics of Earlier

Versus Delayed Presentation of Very Late Drug-Eluting Stent Thrombosis: An Optical Coherence

Tomographic Study. *J Am Heart Assoc*. 2017;6.

119.   Kim C, Kim BK, Lee SY, Shin DH, Kim JS, Ko YG, Choi D, Jang Y and Hong MK. Incidence,

clinical presentation, and predictors of early neoatherosclerosis after drug-eluting stent

implantation. *Am Heart J*. 2015;170:591-7.

120.   Virmani R, Joner M and Sakakura K. Recent highlights of ATVB: calcification. *Arterioscler

Thromb Vasc Biol*. 2014;34:1329-32.

121.   Goto K, Takebayashi H, Kihara Y, Hagikura A, Fujiwara Y, Kikuta Y, Sato K, Kodama S,

Taniguchi M, Hiramatsu S and Haruta S. Appearance of neointima according to stent type and

restenotic phase: analysis by optical coherence tomography. *EuroIntervention*. 2013;9:601-7.

122.   Song L, Mintz GS, Yin D, Yamamoto MH, Chin CY, Matsumura M, Kirtane AJ, Parikh MA,

Moses JW, Ali ZA, Shlofmitz RA and Maehara A. Characteristics of early versus late in-stent

restenosis in second-generation drug-eluting stents: an optical coherence tomography study.

EuroIntervention. 2017;13:294-302.

123.   Tada T, Kadota K, Hosogi S, Miyake K, Ohya M, Amano H, Izawa Y, Kanazawa T, Kubo S,

Ichinohe T, Hyoudou Y, Hayakawa Y, Sabbah MM, Otsuru S, Hasegawa D, Habara S, Tanaka H, Fuku

Y, Katoh H, Goto T and Mitsudo K. Association between tissue characteristics assessed with optical

coherence tomography and mid-term results after percutaneous coronary intervention for in-

stent restenosis lesions: a comparison between balloon angioplasty, paclitaxel-coated balloon

dilatation, and drug-eluting stent implantation. *Eur Heart J Cardiovasc Imaging*. 2015;16:1101-11.

124.   Sakakura K, Joner M and Virmani R. Does neointimal characterization following DES

implantation predict long-term outcomes? *JACC Cardiovasc Imaging*. 2014;7:796-8.

125.   Rinfret S, Ribeiro HB, Nguyen CM, Nombela-Franco L, Urena M and Rodes-Cabau J. Dissection and re-entry techniques and longer-term outcomes following successful percutaneous coronary intervention of chronic total occlusion. *Am J Cardiol*. 2014;114:1354-60.

126.   Amsavelu S, Christakopoulos GE, Karatasakis A, Patel K, Rangan BV, Stetler J, Roesle M, Resendes E, Grodin J, Abdullah S, Banerjee S and Brilakis ES. Impact of Crossing Strategy on Intermediate-term Outcomes After Chronic Total Occlusion Percutaneous Coronary Intervention. *Can J Cardiol*. 2016;32:1239 e1-1239 e7.

127.   Azzalini L, Dautov R, Brilakis ES, Ojeda S, Benincasa S, Bellini B, Karatasakis A, Chavarria J, Rangan BV, Pan M, Carlino M, Colombo A and Rinfret S. Impact of crossing strategy on midterm outcomes following percutaneous revascularisation of coronary chronic total occlusions. *EuroIntervention*. 2017;13:978-985.

128.   Wilson WM, Walsh SJ, Bagnall A, Yan AT, Hanratty CG, Egred M, Smith E, Oldroyd KG, McEntegart M, Irving J, Douglas H, Strange J and Spratt JC. One-year outcomes after successful chronic total occlusion percutaneous coronary intervention: The impact of dissection re-entry techniques. *Catheter Cardiovasc Interv*. 2017;90:703-712.

129.   Azzalini L, Dautov R, Brilakis ES, Ojeda S, Benincasa S, Bellini B, Karatasakis A, Chavarria J, Rangan BV, Pan M, Carlino M, Colombo A and Rinfret S. Procedural and longer-term outcomes of wire- versus device-based antegrade dissection and re-entry techniques for the percutaneous revascularization of coronary chronic total occlusions. *Int J Cardiol*. 2017;231:78-83.

130.   Werner GS, Emig U, Mutschke O, Schwarz G, Bahrmann P and Figulla HR. Regression of collateral function after recanalization of chronic total coronary occlusions: a serial assessment by intracoronary pressure and Doppler recordings. *Circulation*. 2003;108:2877-82.

131.   Kotsia A, Navara R, Michael TT, Sherbet DP, Roesle M, Christopoulos G, Rangan BV, Haagen D, Garcia S, Maniu C, Pershad A, Abdullah SM, Hastings JL, Kumbhani DJ, Luna M, Addo T, Banerjee

S and Brilakis ES. The AngiographiC Evaluation of the Everolimus-Eluting Stent in Chronic Total Occlusion (ACE-CTO) Study. *J Invasive Cardiol*. 2015;27:393-400.

132.   Heeger CH, Busjahn A, Hildebrand L, Fenski M, Lesche F, Meincke F, Kuck KH and Bergmann MW. Delayed coverage of drug-eluting stents after interventional revascularisation of chronic total occlusions assessed by optical coherence tomography: the ALSTER-OCT-CTO registry. *EuroIntervention*. 2016;11:1004-12.

133.   Sherbet DP, Christopoulos G, Karatasakis A, Danek BA, Kotsia A, Navara R, Michael TT, Roesle M, Rangan BV, Haagen D, Garcia S, Maniu C, Pershad A, Abdullah SM, Hastings JL, Kumbhani DJ, Luna M, Addo T, Banerjee S and Brilakis ES. Optical coherence tomography findings after chronic total occlusion interventions: Insights from the "AngiographiC evaluation of the everolimus-eluting stent in chronic Total occlusions" (ACE-CTO) study (NCT01012869). *Cardiovasc Revasc Med*. 2016;17:444-449.

134.   Finn AV, Joner M, Nakazawa G, Kolodgie F, Newell J, John MC, Gold HK and Virmani R. Pathological correlates of late drug-eluting stent thrombosis: strut coverage as a marker of endothelialization. *Circulation*. 2007;115:2435-41.

135.   Foin N, Lu S, Ng J, Bulluck H, Hausenloy DJ, Wong PE, Virmani R and Joner M. Stent malapposition and the risk of stent thrombosis: mechanistic insights from an in vitro model. *EuroIntervention*. 2017;13:e1096-e1098.

136.   Inoue T, Shite J, Yoon J, Shinke T, Otake H, Sawada T, Kawamori H, Katoh H, Miyoshi N, Yoshino N, Kozuki A, Hariki H and Hirata K. Optical coherence evaluation of everolimus-eluting stents 8 months after implantation. *Heart*. 2011;97:1379-84.

137.   Barlis P, Regar E, Serruys PW, Dimopoulos K, van der Giessen WJ, van Geuns RJ, Ferrante G, Wandel S, Windecker S, van Es GA, Eerdmans P, Juni P and di Mario C. An optical coherence

tomography study of a biodegradable vs. durable polymer-coated limus-eluting stent: a LEADERS trial sub-study. *Eur Heart J*. 2010;31:165-76.

138.   Andreasen LN, Holm NR, Balleby IR, Krusell LR, Maeng M, Jakobsen L, Veien KT, Hansen KN, Kristensen SD, Hjort J, Kaltoft A, Dijkstra J, Terkelsen CJ, Lassen JF, Madsen M, Botker HE, Jensen LO and Christiansen EH. Randomized comparison of sirolimus eluting, and biolimus eluting bioresorbable polymer stents: the SORT-OUT VII optical coherence tomography study. *Eur Heart J Cardiovasc Imaging*. 2018;19:329-338.

139.   Koppara T, Joner M, Bayer G, Steigerwald K, Diener T and Wittchow E. Histopathological comparison of biodegradable polymer and permanent polymer based sirolimus eluting stents in a porcine model of coronary stent implantation. *Thromb Haemost*. 2012;107:1161-71.

140.   Chin-Quee SL, Hsu SH, Nguyen-Ehrenreich KL, Tai JT, Abraham GM, Pacetti SD, Chan YF, Nakazawa G, Kolodgie FD, Virmani R, Ding NN and Coleman LA. Endothelial cell recovery, acute thrombogenicity, and monocyte adhesion and activation on fluorinated copolymer and phosphorylcholine polymer stent coatings. *Biomaterials*. 2010;31:648-57.

141.   Steigerwald K, Ballke S, Quee SC, Byrne RA, Vorpahl M, Vogeser M, Kolodgie F, Virmani R and Joner M. Vascular healing in drug-eluting stents: differential drug-associated response of limus-eluting stents in a preclinical model of stent implantation. *EuroIntervention*. 2012;8:752-9.

142.   Nakazawa G, Vorpahl M, Finn AV, Narula J and Virmani R. One step forward and two steps back with drug-eluting-stents: from preventing restenosis to causing late thrombosis and nouveau atherosclerosis. *JACC Cardiovasc Imaging*. 2009;2:625-8.

143.   Gada H, Kirtane AJ, Newman W, Sanz M, Hermiller JB, Mahaffey KW, Cutlip DE, Sudhir K, Hou L, Koo K and Stone GW. 5-year results of a randomized comparison of XIENCE V everolimus-eluting and TAXUS paclitaxel-eluting stents: final results from the SPIRIT III trial (clinical evaluation

of the XIENCE V everolimus eluting coronary stent system in the treatment of patients with de novo native coronary artery lesions). *JACC Cardiovasc Interv*. 2013;6:1263-6.

144.   Kereiakes DJ, Ellis SG, Metzger C, Caputo RP, Rizik DG, Teirstein PS, Litt MR, Kini A, Kabour A, Marx SO, Popma JJ, McGreevy R, Zhang Z, Simonton C, Stone GW and Investigators AI. 3-Year Clinical Outcomes With Everolimus-Eluting Bioresorbable Coronary Scaffolds: The ABSORB III Trial. *J Am Coll Cardiol*. 2017;70:2852-2862.

145.   Yamaji K, Ueki Y, Souteyrand G, Daemen J, Wiebe J, Nef H, Adriaenssens T, Loh JP, Lattuca B, Wykrzykowska JJ, Gomez-Lara J, Timmers L, Motreff P, Hoppmann P, Abdel-Wahab M, Byrne RA, Meincke F, Boeder N, Honton B, O'Sullivan CJ, Ielasi A, Delarche N, Christ G, Lee JKT, Lee M, Amabile N, Karagiannis A, Windecker S and Raber L. Mechanisms of Very Late Bioresorbable Scaffold Thrombosis: The INVEST Registry. *J Am Coll Cardiol*. 2017;70:2330-2344.

146.   Bocan TM, Mazur MJ, Mueller SB, Brown EQ, Sliskovic DR, O'Brien PM, Creswell MW, Lee H, Uhlendorf PD, Roth BD and et al. Antiatherosclerotic activity of inhibitors of 3-hydroxy-3-methylglutaryl coenzyme A reductase in cholesterol-fed rabbits: a biochemical and morphological evaluation. *Atherosclerosis*. 1994;111:127-42.

147.   Cannon CP, Braunwald E, McCabe CH, Rader DJ, Rouleau JL, Belder R, Joyal SV, Hill KA, Pfeffer MA, Skene AM, Pravastatin or Atorvastatin E and Infection Therapy-Thrombolysis in Myocardial Infarction I. Intensive versus moderate lipid lowering with statins after acute coronary syndromes. *N Engl J Med*. 2004;350:1495-504.

9. ACKNOWLEDGEMENTS

Finally, and most importantly, I would like to thank my parents, Rezar and Betina Xhepa, and my family (Ariana, Matteo, Jasmine, Nerejda, Alba and Andrea) for their patience and support as well as for being a constant source of inspiration. This work is dedicated to them.

10. CURRICULUM VITAE

122

Dr. Erion Xhepa

Nationality: Albanian

Date of birth: 23 July 1979

Professional Experience

2014-   ISAResearch Centre

• Deutsches Herzzentrum, Munich, Germany

2011-2013   Interventional cardiologist

• Department of Cardiology of the Hospital of Varese and Gallarate, Varese, Italy

2006-2011   Cardiology Fellowship

• Department of Cardiology, Hospital of Varese, University of Insubria, Varese, Italy

2003   Internship

• Department of Cardiology, Ullevaal University Hospital, Oslo, Norway

Education

2015-2019   Technische Universität, Munich, Germany

• Ph.D Programme in Medical Life Science and Technology

2006-2011   Specialization degree in Cardiology, University of Insubria, Varese, Italy

- Final grading 50/50 "magna cum laude"

123

1999-2006   Faculty of Medicine and Surgery, University of Insubria, Varese, Italy

- Final grading 110/110 "magna cum laude"

July 1998   Bachelor at the high school "Petro Nini Luarasi", Tirana, Albania

- Final grading 10/10

11. LIST OF PUBLICATIONS

Book Chapters

Xhepa E, Koppara T, Kufner S, Radu MD, Räber L, Joner M. Validation of OCT by histology
In: The clinical atlas of optical coherence tomography, 2nd Edition
Editors: Maria D. Radu, Lorenz Räber, Yoshinobu Onuma, Patrick W. Serruys. PCR Publishing

Koppara T, Xhepa E, Kufner S, Radu M, Joner M. Neoatherosclerosis: the histopathological view.
In: The clinical atlas of optical coherence tomography, 2nd Edition
Editors: Maria D. Radu, Lorenz Räber, Yoshinobu Onuma, Patrick W. Serruys. PCR Publishing

Scientific Manuscripts

Xhepa E, Cassese S, Rroku A, Joner M, Pinieck S, Ndrepepa G, Kastrati A, Fusaro M. Subintimal versus intraplaque revascularization of coronary chronic total occlusions – Mid-term angiographic and optical coherence tomography findings from the ISAR-OCT-CTO registry. JACC Cardiovasc Interv *in press*

Rai H, Hussein H, Colleran R, Xhepa E, Wiebe J, Pinieck S, Cassese S, Joner M, Kastrati A, Byrne RA, Foley DP. Optical coherence tomography tissue coverage and characterization with grey-scale signal intensity analysis after bifurcation stenting with a new generation bioabsorbable polymer drug-eluting stent. Cardiovasc Revasc Med. 2019 May 8. pii: S1553-8389(19)30302-1. doi: 10.1016/j.carrev.2019.05.004. [Epub ahead of print] PubMed PMID: 31155492.

Xhepa E, Byrne RA, Rivero F, Rroku A, Cuesta J, Ndrepepa G, Kufner S, Valiente TB, Cassese S, Garcia-Guimaraes M, Lahmann AL, Rai H, Schunkert H, Joner M, Pérez-Vizcayno MJ, Gonzalo N, Alfonso F, Kastrati A. Qualitative and quantitative neointimal characterization by optical coherence tomography in patients presenting with in-stent restenosis. Clin Res Cardiol. 2019 Feb 19. doi: 10.1007/s00392-019-01439-5. [Epub ahead of print] PubMed PMID: 30783752.

Joner M, Koppara T, Byrne RA, Castellanos MI, Lewerich J, Novotny J, Guagliumi G, Xhepa E, Adriaenssens T, Godschalk TC, Malik N, Alfonso F, Tada T, Neumann FJ, Desmet W, Ten Berg JM, Gershlick AH, Feldman LJ, Massberg S, Kastrati A; Prevention of PRESTIGE Investigators.

Neoatherosclerosis in Patients With Coronary Stent Thrombosis: Findings From Optical Coherence Tomography Imaging (A Report of the PRESTIGE Consortium). JACC Cardiovasc Interv. 2018 Jul 23;11(14):1340-1350. doi: 10.1016/j.jcin.2018.02.029. PubMed PMID: 30025727.

Xhepa E, Kastrati A. Reduction of thrombus burden: a still unmet need in patients with ST-segment elevation myocardial infarction. Coron Artery Dis. 2018 May;29(3):181-182. doi: 10.1097/MCA.0000000000000584. PubMed PMID: 29629961.

Koppara T, Tada T, Xhepa E, Kufner S, Byrne RA, Ibrahim T, Laugwitz KL, Kastrati A, Joner M. Randomised comparison of vascular response to biodegradable polymer sirolimus eluting and permanent polymer everolimus eluting stents: An optical coherence tomography study. Int J Cardiol. 2018 May 1;258:42-49. doi: 10.1016/j.ijcard.2018.01.011. PubMed PMID: 29544956.

Cassese S, Ndrepepa G, Byrne RA, Kufner S, Lahmann AL, Mankerious N, Xhepa E, Laugwitz KL, Schunkert H, Fusaro M, Kastrati A, Joner M. Outcomes of patients treated with ultrathin-strut biodegradable polymer sirolimus-eluting stents versus fluoropolymer-based everolimus-eluting stents: a meta-analysis of randomised trials. EuroIntervention. 2018 Jun 20;14(2):224-231. doi: 10.4244/EIJ-D-18-00024. PubMed PMID: 29537375.

Cassese S, Xhepa E, Ndrepepa G, Kufner S, Colleran R, Giacoppo D, Koppara T, Mankerious N, Byrne RA, Laugwitz KL, Schunkert H, Fusaro M, Kastrati A, Joner M. Vascular response to percutaneous coronary intervention with biodegradable-polymer vs. new-generation durable-polymer drug-eluting stents: a meta-analysis of optical coherence tomography imaging trials. Eur Heart J Cardiovasc Imaging. 2018 Nov 1;19(11):1294-1301. doi: 10.1093/ehjci/jex334. Review. PubMed PMID: 29300853.

Nicol P, Xhepa E, Bozhko D, Joner M. Neoatherosclerosis: from basic principles to intravascular imaging. Minerva Cardioangiol. 2018 Jun;66(3):292-300. doi: 10.23736/S0026-4725.17.04573-X. Epub 2017 Nov 20. Review. PubMed PMID: 29160047.

Adriaenssens T, Joner M, Godschalk TC, Malik N, Alfonso F, Xhepa E, De Cock D, Komukai K, Tada T, Cuesta J, Sirbu V, Feldman LJ, Neumann FJ, Goodall AH, Heestermans T, Buysschaert I, Hlinomaz O,

Belmans A, Desmet W, Ten Berg JM, Gershlick AH, Massberg S, Kastrati A, Guagliumi G, Byrne RA; Prevention of Late Stent Thrombosis by an Interdisciplinary Global European Effort (PRESTIGE) Investigators. Optical Coherence Tomography Findings in Patients With Coronary Stent Thrombosis: A Report of the PRESTIGE Consortium (Prevention of Late Stent Thrombosis by an Interdisciplinary Global European Effort). Circulation. 2017 Sep 12;136(11):1007-1021. doi: 10.1161/CIRCULATIONAHA.117.026788. Epub 2017 Jul 18. PubMed PMID: 28720725; PubMed Central PMCID: PMC5598909.

Kufner S, Joner M, Schneider S, Tölg R, Zrenner B, Repp J, Starkmann A, Xhepa E, Ibrahim T, Cassese S, Fusaro M, Ott I, Hengstenberg C, Schunkert H, Abdel-Wahab M, Laugwitz KL, Kastrati A, Byrne RA; ISAR-DESIRE 4 Investigators. Neointimal Modification With Scoring Balloon and Efficacy of Drug-Coated Balloon Therapy in Patients With Restenosis in Drug-Eluting Coronary Stents: A Randomized Controlled Trial. JACC Cardiovasc Interv. 2017 Jul 10;10(13):1332-1340. Doi 10.1016/j.jcin.2017.04.024. PubMed PMID: 28683939.

Joner M, Xhepa E. Consequences of Vascular Calcification: Implications for Bioresorbable Vascular Scaffolds. JACC Cardiovasc Imaging. 2017 Oct;10:1162-1164. doi: 10.1016/j.jcmg.2016.12.012. Epub 2017 Mar 15. PubMed PMID: 28330667.

Cassese S, Ndrepepa G, Byrne RA, Kufner S, Xhepa E, de Waha A, Rheude T, Colleran R, Giacoppo D, Harada Y, Laugwitz KL, Schunkert H, Fusaro M, Kastrati A. Outcomes of patients treated with durable polymer platinum-chromium everolimus-eluting stents: a meta-analysis of randomised trials. EuroIntervention. 2017 Oct 20;13(8):986-993. doi: 10.4244/EIJ-D-16-00871. PubMed PMID: 28067198.

Kufner S, Xhepa E, Lutter C, Cassese S, Joner M. Optical coherence tomography in drug-eluting stent restenosis: a technique in need of a strategy. Minerva Cardioangiol. 2017 Feb;65(1):61-67. doi: 10.23736/S0026-4725.16.04241-9. Epub 2016 Sep 27. Review. PubMed PMID: 27676648.

Cassese S, Xhepa E, Kastrati A. Biodegradable-polymer drug-eluting stents: back to the future? Heart. 2017 Jan 15;103(2):91-92. doi: 10.1136/heartjnl-2016-310213. Epub 2016 Sep 14. PubMed PMID: 27628493.

Rheude TA, Xhepa E, Byrne RA. Markedly different tissue types on optical coherence tomography imaging in a patient with multiple lesion drug-eluting stent in-stent restenosis. Catheter Cardiovasc Interv. 2017 May;89(6):E181-E184. doi: 10.1002/ccd.26694. Epub 2016 Aug 16. PubMed PMID: 27527355.

Xhepa E, Tada T, Kufner S, Ndrepepa G, Byrne RA, Kreutzer J, Ibrahim T, Tiroch K, Valgimigli M, Tölg R, Cassese S, Fusaro M, Schunkert H, Laugwitz KL, Mehilli J, Kastrati A. Long-term prognostic value of risk scores after drug-eluting stent implantation for unprotected left main coronary artery: A pooled analysis of the ISAR-LEFT-MAIN and ISAR-LEFT-MAIN 2 randomized clinical trials. Catheter Cardiovasc Interv. 2017 Jan;89(1):1-10. doi: 10.1002/ccd.26645. Epub 2016 Aug 12. PubMed PMID: 27515100.

Otsuka F, Byrne RA, Yahagi K, Mori H, Ladich E, Fowler DR, Kutys R, Xhepa E, Kastrati A, Virmani R, Joner M. Neoatherosclerosis: overview of histopathologic findings and implications for intravascular imaging assessment. Eur Heart J. 2015 Aug 21;36(32):2147-59. doi: 10.1093/eurheartj/ehv205. Epub 2015 May 20. Review. PubMed PMID: 25994755.